GROUND RADIOMETRIC INVESTIGATION IN THE SOUTHERN PART OF THE KERRI–KERRI FORMATION, GOMBE STATE, NORTHEASTERN NIGERIA

By

DAVID BACHAMA YUSUF

DEPARTMENT OF PHYSICS

AHMADU BELLO UNIVERSITY, ZARIA

NIGERIA

JUNE, 2016

GROUND RADIOMETRIC INVESTIGATION IN THE SOUTHERN PART OF THE KERRI–KERRI FORMATION, GOMBE STATE, NORTHEASTERN NIGERIA

By

David Bachama YUSUF, B.Sc. (A.B.U.) 1986, M.Sc. (A.B.U.) 2000
PhD/SCI/14040/2011-2012

A THESIS SUBMITTED TO THE SCHOOL OF POSTGRADUATE STUDIES,

AHMADU BELLO UNIVERSITY, ZARIA

IN PARTIAL FULFILMENT OF THE REQUIREMENTS FOR THE AWARD

OF A

DEGREE OF DOCTOR OF PHILOSOPHY IN APPLIED GEOPHYSICS

DEPARTMENT OF PHYSICS

FACULTY OF SCIENCE

AHMADU BELLO UNIVERSITY, ZARIA

NIGERIA

JUNE, 2016

CERTIFICATION

This thesis entitled "GROUND RADIOMETRIC INVESTIGATION IN THE SOUTHERN PART OF THE KERRI–KERRI FORMATION, GOMBE STATE, NORTHEASTERN NIGERIA" by David Bachama YUSUF meets the regulations governing the award of the degree of Doctor of Philosophy of the Ahmadu Bello University, and is approved for its contribution to knowledge and literary presentation.

Dr. A. A. Lawal (Signature) _____

Chairman Supervisory Committee Date _____

Prof. K. M. Lawal (Signature) _____

Member Supervisory Committee Date _____

Dr. A. S. Arabi (Signature) _____

Member Supervisory Committee Date _____

Dr. Y. I. Zakari (Signature) _____

Head of Department of Physics Date _____

Prof. Kabiru Bala (Signature) _____

Dean School of Postgraduate Studies Date _____

DECLARATION

I declare that the work in this Thesis entitled "Ground Radiometric Investigation in the Southern Part of the Kerri–Kerri Formation, Gombe State, Northeastern Nigeria" has been carried out by me in the Department of Physics, Faculty of Science, Ahmadu Bello University, Zaria. The information derived from the literature has been duly acknowledged in the text and a list of references provided. No part of this thesis was previously presented for another degree or diploma at this or any other Institution.

David Bachama YUSUF

Name	Signature	Date

ACKNOWLEDGEMENT

First and foremost, I am grateful to God Almighty for His care, support, protection, provisions and guidance in my life. He has granted me safe journey mercies throughout the period of this work and made it possible for me to meet up with all the financial obligations involved. To Him be all the glory.

Many people have contributed in one way or the other to the success of this work.

Dr. Ahmed A. Lawal of the Department of Physics, (A.B.U.), Zaria suggested the topic and served as the Chairman Supervisory Committee. I am very grateful for his support, contributions and encouragement. Prof. Kola M. Lawal of the Department of Physics, A.B.U., a member of the Supervisory Committee made a lot of useful suggestions and contributions to this work. Dr. Abdullahi, Suleiman Arabi of the Centre for Energy Research and Training, (CERT), A.B.U., also a member of the Supervisory Committee contributed immensely to the success of this work.

To Dr. Umar Sadiq (Former Head of Department of Physics), Dr. Y. I. Zakari, (Head of Department of Physics), Dr. P. Sule (Geophysics Coordinator, Dept. of Physics) and Dr. M. I. Mamunu (Former Seminar Coordinator, Dept. of Physics), I am very grateful for their support and cooperation. Prof. Rabiu Nasiru is appreciated for his encouragement and advice. The following members of staff of Dept. of Physics, A.B.U.; L. O. Sule, Boniface, Madam Mary (Late), Mrs. Mary Dada, Miss Grace C. Ukeje, Malam Isiyaku Jafaru, Bala Bello and Auwal Jibrin are acknowledged for their support and assistance. In the Dept. of Geology, A.B.U., I appreciate the support of Dr. H. Hamza, Malam Shehu Magaji and Mr. Olufemi Adeleye (who produced some of the maps).

Prof. Abdullahi Mahdi (Pioneer V/C Gombe State University), Prof. I. M. Umar (V/C Gombe State University), Prof. Abubakar I. Waziri (Deputy V/C Gombe State University), Malam M. A. Yuguda (Registrar Gombe State University) and Dr. N. Y. Tadi (Director, SBRS), Freda Yazu (Deputy Registrar) and Zephania Shehu (Chief Accountnt) are hereby acknowledged for their support. To Dr. Esrom Jokthan (Provost. FCE Billiri), I am grateful. I also appreciate the support of Musa Sarki, Danladi Aliyu, Salihi I. Muktar (My neighbours), Asinah Pisagih, Ruth Beli, Adamu Pela, Salisu B. Hamza, Juliet D. Aluke, Verla Hilda, Sarki Apolos (Baba), Takkani Jigai (Arase), Edward F. Baka, Erasmus I. Sulai, Kachalla Aliyuda, Sa'adu Bappah Idaya, Hamisu Ya'u, Sidi U. Reme and Auwal Baba (SBRS Physics Lab.).

I am also grateful to Mr. Gana J. Sunday (NGSA, Kaduna) for his contributions. To Mr. Mohammed and Ekele (Technical Staff of NGSA, Kaduna) who assisted me in conducting the Spectrometric Survey, I am very grateful. To Isaac Istifanus Aiki who assisted me in the Scintillometric Survey, thank you.

Abdu B. Zargina (Galadiman Degri) of Ministry of Lands, Gombe State assisted me a lot. To Surveyor Zakariya A. Difa (Ministry of Lands, Gombe State and most hard working staff Award Winner 2015 of Gombe State), I am very grateful. Thank you to Asst. Surveyor Idris A. Difa for a good job. To Eng. A. Musliu and his boys, thank you.

I cannot forget to thank and acknowledge my sister, Mrs. Ruskana P. Ali of the Department of Industrial Design, A.B.U. who has supported me from my undergraduate level to this stage. May God continue to bless and strengthen her. To her children Abba Ali & his wife Ruth, Yusuf Ali (Nigeria Overall Award Winner for Graduate Animal Scientist 2015), Agnes, Rifkatu and Kanadi, I say thank you all. I also acknowledge the support of her colleagues, Dr. Adele Garkida and Rev. Dr. C. M. Gonah of Industrial Design Dept., A.B.U. To her neighbour, Maman Glory (The Senator), I am grateful. To my sister Mrs. Victoria N. D. Jamiyal and her family, I am very grateful for their support and encouragement. I acknowledge my brother Dr. Nigel Y. Bachama

and his family for their support, prayers and encouragement. I appreciate my mother Hannatu Ibrahim for her constant support.
I acknowledge Tertiary Education Trust Fund (TETFUND) for assisting me with two-thirds (2/3) of the amount given to other PhD science students in Nigeria.
I also want to thank Markus Maigari for staying with my children each time I travel out of Gombe. Thank you for sparing your time. God will reward you abundantly.
Last but not the least are my wife Mrs. Rahila D. Bachama and children; Deborah, Peace and Glory who have given me their support and endured my absence throughout the course of this work. Thank you for your support and prayers. God will bless you abundantly.
May God grant each and every one his/her heart desires. It is my hope, wish and prayer that our dear country Nigeria will regain its lost glory and be in peace. Thank you all and God bless.

DEDICATION

I dedicate this work to my late father Mr. Yusufu Bachama Mwanai, my mother Mrs. Naye Y. Bachama, and my dear children Deborah David, Peace David and Glory David. To God Almighty be all the glory.

TABLE OF CONTENTS

		Page
Title Page	. . . . .	i
Certification.	. . . . .	ii
Declaration	. . . . .	iii
Acknowledgement	. . . . .	iv
Dedication	. . . . .	vi
Table of Contents	. . . . .	vii
List of Tables	. . . . .	xi
List of Figures	. . . . .	xiii
List of Appendices	. . . . .	xvi
List of Plates	. . . . .	xvii
Abstract	. . . . .	xviii
1.0 GENERAL INTRODUCTON.	. . . . .	1
1.1 Overview	. . . . .	1
1.2 Justification	. . . . .	6
1.3 Aim and Objectives of the Study	. . . . .	7
1.4 Scope and Limitation of the Study	. . . . .	8
1.5 Location of the Study Area	. . . . .	8

1.6 Geology of the Study Area 9

1.7 Vegetation and Climate of the Study Area 13

1.8 Relief & Drainage of the Study Area 14

2.0 LITERATURE REVIEW 16

2.1 Basic Principles of Radiometrics 16

2.2 Gamma Ray Spectrometry 19

2.3 Decay Chain Series of Uranium, Potassium and Thorium . . 20

2.4 Radioactive Equilibrium / Disequilibrium 24

2.5 Secular Equilibrium 27

2.6 Cosmic Rays and Background Corrections 29

2.7 Uranium Minerals Associated with Common Rocks . . . 31

2.8 Radiometric Anomalies 35

2.9 Radiometric Exploration Methods 37

2.10 Radiometric Measuring Instruments 39

2.10.1 Ionization chambers 40

2.10.2 Proportional counters 40

2.10.3 Geiger-Mueller (GM) counters 41

2.10.4 Scintillation detectors 41

2.11 Radiometric Data Processing 43

2.12 Radiometric Data Presentation 47

3.0 MATERIALS AND METHODOLOGY 49

3.1 Ground Scintillometric Survey 49

3.1.1 Materials for the scintillometric survey 49

3.1.2 Methodology for the scintillometric survey 50

3.2 Ground Spectrometric Survey 51

3.2.1 Materials for the ground spectrometric survey 51

3.2.2 Methodology for the spectrometric survey. 52

3.2.3 Spectrometric data processing. 54

3.3 Collection and Preparation of Rock Samples 56

4.0 RESULTS 58

4.1 Scintillometric Data Analysis. 58

4.2 Spectrometric Data Analysis 60

4.2.1 Image maps for the PGIS-SP data 61

4.2.2 Image maps for the rock samples 64

4.2.3 Ternary maps for the PGIS-SP data 66

4.2.4 Ratio maps for the PGIS-SP data 68

4.2.5 Variation of concentration of radioelements with topography of the study area 72

4.2.6 Variation of concentration of radioelements with geology of the study area 74

4.3 Statistical Analysis of the Data 77

4.3.1 Average crustal abundance of concentration of the radioelements . . 78

4.3.2 Diagnostic ratio analysis of the data 78

4.3.3 Correlations between the concentrations of the radioelements . . 79

4.3.4 Threshold method of data analysis 80

5.0 DISCCUSSION OF RESULTS 84

5.1 Interpretation of Data 84

5.1.1 Map assessment 84

5.1.2 Statistical assessment 87

5.1.3 Activity ratios of the concentrations of the radioelements . . . 88

5.1.4 Correlations between activity concentrations of the radionuclides . . 89

5.1.5 Absorbed dose rate 89

6.0 CONCLUSIONS AND RECOMMENDATIONS 91

6.1 Conclusions 91

6.2 Recommendations 93

REFERENCES 94

APPENDICES 102

PLATES 122

LIST OF TABLES

Table No.		Page
1.1	Lithostratigraphical subdivisions for the Gongola Basin . . .	11
2.1	International Atomic Energy Agency (IAEA) Recommended Energy Windows	20
2.2	The U^{238} decay chain series	21
2.3	Decay chain series of U^{235}	21
2.4	The Th^{232} decay chain series	22
2.5	Types of Important Uranium Deposits	33
2.6	Relative Abundance of Uranium in Some Rocks	34
2.7	Mean Contents of Radio - Elements in Various Rock Types . . .	36
4.1	Statistical analysis of the PGIS-SP data	77
4.2	Statistical analysis of laboratory gamma spectrometer results of the rock samples	77
4.3	Ratios of activity concentrations of the radionuclides for the PGIS-SP data	78
4.4	Ratios of activity concentrations of the radionuclides for the rock samples	78

4.5 Correlation between U, Th and K for the PGIS-SP data . . . 79

4.6 Correlation between ^{226}Ra, ^{232}Th and ^{40}K for the rock samples . . 79

LIST OF FIGURES

Figure No.		Page
1.1	Ternary image map of Gombe Sheet 152 S.W	7
1.2	Location of the Study Area in Akko Local Government Area of Gombe State	9
1.3	Geologic map of the study area	13
1.4	Drainage pattern of the study area	15
2.1	Spectograms obtained from U, K, and Th samples on Granite outcrop	22
2.2	Variations as a function of time of four successive members of decay series	27
2.3	Relative Proportion of Uranium (U), Potassium (K) and Thorium (Th) on a Ternary Image Ratio	47
3.1	Location of data points and direction of profiles for the Spectrometric survey	54
3.2	Locations of rock samples collected and composite samples formed .	57
4.1	Contour map of count rates of gamma ray energy of the study area . .	58
4.2	Frequency Distribution of Total Count Rates of Gamma ray Energy of the Study Area	59
4.3	Total count map of the study area for the PGIS-SP data . . .	61

4.4 Uranium concentration (eU) map of the study area for the PGIS-SP data 62

4.5 Thorium concentration (eTh) map of the study area for the PGIS-SP data 62

4.6 Potassium concentration (%K) map of the study area for the PGIS-SP data 63

4.7 Absorbed dose rate map of the study area 64

4.8 Uranium (^{238}U) map of rock samples 65

4.9 Thorium (^{232}Th) map of rock samples 65

4.10 Potassium (^{40}K) map of rock samples. 66

4.11 Standard Ternary Map of the Study Area 67

4.12 Normalised Ternary Map of the Study Area 68

4.13 U/Th Ratio Map of the Study Area for the PGIS-SP data . . . 69

4.14 Th/K ratio map of the study area for the PGIS-SP data . . . 70

4.15 U/K ratio map of the study area for the PGIS-SP data . . . 70

4.16 U^2/Th Ratio Map of the Study area for the PGIS-SP data . . . 71

4.17 Shuttle Rader Topographic Map of the study area 72

4.18 Uranium map draped on SRTM for PGIS-SP data 73

4.19 Thorium map draped on SRTM for PGIS-SP data 73

4.20 Potassium map draped on SRTM for PGIS-SP data 74

4.21 Geologic map of the spectrometric survey area 74

4.22 Uranium map draped on geologic map of spectrometric survey area . 75

4.23 Thorium map draped on geologic map of spectrometric survey area . 75

4.24 Potassium map draped on geologic map of spectrometric survey area . 76

4.25 Total count map draped on geologic map of the study area for the PGIS-SP data 76

4.26 Bar Chart of mean gamma ray activity of U, Th and K along profiles for PGIS-SP data 80

4.27 Bar chart of gamma ray activity of U, Th and K of Rock Samples . . 80

4.28 Map of concentration of Uranium after separation of threshold value . 81

4.29 Map of concentration of Thorium after separation of threshold value . 82

4.30 Map of concentration of Potassium after separation of threshold value . 82

4.31 Areas of most promising uranium mineralization 83

LIST OF APPENDICES

Appendix No.		Page
I.	Background readings taken in the Pond and Dadin - Kowa Dam . .	102
II.	Corrected Scintillometric Data	103
III.	PGIS-SP Data for Profiles 1 to 10	107
IV.	Results of conversion of activity concentration of radionuclides of rock samples from Bq/kg to ppm and results of calculations of dose rate .	119
V.	Results of laboratory gamma ray spectrometer Analysis . . .	120
VI.	Frequency distribution of total count rates of gamma ray energy of the study area.	121

LIST OF PLATES

Plate No. **Page**

I. The Researcher taking readings with the scintillometer in the Study area 122

II. A Field Assistant recording readings taken by the researcher . . 123

III. The PGIS - SP strapped at the back of the researcher during the spectrometric survey 124

ABSTRACT

The first ground radiometric investigation has been carried out in the present study to confirm the occurrences or otherwise of uranium, thorium and potassium mineralization and also to assess the risks associated with human exposure to these radiations in the southwest of the Kerri–Kerri Formation. Total count readings were taken randomly with a portable ground scintillometer "Exploranium GR-101A". From the analysis of the scintillometric data, an area 2.25 km^2 was identified with higher gamma ray activity (40–60 cps) situated northeast of Tumu in the southwest of the study area bounded by latitudes 10º 00′ 14″ N to 10º 01′ 19″ N and longitudes 11º 00′ 58″ E to 11º 02′ 04″ E. Further ground spectrometric survey was carried out with a "Pico Envirotec Portable Ground Information System Gamma Ray Spectrometer" (PGIS–SP/Model GIS-15), in the area identified with higher gamma ray activity. Rocks samples were also collected in the study area for laboratory gamma spectrometer analysis which was carried out at the Centre for Energy Research and Training (CERT), Ahmadu Bello University (A.B.U.), Zaria. Results from map analysis of both the PGIS-SP data and rock samples indicate the concentration of potassium in the northwestern part of the study area consisting of high alluvium and low level elevation, while uranium and thorium are more concentrated in the central and southern parts of the area consisting of highly weathered ironstones (i.e. hematite). The equivalent thorium image map shows the concentration of thorium in the southwest, southeast and southern end of the area. The mean activity concentration of ^{238}U, ^{232}Th and ^{40}K for the PGIS-SP data are respectively 5 ppm, 16 ppm and 0.6 % while their standard deviations are: 2 ppm for ^{238}U, 6 ppm for ^{232}Th and 0.2 % for ^{40}K. The correlation coefficients between (^{238}U and ^{232}Th), (^{238}U and ^{40}K) and (^{232}Th and ^{40}K) are respectively 0.30, 0.31 and 0.24. For the rock samples, the mean concentrations of ^{238}U, ^{232}Th and ^{40}K are respectively 2 ppm, 15 ppm and 0.3 % while their standard deviations are 1 ppm for ^{238}U, 4 ppm for ^{232}Th and 0.3 % for ^{40}K. For the rocks, a good correlation ($r = 0.50$) exists, between ^{232}Th and ^{40}K while a very weak correlation ($r = 0.05$) exists, between ^{238}U and ^{40}K. The correlation between ^{238}U and ^{232}Th is good but negative ($r = - 0.63$) which indicates the absence of significant accessory minerals in the study area. There is uniformity in the concentrations of the radionuclides as their standard deviations are lower than their mean values. The resulting low eTh/K and eU/K ratios are good indicators of preferential enrichment of potassium to thorium and uranium in the rocks of the area. Results from statistics and map analysis revealed that the concentration of uranium in the study area were far below 250 times the average content in normal rocks and in addition their ratios did not reflect preferential enrichment of uranium to the others. The mean absorbed dose rate for the PGIS-SP data is 15.646 $nGyph^{-1}$ while that of the rocks is 53.6930 $nGyph^{-1}$ both of which are lower than the world average value of 60 $nGyph^{-1}$. Radiations from the rocks of the area are therefore not harmful to humans and the environment. This study has also revealed that the radiometric anomaly observed on the ternary image map of Gombe Sheet 152 S.W. in the study area is mostly due to potassium radiation.

Keywords: Kerri-Kerri Formation, Radiometrics, Activity concentrations, Activity ratios and Absorbed dose rate.

CHAPTER ONE

GENERAL INTRODUCTION

1.1 Overview

Nigeria is blessed with abundant solid mineral resources distributed in all the states of the federation. According to reports by the Nigerian Geological Survey Agency (NGSA, 2004), Nigeria has about 34 known major mineral deposits distributed in different locations across the country and offer a lot of attractions for investors. These viable solid minerals could be explored and exploited to boost the country's economy and supplement the revenue derived from other resources.

The need for reliable geophysical data cannot be overemphasized in any economy, especially in economies blessed with natural resources as Nigeria. For many years, the absence of reliable geophysical data has been seen as one of the many challenges hindering the development of the mining sector in Nigeria. These challenges have stood for as bottlenecks against the development of the sector and have also been one of the put - offs towards getting foreign investors to come in, as many have argued that investing in economies without reliable bankable data is a risk no investor is willing to take.

Being a prime ingredient in the production of nuclear power, uranium is of great importance and great danger at the same time for the peace of the world. Uranium gained importance with the development of practical uses of nuclear energy. The first atomic bomb used in warfare was a uranium bomb. This bomb contained enough of the ^{235}U isotope to start a chain reaction which in a fraction of a second caused a large number of the uranium atoms to undergo fission, thereby releasing a fireball of energy (Lenntech, 2013).

The main use of uranium in the civilian sector is to fuel commercial nuclear power plants. This requires uranium to be enriched with the U^{235} isotope and the chain reaction to be controlled so that the energy is released in a more manageable way. The isotope U^{238} is also

used to estimate the age of rocks in radiometric dating. Other uses of uranium include: making of phosphate fertilizers, yellow glass and pottery glass, photographic chemicals, lamp filaments, and in leather and wood stain (Lenntech, 2013).

Thorium is also an important alloying agent in magnesium, as it imparts greater strength and creep resistance at high temperatures. Thorium can be used as a source of nuclear power. It is about three times as abundant as uranium and about four times as abundant as lead and there is probably more energy available from thorium than both uranium and fossil fuels (Tukel *et al.,* 2009).

Potassium is a very important mineral for the proper functioning of all cells, tissues, and organs in the human body. It is also an electrolyte, a substance that conducts electricity in the body, along with sodium, chloride, calcium, and magnesium (UMMC, 2013). Potassium is crucial to heart function and plays a key role in skeletal and smooth muscle contraction, making it important for normal digestive and muscular function (UMMC, 2013). Many foods contain potassium, including some types of fish (such as salmon, cod, and flounder), and many fruits, vegetables, and legumes. Dairy products are also good sources of potassium (UMMC, 2013). Uranium, thorium and potassium are therefore valuable elements with lots of economic importance.

Geological survey in Nigeria evolved as far back as early 1960's when the Mineral Surveys of the Southern and Northern Protectorates of Nigeria were established respectively by the British Secretary of State for the Colonies (Dada *et al.*, 1982). The Mineral Surveys were mandated to carry out broad reconnaissance survey of mineral resources of the two Protectorates for use as raw materials for industries in Britain. In the course of their activities, such deposits as ironstone, columbite, limestone and bitumen, lead and zinc ores, coal, pottery clays, iron ore, gold, and marble, etc, were discovered in various parts of the country (Dada *et al.*, 1982).

Government's efforts towards the provision of credible geophysical data began in 1972 when Hunting Geology and Geophysics Limited and Fairy Surveys Limited were commissioned to carry out airborne surveys of the entire country except the Southwest and Chafe blocks (Dada *et al.*, 1982). The country was divided into six (6) zones namely;

1. Niger Delta and Offshore Regions;
2. Lower Benue;
3. Upper Benue;
4. Chad Basin;
5. North Central and
6. Sokoto and Middle Niger

Magnetic and radiometric surveys were carried out in Zones 2, 3 and 6, while only magnetic surveys were carried out in zones 1 and 4 (Dada *et al.*, 1982). As a follow up to this, Airborne Geophysical survey of southwestern Nigeria commenced in 2003 by Fugro Airborne Surveys Limited. Fixed wing airborne gradiometer and radiometric geophysical survey over Ogun State also started in 2003 and were completed in 2004 (Dada *et al.*, 1982).

The aim and objective of these surveys were to detect mineral occurrences and deposits in the country through geological mapping. The overall strategy envisaged that Nigeria should be self sufficient in the production of industrial minerals for local industries, while exploration would be concentrated on gathering and acquiring geological data on precious metals, base metals and gemstones in order to attract foreign investors to develop these minerals for export and foreign exchange earnings.

Dada *et al*. (1982) reported that the Geological Survey Department (GSD) contracted out the airborne gamma spectrometer survey of four contiguous areas in 1973/74, namely:

1. Sokoto and Middle Niger
2. North Central (Kaduna - Jos)

3. Lower Benue and Adjoining regions
4. Upper Benue and Adjoining regions

These surveys were completed and reports submitted in 1975/76. The Geological Survey Department commenced a group follow - up in 1976. The programme consisted of traversing identified areas with gamma spectrometers and scintillometers, followed by detailed radiometric survey on grids, geological mapping, pitting, trenching, and diamond drilling (Dada *et al.,* 1982). Areas covered included about 20,000 km^2 in Sokoto State; 10,000 km^2 in Cross River and Benue States; and 8,000 km^2 in the Niger and Benue rivers confluence area of Northern Nigeria (Dada *et al.,* 1982). No appreciable quantity of uranium was found; therefore no further drilling was carried out (OECD and IAEA, 1979).

In 1975, the Nigeria Mining Corporation carried out a feasibility study on the prospect of uranium mineralization in Nigeria (Dada *et al.,* 1982). This was followed by a geochemical and reconnaissance ground traversing with scintillometers. A total area of 35,000 km^2 in northeastern Nigeria was covered in the programme. The programme was expanded in 1981 to include the central area of Nigeria and reconnaissance fieldwork commenced in October, 1981. Readings were taken using total count scintillometers (SSP2) and the results were contoured on a map of 1:100,000 standard sheets (Dada *et al.*, 1982). In a report in 1979, OECD and IAEA (1979) expected an increase in the success of the efforts. It however noted that the Federal Government's position on Uranium exploration was not clear although decrees establishing the Nigeria Atomic Energy Commission (NAEC) and Energy Commission of Nigeria (ECN) were promulgated. The need for such commissions necessarily means an increase in the area of uranium exploration or in the exploration of the radio - elements to the industry and Government establishments. Also, the need for nuclear energy to play a prominent role in future energy supply was clearly demonstrated in the concluding report of the World Energy Conference (WEC) released in September 1978. All

these mean that there is going to be an increase in Uranium exploration both locally and internationally.

Although intensive ground follow - up surveys have been carried out in some areas since 1977, for example by the Nigeria Uranium Mining Company (NUMCO), Nigerian Mining Corporation, Geological Survey of Nigeria (now Nigerian Geological Survey Agency, NGSA) and University of Ife, there is very little information on uranium occurrences in Nigeria. The only little available information on uranium occurrences in Nigeria are mainly from individuals who have analyzed a few rock samples and uranium ores from some locations around the Nigerian younger granite province. However, the works of Uwah (1984), Dewu (1986), and Ahmed (2006) who carried out detailed investigations of radiometric anomalies in the Sokoto Basin, Bisichi and Jingir areas of Sokoto and Plateau States respectively, form a very important step for a large scale exploration of uranium and allied minerals. Arabi *et al.* (2012) assessed the levels of concentration of uranium in groundwater to ascertain its compliance with the World Health Organization's and United State Environmental Protection Agency's guidelines for uranium in drinking water in the northeastern part of Nigeria (Gombe Sheet 152). Other individuals who have recently carried out research in Radiometrics in the northern and northeastern part of Nigeria include: Ayodeji *et al.* (2011), Abdullahi (2013), Bute (2013), Taiwo *et al.* (2014) and Arabi *et al.* (2012; 2015).

The main requirement of the future of nuclear power is the development of hidden ore bodies. A fuel supply is intrinsically fundamental to the sustainability of any energy system. Therefore it is essential that all stake holders with interest in understanding nuclear fuel supply have available a systematic analysis of the long term uranium supply (STI/PUB, 2001). The abundance of uranium in the earth's crust according to Tukel *et al.* (2009) is about 4×10^{-4} %, roughly the same as that of boron or tungsten. It is a little more common than gold

or rubidium, but thorium and lead are 3 and 4 times more abundant, respectively. Tukel *et al.* (2009) estimated that the world's known petroleum reserves will last 40 years, natural gas will last 61 years and coal reserves will be exhausted in 227 years. Thus, the decrease in fossil fuel reserves due to fast consumption and environmental damages due to increasing environmental pollution makes it necessary to orient towards new and renewable energy resources.

1.2 Justification

The NGSA has in recent years been processing and integrating geophysical data acquired in the country into a data base. The regional airborne radiometric data acquired by Fugro Airborne Surveys were processed and from which image maps were produced by the NGSA. The Airborne ternary image map of Gombe Sheet 152 SW, prepared by the NGSA (2007) shows some radiometric anomalies in some parts of the Kerri - Kerri Formation (Fig.1.1).

Also, in a study on uranium favourability in Nigeria, Oshin (1986) has suggested that the geological setting of the Kerri - Kerri and Bima Formations are potential hosts of uranium mineralization.

Since then there has been no ground radiometric follow up survey to confirm the potentials of uranium, thorium and potassium mineralization in the Kerri - Kerri Formation as suggested by Oshin (1986) and as observed on the airborne radiometric ternary image map of Gombe Sheet 152 SW (Fig. 1.1).

The present work can therefore be considered as the first ground radiometric investigation to confirm the occurrence or otherwise of uranium, thorium and potassium mineralization and if so delineate such areas in the study area. Findings from this study will therefore shed more light on the potentials of uranium mineralization in the Kerri - Kerri Formation and contribute immensely to the general knowledge of uranium occurrences in Nigeria.

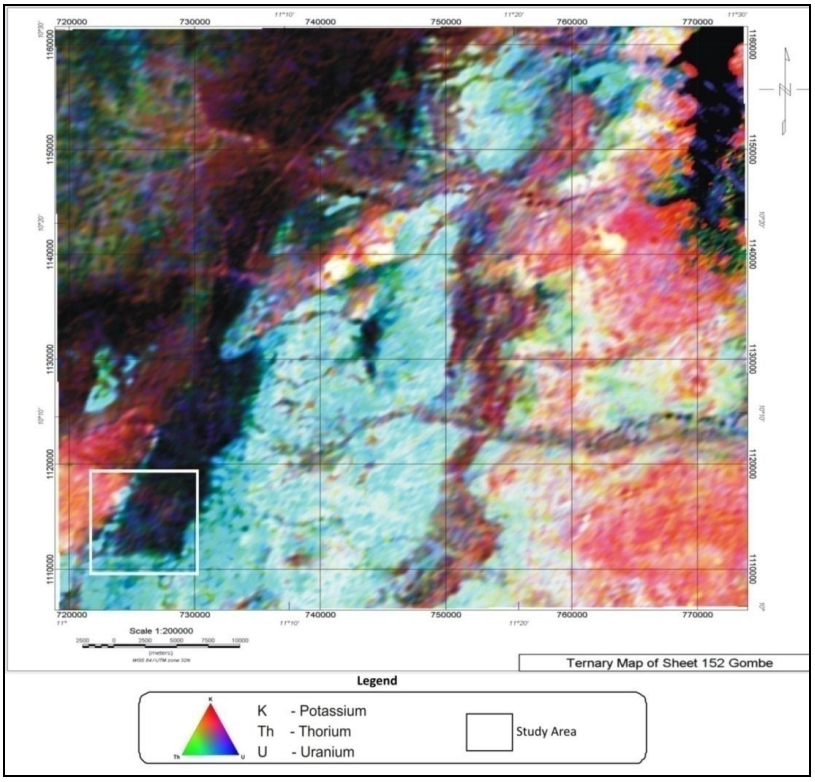


Fig. 1.1: Ternary Image Map of Gombe Sheet 152 SW. (Source: NGSA, 2007).

1.3 Aim and Objectives of the Study

The aim of this present study is to carry out a ground radiometric investigation in the southwestern part of the Kerri–Kerri Formation situated southwest of Gombe Town (Gombe Sheet 152 SW) in order to ascertain whether or not there are uranium, thorium and potassium enrichments in the rocks of the area.

The above aim will be achieved by the following objectives:

i. Carrying out a reconnaissance survey of the study area by taking total count readings randomly with a portable ground scintillometer "Exploranium® GR-101A" in order to identify area/areas with more prominent radioactive anomalies for further ground spectrometric survey.

ii. Carrying out a ground spectrometric survey of the area identified with higher radiometric anomalies in the scintillometric survey with a Portable Ground

Information System Gamma Ray Spectrometer (PGIS-SP) at grid points along profiles in the area/areas.

iii. Collecting rock samples within the study area for laboratory gamma ray spectrometric analysis.

iv. Processing of the acquired data to produce; contour maps, image maps, ratio maps and ternary image maps of the radio – elements for analysis and interpretation..

v. Analysis and interpretation of the processed spectrometric data and laboratory gamma ray spectrometric results of the rock samples with a view to delineate areas of probable uranium, thorium and potassium mineralization and

vi. Assessing the absorbed dose rate to determine if the rocks of the area are harmful or not to human beings and the environment.

1.4 Scope and Limitation of the Study

This study was limited to ground radiometric investigation to confirm the occurrence or otherwise of uranium, thorium and potassium in the southwestern part of the Kerri - Kerri Formation. While the thickness of the Kerri-Kerri Formation ranges from 200 m to 300 m (Carter *et al*., 1963), the penetration of gamma rays detected from rocks and soils in Radiometrics does not exceed 35 cm. Gamma ray spectrometry is therefore limited to the measurement of gamma rays emitted by the radio-elements uranium, thorium and potassium only from the surface to a depth of 35 cm to 40 cm.

1.5 Location of the Study Area

The area of study lies between latitudes 10^0 $00^{'}$ N and 10^0 07'N and longitudes 11^0 00'E and 11^0 06'E on the topographic map of Gombe Sheet 152 SW. The area is located within the southwest end of the Kerri - Kerri Formation and Gombe Sandstone both of which are

situated in the Upper Benue Trough, Northeastern Nigeria. The study area is situated southwest of Gombe Town and covers an area of about 145 km^2 (Fig. 1.2).

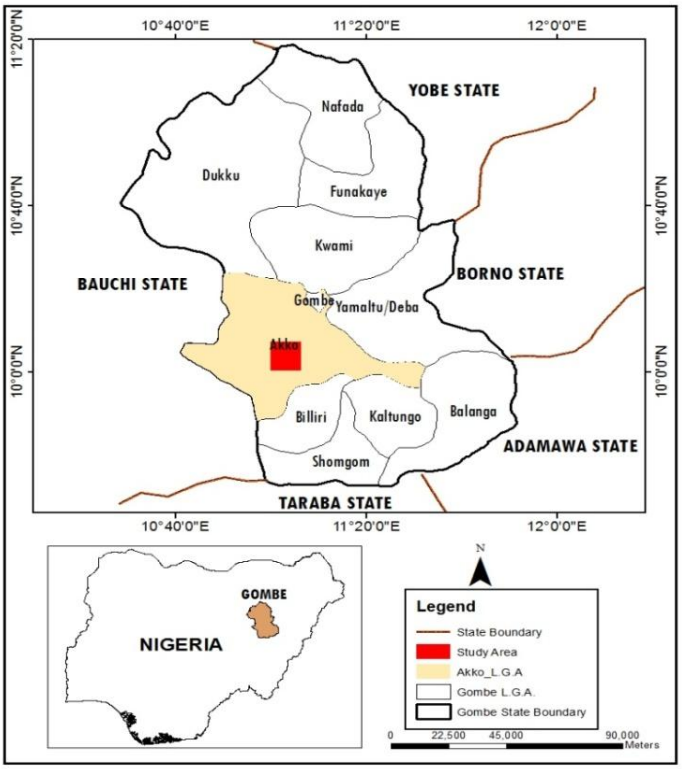


Fig. 1.2: Location of the Study Area in Akko Local Government Area of Gombe State (Derived from Google Earth Satellite Image)

1.6 Geology of the Study Area

The Kerri - Kerri Formation was laid down in a Continental environment ranging from lacustrine to deltaic (Carter *et al.,* 1963) which was derived from the weathering of the basement rocks as well as of Cretaceous sedimentary formations. The formation is an extensive clastic unit outcropping over an area more than 3,000 km^2 - widest in the north and tapering southwards (Olabode *et al.,* 2015). In the western part of the Kerri - Kerri Plateau, the formation overlies the basement complex, but the contact is almost completely masked by abundant alluvial deposits (Carter *et al.,* 1963). The maximum thickness of the Kerri - Kerri Formation ranges from 200 m to 300 m (Carter *et al.,* 1963). The Kerri–Kerri Formation is composed of flat-lying to gently dipping conglomerate, grit, sandstone, siltstone and clay which unconformably overstep the Gombe Sandstone (Carter *et al.,* 1963). The Formation is

characterized by felspathic sediments and the grade of its sandstone is coarser. An increase in sandstone content and coarseness of sand grains at the lower part of the Kerri - Kerri Formation is interpreted as the shallowing of the basin during sediment fill (Odedede and Adaikpoh, 2011). The Kerri - Kerri Formation has not been subjected to folding and has the lowest fracture density of all the formations present in the area. This is probably because it was laid down after the main tectonic phase has occurred, and on the poorly cemented nature of the lithological components of its upper part (Carter *et al.*, 1963).

The heavy mineral suite in the Kerri - Kerri Formation includes: rutile, zircon, kyanite, stauronite, limonite, tremolite, sillimanite, pyroxene, hornblend and tourmaline, which are indicative of derivation from the nearby basement complex and older sedimentary rocks (Adegoke *et al.*, 1986). The rare basal conglomerates, well-bedded siltstones and the presence of shrinkage cracks, clay-supported grits, local channel sandstones and thin horizons of coal and carbonaceous clay suggest a typical fluvial, deltaic and marginal lacustrine environment of deposition (Adegoke *et al.*, 1986).

The lithology of the Kerri - Kerri Formation is basically an alternation of claystones and cross-bedded sandstones suggesting a mix of Lacustrine and deltaic environments (Olabode *et al.*, 2015). The sandstones are characteristically friable, with a grain size that range from medium to coarse, poorly sorted and clayey (Olabode *et al.*, 2015). Exposures in other locations and the numerous boreholes sunk by both the Geological Survey of Nigeria and the Bauchi State Government, established its diversity of facies and depositional environments, including alluvial fans, fan deltas, braided river and marginal marine settings (Dike, 1993).

The stratigraphy (Table 1.1) of the Gongola Basin in the Upper Benue Trough consists of the youngest to the oldest: Alluvium, Kerri - Kerri Formation, Gombe Sandstone, Pindiga Formation, Yolde Formation, Bima Group and the Basement Complex rocks (Odedede and Adaikpoh, 2011).

Table 1.1: Lithostratigraphical Subdivisions for the Gongola Basin (Adapted from: Zaborski *et al.*, 1997 and Haq *et al.*, 1988)

GONGOLA BASIN		AGE		Time Scale (Ma) (Haq et al., 1988)
		PLEISTOCENE		
Kerri-Kerri Formation		PALEOCENE (at least in part)		
Gombe Sandstone		MAASTRICHTIAN		--- 65 --- 70
Pindiga Formation	Fika Member	CAMPANIAN		--- 75
		unconformity		
		SANTONIAN		--- 80
		CONIACIAN		--- 85
	Dunbulwa Gulani/ Daba Fulani Member	Upper	TURONIAN	--- 90 --- 95
		Middle		--- 100
	Kanawa Member	Lower		--- 105
		CENOMANIAN		--- 110 --- 115 --- 120
Yolde Formation				
Bima Group	Upper Bima Formation	ALBIAN		--- 125
	Middle Bima Formation			--- 130
	Lower Bima Formation	APTIAN		--- 135
		PRE-APTIAN		--- 140 --- 145
Crystalline Basement		PRECAMBRIAN		

Alluvium includes most soils and comprises those deposits formed in - situ by the chemical and physical decomposition of the bedrocks which are generally poorly developed over the arenaceous member of the Cretaceous Formation (Carter *et al.,* 1963). The extent of alluvium cover increases westwards but it can be estimated that 10 % of the Gombe Sandstone is covered by alluvium (Carter *et al.,* 1963).

The Gombe Sandstone is a continental sequence of sandstone, shale, siltstones and ironstones, with maximum thickness of 300 m and its sequence can be divided into two parts; the upper 223 m mainly consists of sandstones while the rest of the lower part consists of shales containing ironstone layers (Carter *et al.,* 1963). Siltstones and flaggy sandstones form the greater part of the Gombe Sandstone. The rocks are soft and light grey in colour when

fresh, but on exposure give rise to dark red, flaggy debris which characteristically mantles the Gombe Sandstone hill (Carter *et al.,* 1963).

The Gombe Sandstone outcrops in the southern end, southeast, southwest and northwest of the study area where it conformably lies on shale and limestone of the Pindiga Formation and is unconformably covered by the Kerri - Kerri Formation. Sedimentary structures encountered in the Gombe Sandstone include parallel bedding, internal lamination, and biogenic structures; dwelling traces of skolithos while planar cross bedded structures are exhibited by the Kerri - Kerri Formation (Odedede and Adaikpoh, 2011). According to Zaborski *et al.* (1997), the bedded facies of the Gombe Sandstone was laid down in shallow, quiet, perhaps Hyposaline Sea.

The Pindiga Formation conformably overlies the Yolde Formation. The Pindiga Formation consists of a series of marine, blue-black shale with interblended fossilferous limestone at the base (Carter *et al.,* 1963).

The Yolde Formation conformably overlies the massive coarse sandstones of the Bima Formation (Aptian - Cenomanian) and is conformably bounded at the top by the marine shale of the Pindiga Formation.

The Bima Formation is the oldest, most extensive and thickest of the Cretaceous sedimentary formations in the Upper Benue Trough (Carter *et al.,* 1963). The Bima Formation rests unconformably on the Precambrian Basement Complex. The Bima Formation consists of yellow-brown, massive cross-bedded felspathic sandstones, with some white saccharoid sandstones, ferruginous sandstones and pebble bands (Carter *et al.,* 1963).

The basement complex includes all the Pre-Mesozoic rocks and is thus the oldest rock of the Nigerian Stratigraphic Series (Carter *et al.,* 1963). It is composed mainly of granites, gneisses and migmatites with subordinate basic rocks. Fig. 1.3 is the geologic map of the study area.

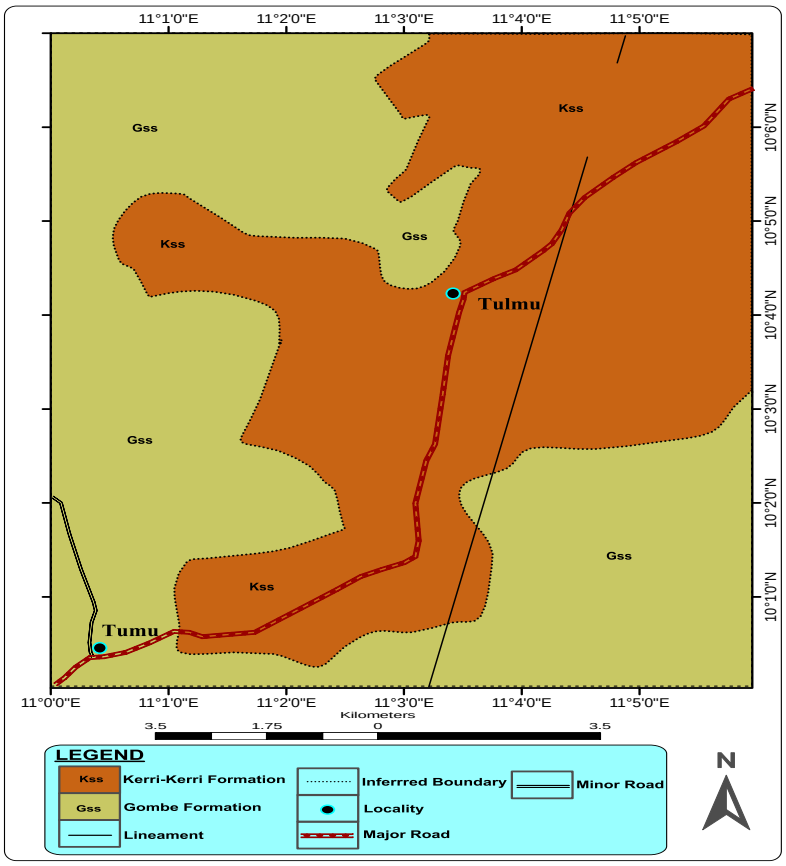


Fig. 1.3: Geologic Map of the Study Area (Source: NGSA, 2004, 2006)

1.7 Vegetation and Climate of the Study Area

Vegetation in Gombe State is Guinea Savannah grassland with concentration of woodland in the southeast and southwest. The central part is predominantly wooded shrub land while the northern part of the state exhibits a mosaic of shrubbed grassland and with the preponderance of Acacia (OnlineNigeria.com., 2015).

The climatic conditions in Gombe as the case in northeastern part of Nigeria exhibit only two different seasons, namely, a short wet season and a prolonged dry season. Temperatures during the day remain constantly high while humidity is relatively low throughout the year, with little or no cloud cover. There are, however, wide diurnal ranges in temperature (between nights and days) particularly in the very hot months. The mean monthly temperatures during the day exceed 30 °C while the mean monthly temperatures at night fall, at most times, to below 22 °C (OnlineNigeria.com., 2015). The long dry season extends from

October to mid - May while the wet season covers a relatively short period, from June to September.

1.8 Relief and Drainage of the Study Area

Gombe State is part of the central Nigeria highlands; but the flat landscape in the northern and southern parts of the state have isolated hills. While the elevation of the plain is at about 600 m above sea level, the hills reach between 700 m and 800 m (OnlineNigeria.com., 2015). The topography is mainly mountainous, undulating and hilly to the southeast and flat open plains in the central, north and northeast, west and northwest.

The Gongola River is the main drainage system, running approximately north to south towards the Benue River Basin, but with principal tributataries draining from west to east into River Gongola (OnlineNigeria.com., 2015). The streams in the study area (Fig. 1.4) are seasonal.

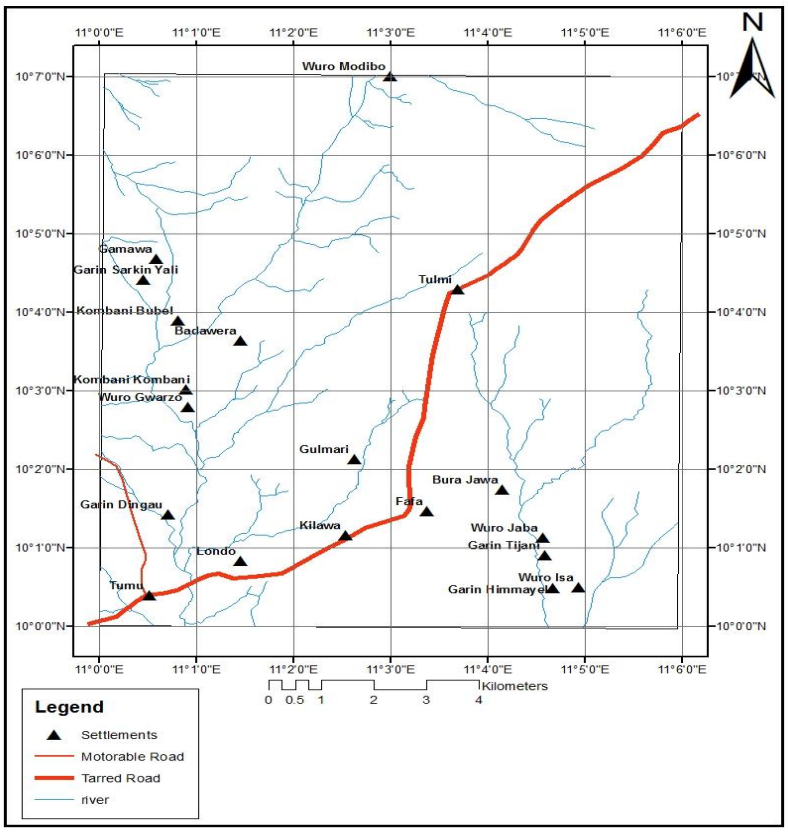


Fig.1.4: Drainage Pattern of the Study Area (Derived from Google Earth Satellite Image)

CHAPTER TWO

LITERATURE REVIEW

2.1 Basic Principles of Radiometrics

Radiometrics or Gamma ray spectrometry is a geophysical method used to estimate the concentrations of the radio-elements; potassium, uranium and thorium by measuring the gamma rays emitted by the radioactive isotopes of these elements during radioactive decay.

Potassium (K^{40}), Uranium (U^{235}, U^{238}) and Thorium (Th^{232}) are the three principal natural radioactive elements of the earth's crust. The most abundant of the three is K^{40}, found mainly in feldspar, mica, leucites and nepheline (Galbraith and Saunders, 1983). These radio - elements are contained in most crustal rocks in at least trace quantities. The natural radiation pattern at the surface of the earth originates mainly from the decay of potassium and the radioactive decay products of uranium and thorium.

While many naturally occurring elements have radioactive isotopes, only potassium, uranium and thorium decay series have radioisotopes that produce gamma rays of sufficient energy and intensity to be measured by gamma ray spectrometry (IAEA, 2003). Average crustal abundances of these elements quoted in literature are in the range of 2 - 2.5% Potassium (K), 2 - 3 ppm Uranium (U) and 8 - 12 ppm Thorium (Th) (IAEA, 2003).

Potassium (K^{40}) is the radioactive isotope of potassium, and occurs as 0.012% of natural potassium which decays to Ar^{40} with the emission of gamma rays with energy 1.46 MeV (IAEA, 2003). Since K^{40} occurs as a fixed proportion of K in the natural environment, these gamma rays can be used to estimate the total amount of K present. The half - life of K^{40} is 1.3 x 10^9 years.

Uranium occurs naturally as the radioisotopes U^{238} and U^{235} which give rise to the decay series that terminate in the stable isotopes of Pb^{206} and Pb^{207} respectively. The half-lives of U^{238} and U^{235} are respectively 4.46 x 10^9 and 7.13 x 10^8 years. Thorium occurs naturally as

the radioisotope Th^{232} which gives rise to a decay series that terminates in the stable isotope Pb^{208}. The half - life of Th^{232} is 1.39×10^{10} years. The gamma rays emitted by the radioactive daughter products U^{238} and Th^{232} are used to estimate their concentrations (IAEA, 2003). Each gamma ray photon has a discreet energy, and this energy is characteristic of the source isotope. This forms the basis of gamma ray spectrometry; by measuring the energies of gamma ray photons, we can determine the source of the radiation (IAEA, 2003).

In other geologic materials, gamma radiation specific to uranium, thorium and potassium may be necessary to distinguish rock types or environmental concerns (Stanley, 1990). In areas of few outcrops, the surface material must be reasonably representative of the underlying bedrock and must be either residual or locally derived before gamma ray spectrometry can be applied successfully (Ahmed, 1998). The usefulness of radioactivity surveys for geologic mapping will therefore vary from place to place depending upon the nature of the overburden.

All rocks and soils contain radioactive isotopes, and almost all the gamma rays detected near the surface of the earth are the result of the natural radioactive decay of potassium, uranium and thorium. Gamma rays are packets of electromagnetic radiation characterized by their high frequency and energy. Each of the radioisotopes emits gamma - radiation of characteristic energy and the gamma ray spectrum of a rock exhibits peaks of varying intensities corresponding to these characteristic energies (Uwah, 1984). It is therefore possible to relate measurements of intensity in three selected regions of the spectrum to the K, U and Th content of the rock.

Gamma ray spectroscopy has many applications but is primarily used as a geologic mapping tool. Changes in lithology, or soil type, are often accompanied by changes in the concentrations of the radio - elements. The method is capable of directly detecting mineral deposits. Potassium alteration, which is often associated with hydrothermal ore deposits, can

be detected using the gamma ray spectrometric method. It is also used for uranium and thorium exploration, heat flow studies and environmental mapping.

The Radiometrics technique most useful in the detection and assessment of radio-element resources is Gamma ray spectrometry (Morce, 1977). Gamma ray spectrometry is effective as a mapping tool in the geologic environment and in the location and characterization of radioactive environmental contamination (Ahmed, 1998). Concentrations of uranium, thorium and potassium vary sympathetically in many geologic materials. However, selective concentrations or depletion of each of these elements occur in certain geologic materials, the total gamma radiation arising from the uranium, thorium and potassium radioactive decay process is sufficient as an indication of rock type (Ahmed, 1998).

Only a limited number of isotopes of natural elements emit gamma rays; and among these, there are only three which are common enough within earth materials to make them geologically useful (Urquhart, 2009). These three are Bi^{214}, Ti^{208}, and K^{40}. Bi^{214} comes from the decay of U^{238} and is, therefore, an indication of the concentration of uranium in the earth materials that lie within the range of the detector. Ti^{208} comes from the decay of Th^{232} and is an indicator of thorium content while K^{40} is one of the minor natural isotopes of potassium and the only isotope of K that is radioactive (Urquhart, 2009). It makes up only 0.012% of the total potassium in rocks and soils, but because this fraction remains constant, even during weathering and metamorphism, the gamma radiation from it is a good indicator of changes in the amount of potassium in rocks (Urquhart, 2009).

Gamma rays are defined by their energies, measured in electron volts (eV), (Urquhart, 2009). The Gamma rays from Ti^{208}, the Th indicator, have energy of 2.62 MeV. The Gamma rays from Bi^{214} have energy of 1.76 MeV; while those from K^{40} have energy of 1.46 MeV (Urquhart, 2009). All three of these energies are constant; they never change, they therefore constitute well defined peaks in the energy spectrum emanating from rocks (Urquhart, 2009).

Thus, in principle, if gamma ray spectra over different regions of exposed rock are measured and compared then changes in the heights of the 1.46, 1.76 and 2.62 MeV peaks can be translated into corresponding variations in the concentrations of potassium, uranium and thorium within different rocks (Urquhart, 2009).

2.2 Gamma Ray Spectrometry

The most useful radiometric technique in the detection and assessment of radioactive elements is the gamma ray spectrometry (Ahmed, 1998). It involves the detection of gamma rays of varying intensities by scintillation or solid state detectors. The scintillations are amplified, sorted out and stored as energy by single channel or multichannel height analyzers. The spectral data can then be treated by computers to yield abundances of the individual radio - elements.

There are three major categories of Gamma ray spectrometry, namely, threshold (integral), multichannel and window (Darnley, 1973). Multichannel spectrometry involves obtaining count rates from the full spectrum in a series of discrete steps or channels. Threshold spectrometry involves summing the counts from the spectrum in a series overlapping steps by varying the energy threshold at which counting commence. For example, threshold of 1.36, 1.66 and 2.42 MeV could be used respectively to measure the sums K + U + Th, U + Th and Th alone respectively.

"Window spectrometry", which is the most commonly used in most airborne and ground surveys and laboratory analyses (Grasty, 1975) involves measuring the count rates only from portions of the spectrum encompassing the photo peaks of interest. Typical window settings adopted in most "window spectrometry" and as recommended by IAEA (1979) are shown in Table 2.1.

Table 2.1: International Atomic Energy Agency (IAEA) Recommended Energy Windows

Element	Radionuclide	Energy (MeV)	Window Energy (KeV)
Potassium	^{40}K	1.461	1370 – 1570
Uranium	^{214}Bi	1.764	1660 – 1860
Thorium	^{208}Ti	2.615	2410 – 2810
Total			410 - 2810

2.3 Decay Chain Series of Uranium, Potassium and Thorium

Radioactivity is a spontaneous and self - destructive nuclear activity leading to the break - up of the element. It is spontaneous in the sense that it is intrinsic and is unaffected by external agents, either physical or chemical. All radioactive substances in nature undergo this disintegration / decaying process emitting three distinct types of radioactive rays and resulting in the formation of new elements.

The decay chain refers to the radioactive decay of different discrete radioactive decay products as a chained series of transformations. Most radioactive elements do not decay directly to a stable state, but rather undergo a series of decays until eventually a stable isotope is reached.

Decay stages are referred to by their relationship to previous or subsequent stages. A parent isotope is one that undergoes decay to form a daughter isotope. The daughter isotope may be stable or it may also decay to form a daughter isotope of its own. The daughter of a daughter isotope is sometimes called a granddaughter isotope. Natural radioactivity is confined principally to the disintegration products of Potassium (K), Uranium (U) and Thorium (Th). In addition to these include: rubidium (Rb) and the rare earth elements samarium (Sm) and lutecium (Lu).

While potassium undergoes a simple form of radioactive decay, the decay of uranium and thorium are complex and proceeds sequentially along a chain of disintegration. Each of the particles emitted during radioactive decay has its own characteristics and the emitted gamma rays are characteristics of the elements which emit them. Natural sources of gamma radiation

in rocks originate from the decay of radioactive products in the uranium and thorium decay chains and the decay of potassium. The decay chains series of U^{238}, U^{235}, Th^{232} and some of the gamma rays emitted by their daughters are given in Tables 2.2, 2.3 and 2.4 respectively.

Table 2.2: The U^{238} decay chain series (After Evans, 1955)

	Name of Isotope	Nuclide	Particle Emitted	Half- life	Particle Energy (MeV)
URANIUM GROUP	Uranium	U^{238}	α	4.507×10^9 y	4.200
	Thorium	Th^{234}	β	24.1 d	0.190
	Protactinium	Pa^{234}	β	1.18 m	*0.074*
	Uranium	U^{234}	α	2.48×10^5 y	4.770
	Thorium	Th^{230}	α	7.52×10^4 y	4.680
RADIUM GROUP	Radium	Ra^{226}	α	1600 y	4.780
	Radon	Rn^{222}	α	3.825 d	5.490
	Polonium	Po^{218}	α	3.05 m	5.000
	Lead	Pb^{214}	β	26.8 m	1.030
	Bismuth	Bi^{214}	β	19.7 m	3.260
	Polonium	Po^{214}	α	1.58×10^{-4} s	7.680
	Lead	Pb^{210}	β	22.3 y	0.061
	Bismuth	Bi^{210}	β	5.02 d	1.160
	Polonium	Po^{210}	α	138.4 d	5.300
	Lead	Pb^{206}	Stable	--	--

Table 2.3: Decay chain series of U^{235} (After Evans, 1955)

Name of Isotope	Nuclide	Particle Emitted	Half- life	Particle Energy (MeV)
Uranium	U^{235}	α	7×10^8 y	4.180 - 4.560
Thorium	Th^{231}	β	25.6 h	0.300
Protactinium	Pa^{231}	α	3.4×10^4 y	4.660 - 5.046
Actinium	Ac^{227}	α	22 y	4.940
Thorium	Th^{227}	α	18.2 d	5.708
Francium	Fr^{223}	β	22 m	1.500
Radium	Ra^{223}	α	11.43 d	5.979
Radon	Rn^{219}	α	3.9 s	6.547
Polonium	Po^{215}	α	1.8×10^{-3} s	7.360
Lead	Pb^{211}	β	36 m	0.500
Bismuth	Bi^{211}	α	2.16 m	6.617
Polonium	Po^{211}	α	9.52 s	6.570
Thallium	Tl^{207}	β	4.79 m	1.440
Lead	Pb^{207}	Stable	--	--

Table 2.4: The Th^{232} decay chain series (After Evans, 1955)

Name of Isotope	Nuclide	Particle Emitted	Half- life	Particle Energy (MeV)
Thorium	Th^{232}	α	$1.4x10^{10}$ y	4.010
Radium	Ra^{228}	β	6.7 y	0.053
Actinium	Ac^{228}	β	6.13 h	2.110
Radothorium	Th^{228}	α	1.91 y	5.430
Radium	Ra^{224}	α	3.64 d	5.680 - 6.290
Radon	Rn^{220}	α	55.3 s	6.780
Polonium	Po^{216}	α	0.168 s	0.580
Lead	Pb^{212}	β	11 h	0.299
Bismuth	Bi^{212}	β	61 m	2.250
Polonium	Po^{212}	α	$3.04x10^{-7}$ s	8.780
Thallium	Tl^{208}	β	3.1 m	1.800
Lead	Pb^{208}	Stable	--	--

Each of the radioisotopes emits gamma radiation of characteristic energy and the gamma ray spectrum of a rock exhibits peaks of varying intensities corresponding to these characteristic energies (Fig. 2.1). It is therefore possible to relate measurement of intensity in three selected regions of the spectrum to the K, U, and Th content of a rock.

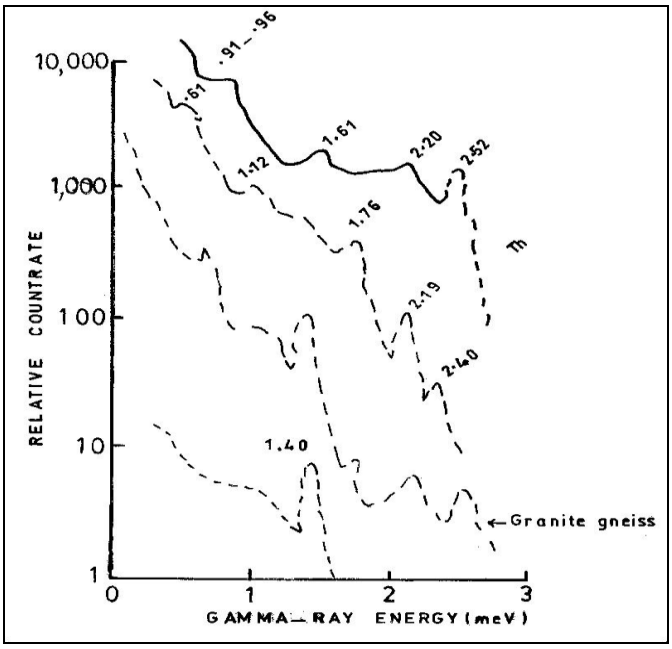


Fig. 2.1: Spectograms obtained from U, K and Th samples on granite outcrop (After Doig, 1968)

About 11 % of natural K^{40} which itself is only about 0.012 % of the natural potassium decays by electron capture to Ar^{40} yielding gamma rays of energy 1.46 MeV (Doig, 1968). Gamma

rays with this energy are used in gamma ray spectrometry to detect and measure natural potassium in crustal rocks. Due to the relative low abundance (0.012 %) of K^{40} in natural K, the intensities of the 1.46 MeV gamma rays are low (Doig, 1968) as shown in (Fig. 2.1).

Each of the decay chains of the U^{235} and U^{238} has an intermediate nuclide of atomic number 86, which is a gas under normal condition decaying by α emission to solid daughter radium (Doig, 1968). These are Rn^{222} in U^{238} and Rn^{219} in U^{235}. The most promising radiation characteristic is that of Ra^{234} which has energy of 0.001 MeV but this is present at a very low intensity (Doig, 1968). Of particular importance in gamma ray spectrometry is the decay of Bi^{214} to Po^{214} in the U^{238} series. This decay yields several gamma rays of various energies (Table 2.1). In most in - situ and laboratory determinations of uranium in crustal rocks, the 1.76 MeV gamma rays emitted by the beta decay of Bi^{214} to Po^{214} are normally used. The 1.76 MeV peak in the natural rock spectrum though of relatively low intensity is pronounced and has minimum interference from other rays (Doig, 1968).

The combination of the 1.76 and 1.12 MeV gamma rays emitted by Bi^{214} has been used for uranium measurements (Uwah, 1984). A method using the 1.001 MeV gamma rays emitted by Th^{234} of the U^{238} series by its β-decay to Pa^{234} for uranium determination in uranium ores has been described in Kehinde *et al. (*1983). Crossley and Reid (1982) have also described a method of using the whole gamma ray spectrum of a given rock sample to determine its uranium concentration.

The decay chain of thorium is complex as shown in Table 2.3. Thorium is mono isotopic consisting of Th^{232}. Of particular interest in gamma ray spectrometry is the decay of Tl^{208} to Pb^{208} by β - emission. This decay results in the emission of 2.62 MeV gamma rays. The 2.62 MeV peak in the natural rock spectrum is pronounced and free from interference (Fig. 2.1) and is therefore considered as the most suitable for thorium concentration measurements in geologic samples using gamma ray spectrometry. The gamma rays from U and K do not have

sufficient energy to be observed in the Th channel, and for this reason the intensity is proportional to the Th content. The U channel records gamma rays from U and Th, but the potassium channel has no effect on this channel. It is the K channel that records gamma rays from the K channel and from the series of U and Th channels.

2.4 Radioactive Equilibrium / Disequilibrium

As explained in Section 2.3, the process of successive disintegration of a radioactive substance continues until a stable end product is formed. But when the parent source and the daughter products in a sequence are radioactive, the growth of successive daughter products, their emission and their activity levels becomes very complex. At the initial stage, the successive product growth is a function of the decay of the parent.

When a radioisotope decays, producing a radioactive element whose half - life is shorter than that of its parent, a condition of radioactive equilibrium will eventually be attained in which the daughter product is decaying as rapidly as it is being produced (Dewu, 1986). The decay of U^{238} to its stable daughter, Pb^{206} and Th^{232} to Pb^{207} involves nineteen (19) and eleven (11) daughter elements respectively. If none of these daughter elements is removed out of the series, sometimes after the formation of a uranium or thorium bearing crystal, a state of equilibrium is reached whereby the loss of a daughter element due to its decay is made up by the decay of the preceding parent element. This occurs where the half - life of the parent element is much larger than that of the daughter element. If one of the daughter elements is taken out of the system, however, disequilibrium is established and the nuclides above the one, which has been lost, become proportionally more enriched in the series. Similarly, the nuclides developed from the decay of the lost daughter elements are depleted in the series. If the nuclide, which has been lost, has a short half–life, then equilibrium is restored within a short time. On the other hand, the loss of a nuclide with a long half - life will mean that the series takes a long time to regain equilibrium. Due to the exponential character of radioactive

decay, the nuclides in a decay series approach their equilibrium values asymptotically so that 100 % equilibrium is never achieved (Dewu, 1989).

In a decay series containing nuclides of varying half - lives and where the series are headed by parents of long half–life, disequilibrium between the daughter elements and their parents is better described by secular equilibrium. In this case, the daughter elements can attain 99 % equilibrium with their parents and situations are usually quoted for 95 % or 99 % equilibrium. U^{238} decay series contains a number of daughter elements with very long half-lives of 4.5 x 10^5 years, 8 x10^5 years and 1622 years respectively so that it will take approximately 10^6 years for the U^{238} series to attain equilibrium. Thus a loss of U^{234} from the series means that a period of not less than 10^6 years will be required before 99 % equilibrium between the members in the series is restored.

In the Th^{232} decay series, however, the longest lived daughter element, Ra^{228}, has a half - life of just 6.7 years so that equilibrium is restored within a relatively short period of time should a member be lost from the decay series. This makes the assumption of secular equilibrium in the Th^{232} decay series safer than for the U^{238} series (Dewu, 1989).

Disequilibrium is a serious problem in the use of simple gamma ray spectrometers for U and Th determinations because both analyses are based on daughter elements which are far down the decay series. To obtain correct abundances require the existence of equilibrium between the daughter elements and parents; Bi^{214} with U^{238} and Ti^{208} with Th^{232}. In the Th^{232} decay series, this requirement is however largely met in natural environments because of the relatively short half - lives of the members in the series, the longest being Ra^{228} ($t_{1/2}$ = 6.7 years) which attain 99 % equilibrium in less than 45 years (Dewu, 1989). The U^{238} series, however contains a number of very long - lived daughter elements (U^{234}, Th^{230}, Ra^{226}), and a loss of any one of these will mean a much longer period is needed for re - establishment of equilibrium. Of serious concern is the half - life of its gaseous daughter element, Ra^{222} ($t_{1/2}$ =

3.8 days) which is sufficiently long for it to be transported to considerable distances away from its parent (Dewu, 1989).

U^{238} has also been found separated from its other daughter elements in natural environment apart from U^{238} and U^{234} fractionation (Ahmed, 1998). Of importance in disequilibrium studies are the relationship with and between Ra^{226}, Pa^{231}, Rn^{222}, Pb^{210} and Po^{210}. Whereas fractionation between U^{234} and U^{238} may be due to physical processes, fractionation between U^{238} and its other daughters is better explained by the difference in chemical properties. Radium in particular has been found to be more soluble in water than either U or Th and can thus be removed by moving water from the site of its deposit. Titayeva *et al. (*1973) reported excess Ra^{226} over Th^{230} and U^{238} in solids and sediments. This was attributed to either the deposition of Ra^{226} as absorbed ions into clay minerals and organic matter, or preferential leaching of U^{238}. Ra^{226} is also associated with oil field brines and deposits from hot springs (Rosholt, 1959). Chemical fractionation preferentially enriching Pa^{231} relative to Th^{230} in Mn modules has also been reported by (Gascoyne, 1977). High Pa^{231} in high grade black, U mineral was reported by Rosholt (1959).

Rn isotopes, being gases are easily removed from members in the decay series and may be the most important cause of disequilibrium in the U^{238} decay series in environments favourable to Rn diffusion. Rn is also soluble in water and can therefore be transported in aqueous solution. Also, Rn loss can produce artificial disequilibrium during sample preparation for U analysis (Dewu, 1989).

Methods to determine the existence of equilibrium in the U - decay series from gamma spectrometric data and chemical analysis have been suggested. Comparison of the results of chemical analysis and the determination of equivalent Uranium (eU) from gamma spectrometry is one of such methods (Dewu, 1989).

2.5 Secular Equilibrium

If a radioactive nuclide decays to many daughter products to form a series such that the decay constants of the daughters are represented by $\lambda_1, \lambda_2, \lambda_3 \ldots \lambda_n$, the activity of the nth member of the series at a time t is given by the equation

$$C_n = \lambda_n N_0 \left[\frac{1}{(\lambda_2 - \lambda_1)(\lambda_3 - \lambda_1) \ldots (\lambda_n - \lambda_1)(e^{-\lambda_1 t})} + \frac{1}{(\lambda_1 - \lambda_2)(\lambda_3 - \lambda_2) \ldots (\lambda_n - \lambda_2)(e^{-\lambda_2 t})} + \cdots \cdots \cdots \cdots \cdots \cdots \cdots \frac{1}{(\lambda_1 - \lambda_n)(\lambda_2 - \lambda_n) \ldots (\lambda_{n-1} - \lambda_n)(e^{-\lambda_n t})} \right] \ldots \ldots \ldots \ldots \ldots \ldots \ldots \ldots 2.4$$

Where N_0 is the number of atoms of the parent nuclide at time t = 0 (Evans, 1955). Equation 2.4 assumes that the activity of the n^{th} nuclide at t = 0, is zero, and also as $t \rightarrow \infty$, the activity is zero (Fig. 2.2). Fig. 2.2 also shows that the maximum activity for a particular daughter occurs when its activity is equal to that of its immediate parent (Evans, 1955). Where the activities of all members of the series are equal, the ratios of the activities are unity.

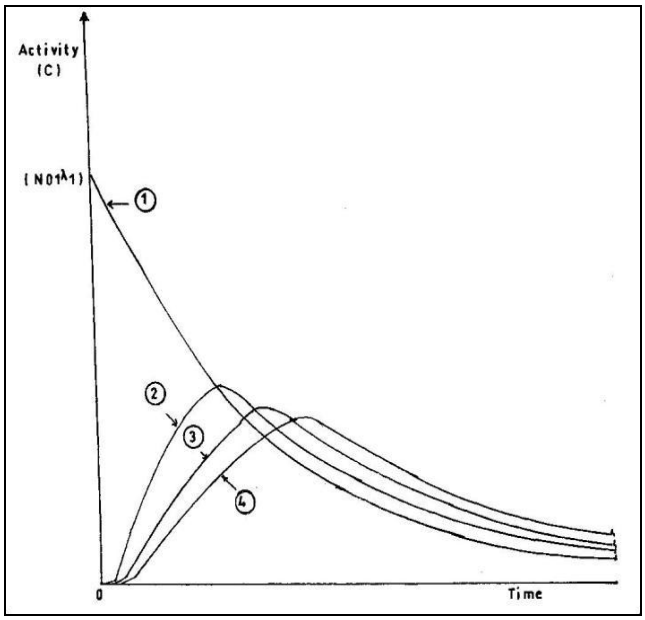


Fig. 2.2: Variations as a function of time of four successive members of decay series. (Adapted from Evans, 1955)

The situation where the rates of decay of all members of a radioactive series are equal is described as secular equilibrium. The radioactive atoms (for example U^{238}) at this point are said to be in secular equilibrium with its disintegration products. Since the activity of any members of a series in equilibrium is equal to that of the parent nuclide, the activity of one of

the daughters can be measured by monitoring the particle or photon it emits provided interference from other daughters and other external sources are checked.

Since the time t (i.e. the length of time between the time of deposition of a mineral and the time of observation) must be higher than the half - lives of the daughter products, then the time t_0 to reach equilibrium will be determined by the half - life of the longest lived daughter of the series. That is, U^{234} ($t_{1/2}$ = 24500 years) in the U^{238} series and Ra^{228} ($t_{1/2}$ = 5.75 years) (Uwah, 1984). Thus while a pure Th source will reach equilibrium in approximately 50 years, a U source requires up to 2 x 10^6 years to reach equilibrium.

Since Th^{232} reaches secular equilibrium in about 50 years, it is often assumed that for most geological samples, the Th decay series will be in equilibrium and the equivalent thorium (eTh), i.e., the amount of Th that would be present if secular equilibrium was established is equal to the Th concentration (Dickson *et al.,* 1982). However Ra^{228} which is the immediate daughter of Th^{232} has been found separated from Th^{232} because of mobility of radium in ground water (Dickson et al., 1982). Then rocks in contact with ground water may have lost Ra^{228} and $Ra^{224}$and Th will not be in equilibrium. This is why Th analysis by gamma ray spectrometry is always reported as eTh.

The U^{238} decay series contains a number of daughters with very long half - lives. U^{234}, Th^{230} and Ra^{226}, which are members in this series, have half - lives of 4.5 x 10^5 years, 8 x 10^6 years and 1622 years respectively so that it will take approximately 10^6 years for the U^{238} series to attain secular equilibrium. Rn^{222}, which is a decay product of Ra^{226} of the U^{238} series, is a gas. It can easily be separated from the parent nuclides. Gamma ray spectrometric analysis of uranium are therefore always reported as gamma equivalent uranium (eU) since they are considered as measuring Ra^{226} content of the analyzed sample (Dickson *et al.,* 1982).

The need to assume secular equilibrium in a four channel gamma ray spectrometry is a problem in the use of the method for uranium exploration (Ahmed, 1998). This is because

several physical and chemical factors cause disequilibrium to occur especially in the uranium decay series as described above.

2.6 Cosmic Rays and Background Corrections

It is unfortunate that nature is not cooperative because not all the gamma rays with energies of 1.76 MeV come from Bi^{214}, nor do all the energies of 1.46 MeV come from K^{40}. This gives rise to a general increase in the gamma ray count measured. There is therefore the need to measure, not the absolute value of the peaks of the gamma ray counts spectrum, but their value relative to the general background which may vary from one region to another.

The most important cause of the rise in background activity towards the lower energies is Compton scattering.

Compton scattering occurs because, when a gamma ray collides with an electron it gives the electron some of its energy, somewhat like a cue ball in billiards slowing down after it strikes another ball. Extending this analogy, the gamma ray is deflected from its path, like the cue ball, and moves away in a different direction with lower energy, hence the gamma ray will have a lower frequency. Energy is invariably lost by scattering. Millions of gamma rays starting out with well defined energies will, after making numerous collisions, from a continuum of energies with a steady rising proportion falling towards lower energy levels. Compton scattering thus accounts for the general shape of the gamma ray spectrum, whose rising background trend towards lower energies is usually called the "Compton continuum".

There are other non - geologic sources of gamma radiation which contribute to the Compton continuum. Cosmic rays are the most important of these other sources. Charged particles from outer space collide with nuclei in the earth's atmosphere and produce high energy gamma rays (3 - 6 MeV) which in turn are converted to lower energies by Compton scattering. Thus, gamma rays resulting from cosmic ray bombardment constitute a source of background noise in radiometric surveys that affects all parts of the spectrum. This noise is

generally less severe towards the lower latitudes because of the shielding effect of the earth's magnetic field. It becomes more intense with increasing altitude, although it is discernible at normal surveying elevations.

A further source of non - geologic gamma radiation is atmospheric radiation (i.e. radon gas). In company with dust particles containing K^{40} and other radio - isotopes, it occurs in layers or clouds, particularly when there is little or no wind to disperse it, at heights of up to 300 m or more above the ground. Because the radiation from these sources is indistinguishable from geologic radioactivity, special measures have to be taken to correct for this effect.

"Background" refers to the general background count rate that prevails in each channel, or spectral window, that is due to non - geologic sources, primarily atmospheric radon and cosmic rays. Cosmic radiation tends to remain fairly constant over short periods of time. During an aero - radiometric survey it can be monitored at the beginning and end of each line, or flight, by climbing to an altitude of 300 m or more where the geologic contribution to the count rate is effectively zero, or by flying over a lake where the water shields the sensor from geologic radiation. In ground radiometric surveys, it is monitored by taking count readings in the middle of a large pond or a river at the beginning (i.e. in the morning) and end (i.e. in the evening) of a survey. In the absence of a river/large pond near the survey area, total count readings can be taken in an area with thick vegetation.

A superior method of monitoring the background in air - borne radiometric survey uses crystals that are shielded from radiation coming from below the aircraft. These "upward looking crystals" detect only the gamma rays which originate from cosmic or spatially variable atmospheric background. This provides a method of continuously monitoring the background during the survey and thus, in principle, could permit corrections to be made for it in real time.

2.7 Uranium Minerals Associated with Common Rocks

An ore mineral can be defined as "a mineral which may be used for the extraction of one or more metals" (Robert, 1954). A Uranium ore mineral is therefore a mineral possessing such physical and chemical properties and occurring in a deposit in such concentrations that it may be used for the profitable extraction of uranium, either alone or together with one or more other metals. There are only a few of the many uranium minerals that meet these qualifications and still fewer in which uranium is the major constituent. Pitchblende and Uraninite contain theoretically up to 85 % uranium but actually between 50 and 80 % (Robert, 1954) while Carnotite, torbernite, tyuyamunite, autunite, uranophane, and brannerite, contain 45 to 60 %.

In other minerals such as davidite, samarskite, and euxenite, uranium is an important but relatively minor constituent mineral which contain only 1 to 18 % (Robert, 1954). Majority of uranium bearing minerals, however, contains uranium in small or trace amounts as an accessory to other major constituents. The uranium content of a mineral does not of itself, however, determine whether it is a uranium ore mineral. If the uranium is present in a mineral in such complex combinations with other elements that it is too costly to extract, or, if the mineral does not occur in sufficient quantities to make extraction worthwhile, that mineral is not a uranium ore mineral (Robert, 1954). Thus, the definition for an ore mineral, like that for an ore deposit, is dependent upon economics and time, upon the value of uranium and the results of future exploration and metallurgical progress (Robert, 1954). A uranium mineral that is not an ore mineral today may be one tomorrow.

Most of the uranium minerals in pegmatites and placers are refractory; that is, the uranium is present in combinations which are extremely difficult to break down chemically in order to recover the uranium (Robert, 1954). These minerals also usually occur scattered sparsely throughout the deposit so that recovery is difficult and expensive. Therefore, even though

some of the individual minerals may contain up to 50 % uranium, they are not uranium ore minerals (Robert, 1954).

The fact that only a few of the numerous uranium minerals qualify as uranium ore minerals and form uranium ore deposits, uranium in small amount is widely spread throughout the rocks of the earth's crust, which adds greatly to the problem of uranium exploration (Robert, 1954). The uranium prospector gets many "nibbles" but few "bites," and to avoid disillusion and frustration, as well as waste of time, effort, and money, he must know his business well. This is one of the most important factors in searching for uranium, as it is for other metals; the ability to judge the importance of what is found and whether to discard it or follow it up. In this respect, it is of paramount importance to be familiar with the uranium ore minerals.

Uranium is an Oxyphile element occurring in minerals of varying degree of chemical complexity especially in association with the more acidic rocks of the lithosphere (Robert, 1954). Thus certain granites, such as the albite riebeckite granite of the Kaffo valley in Northern Nigeria and the Conway granites of the New Hampshire contain 10 - 12 ppm uranium while normal granites contain about four times as much uranium as in basic igneous rocks (Ahmed, 1998). As far as uranium deposits are concerned, this is rather only of academic interest except in special circumstances (Ahmed, 1998). Concentrations of the order of 1000 ppm are necessary to enable uranium to be produced for commercial quantity (Ahmed, 1998). The knowledge of the natural processes that resulted in uranium being localized in deposits is therefore of fundamental importance.

Pure uranium element does not exist in nature, but it is found as a variety of ores in association with other elements (Hayashi, 1970; Roberts *et al.*, 1974). The chief uranium mineral is the oxide uraninite (pitchblende, (UO_2 or U_3O_8). It occurs mainly in hydrothermal vein deposits, bedded sedimentary rocks, pegmatites and in smaller amounts in a large variety of environments in many parts of the world (Roberts *et al.,* 1974). The ore is always

contaminated by rare earth elements, for example, cerium, thorium, and lead (Wooley, 1978). Other primary uranium ores in terms of economic importance include: davidite, autunite, torbenite, brannerite and coffinite (Roberts *et al.*, 1974).

The classification of uranium deposits just like any other ore deposit is difficult in that it requires an interplay of genetic, geometric, mineralogical, petrographic, tectonic and chemical factors, some of which may be conflicting (Bowie, 1970). The classification shown in Table 2.5 is an attempt to reconcile these numerous factors so that their similarities may be emphasized (Bowie, 1970).

Table 2.5: Types of Important Uranium Deposits (Adapted from Bowie, 1970).

Type of Deposit	Characteristic Element	Characteristic Mineral
Igneous and Metamorphic	Nb, U, Th, Cu, Pl, Ti, Zr	Uranothorianite, Pyrochlore, Betarite, Peroskite, Nicolite, Chalcopyrite, Ilmenite, Apatite and Zircon
Peralkaline Syenites	U, Th, Cu, Pl, Ti, Zr	As in above
Pegmatitic	Th, U, Mo, Nb	Uraninite, Uranothorite, Molybderite, Betafite, Allanite, Fluorite.
Porphyritic	U, Th, Mo, Nb, Ti, Zr	Uraninite, Uranothorite, Monazite, Zircon, Flourite, Sulphites.
Detrital Conglomerate	U, Th, Ti, Re, Au	Uraninite, Brannerite, Pyrite, Monazite.

Except in some shales and igneous metamorphic deposits, uranium is not found in sufficient quantity in the common rock types in the earth's crust to be extracted economically (Uwah, 1984). The average crustal abundance of uranium is about 2 ppm (Rich *et al.*, 1972). The relative abundance of uranium in common rocks of the earth's crust is given in Table 2.6.

	Rock	Relative Abundance (ppm)
Igneous Rocks	Granite	3.000
	Felsic granite and granodiorite	3.500

	Syenite	3.000
	Intermediate	1.800
	Ultrabsic	0.002
	Basalt	0.750
Sediments	Clay and shale	3.500
	Limestone	2.200
	Deep-sea clays	1.300
	Sandstone	0.450

Table 2.6: Relative Abundance of Uranium in Some Rocks (Adapted from Parker and Ruziicka, 1979)

Uranium and thorium may also be found in trace quantities in major minerals such as zircon and xenotine (Uwah, 1984). Some rock samples from the Nigerian Younger granites region shows uranium concentrations of 100 - 350 ppm and U/Th ratios of 0.32–1.05 in the Albite granites from Ririwai and Afu, which indicate preferential enrichment of uranium to thorium in these rocks (Bowden *et al.,* 1981).

According to Wooley (1978), uranium ores fall into two categories:

(i) Those that contain uranium in its quadrivalent state (U^{4+}) and

(ii) Those that contain uranium in its hexavalent state (U^{6+}) (the uranyl ions)

The first group, which includes Uraninite, Coffinite, Davidite, and most minerals that contain uranium as a vicarious constituent, are generally black in colour, grading to brownish black and dark brown in oxidized materials. They do not fluoresce in ultraviolet (uv) light (Roberts *et al.,* 1974; Wooley, 1978). Most uranium minerals occur as uranyl compounds. They

generally have lemon yellow to green or orange colour, and fluoresce a bright lemon yellow colour in ultraviolet light (Wooley, 1978).

The important thorium minerals are thorianite (ThO_2), monazite ($ThPO_4$) and thorite ($ThSiO_4$) (Wooley, 1978). Monazite occur widespread throughout the world as a detrital mineral in place deposits, beach and river sands, pegmatites, metamorphic rocks, and vein deposits (Wooley, 1978) which has various colours ranging from reddish – brown, brown, and yellowish – brown, greenish to white. Uranium and thorium may also be found in trace quantities in major minerals such as zircon and xenotine (Wooley, 1978).

2.8 Radiometric Anomalies

Geological information is the basic key to the interpretation of all radiometric data collected in the field (Uwah, 1984). Identification of the various rock types in the survey area can indicate whether or not rocks had been depleted or enriched in the radio - elements of interest when compared with the normal concentrations of the radio - elements in such rock types (Ahmed, 1998).

Also since the chemical compositions of host rock constitute a source of interference in detecting anomalies, sensitivity of a detector may be greatly influenced by the rock type (Ahmed, 1998). One part per million (ppm) of uranium in a pegmatite and basalt, say, may produce different net counts on the same detector under the same physical conditions (Uwah, 1984). The three radioelements (Potassium K^{40}, Uranium U^{235}, U^{238} and Thorium Th^{232}) in normal rocks seem to vary in concentrations sympathetically with one another thus maintaining average constant ratios among them in all rock types (Darnley, 1973). A list of radio - elements and their ratios in some rock types are given in Table 2.7.

Table 2.7: Mean Contents of Radio - Elements in Various Rock Types. (Adapted

from Galbraith and Saunders, 1983)

ROCK TYPE		Th (ppm)	U (ppm)	K (%)	U/Th	U/K	Th/K
IGNEOUS	Ultra basic	3.4	0.8	1.0	0.23	0.76	3.4
	Basic	6.1	1.7	1.9	2.28	0.91	3.2
	Basic - Intermediate	9.8	3.0	2.4	0.30	1.25	4.1
	Acidic - Intermediate	16.0	3.6	3.0	0.23	1.25	5.3
	Acidic	21.9	4.1	3.5	0.29	1.11	6.3
SEDIMENTARY	Evaporites	0.4	0.1	0.1	0.25	1.00	4.0
	Carbonate	1.6	1.6	0.3	1.00	5.00	5.9
	Sandstone	5.7	1.9	1.2	0.33	1.67	4.8
	Shale	11.2	3.7	2.7	0.32	1.43	4.1
METAMORPHIC	Amphibolites	2.0	0.9	0.6	0.45	1.43	3.3
	Greenstone	3.4	0.8	1.0	0.23	0.78	3.4
	Greywacke	6.7	2.1	2.8	0.31	0.78	2.4
	Gneiss	10.6	2.3	3.4	0.22	0.67	3.1
	Schist	13.5	4.1	4.1	0.30	1.67	5.5

For any of the radio - elements to be extracted economically, they have to be located where they have already been concentrated by geological processes to many times the average figures presented in Table 2.6. According to Darnley (1972), this must be about 250 times the average content in normal rock and in addition their ratios must reflect preferential enrichment of the particular element to the others (Uwah, 1984).

The task of delineating a radiometric anomalous region involves an initial reconnaissance survey of the area. The purpose of such a survey is to identify areas of high radioactivity that are possibly indicative of radioactive mineralization for further spectrometric survey. This can normally be done by conducting a fast gross count scintillometric survey at a spacing of about 100 m interval. Fairly constant and low counts may indicate absence of uranium enrichment and such areas can be eliminated for further survey (Ahmed, 1998). In most reconnaissance surveys the gross counts are analyzed and contoured to delineate areas of abnormally high radioactivity. Abnormally high radioactive areas are termed anomalous areas.

Gamma ray spectrometry is used both in the reconnaissance and detailed surveys. The anomalies recognized from the preliminary surveys are of great practical importance for they

may be an indication of deposits of radioactive ore (Ahmed, 1998). Gamma ray spectrometry used in these reconnaissance surveys does not measure uranium directly. The Bi^{214} of the U^{238} series measured in the field may be separated from the uranium deposits if there are favourable conditions (e.g. presence of faults and joints) to enhance radon migration (Soonawala, 1974). Because of this and other environmental effects that affect uranium mineralization, most radiometric anomalies may not correlate with uranium mineralization. Hence radiometric anomalies require thorough investigations before conclusions are made as to their economic importance (Ahmed, 1998). According to Baretta (1981), there are more techniques for uranium prospecting than can be found for any other class of minerals. Some of these methods are listed in Bowie and Cameron (1976), Dodd (1977) and Uwah (1984).

2.9 Radiometric Exploration Methods

There are basically two radiometric survey methods; the ground and airborne radiometric surveys. The air - borne radiometric survey otherwise known as aero - radiometric survey can normally be recommended in circumstances where the terrain is not easily accessible and/or large areas need to be covered. The advantage of the technique is that other geophysical techniques can be carried out simultaneously. The aero - surveys are superior to ground surveys for regional reconnaissance work because large areas can be covered in a relatively short time, but there is always the danger of missing important targets.

There are many documented cases of anomalies that were missed by airborne surveys due to too wide flight line spacing as compared to the width of the anomalous body or rugged terrain which could have prevented the aircraft from maintaining a satisfactory ground clearance (Reedman, 1979). Also, signal attenuation is worse in aero - radiometric survey than ground radiometric survey. For example, a uranium deposit consisting of a number of veins produced only a single large anomaly whereas a ground survey with a high density of sampling points defined the individual vein sources as a series of separate anomalies.

For reconnaissance surveys, gross counts may be adequate to delineate areas of higher than normal radioactivity using the gross count scintillometer. However, where the contribution due to the individual radioelement is required, spectrometric surveys are employed. In this technique, the individual contribution due to U, Th and K are obtained in addition to the total count. Determination of the radioelement concentration can then be made assuming the decay series to be in secular equilibrium.

To complement the field surveys in uranium exploration, radiometric mapping and mineral prospecting, laboratory analysis of K, U, Th and Ra in rock samples is employed. Lead is used to shield a NaI (TI) scintillation detector from background radiation in a laboratory, IAEA (2003). With a multichannel analyzer gamma rays emitted by rock samples are detected, analysed and displayed. Quantitative analysis is essentially comparative: the radiation from a rock sample is compared with the radiation from known standards. The accuracy and precision of the results depends on many factors: the size and energy resolution of the detector; the mass and geometry of the sample; the shielding of laboratory background; counting time; data processing procedures; and the quality of the radioactive standards (IAEA, 2003).

High - resolution Ge laboratory spectrometers can be used for more sophisticated applications. These include the identification of environmental isotopic pollution, the identification of unknown gamma radiation sources, and detailed studies of radioactive equilibrium and the distribution of radionuclides in soil and rock samples.

A typical laboratory scintillation gamma ray spectrometer consists of a NaI (Tl) scintillation detector with a minimum size of 76×76 mm NaI (Tl), a preamplifier, a multichannel analyzer (1024 - 4096 channels), a stabilized high voltage supply, a display unit, and a data recording unit. The sample and detector are enclosed within 6 - 10 cm of lead shielding to reduce the

background radiation. A 5 mm thick brass plate is installed inside the lead shielding to minimize the effect of induced X - ray radiation in the lead shielding.

The performance characteristics of a particular laboratory spectrometer should be known, as this affects the selection of the best method of analysis. The energy resolution of the detector can be measured using the ^{137}Cs peak at 662 KeV. This can be used to select an appropriate channel width setting. The noise level in the 10 - 30 KeV energy range should be experimentally determined and eliminated by correctly setting the instruments lower energy discriminator. The stability of the instrument may be tested by a series of repeat measurements of a reference source. The measured standard deviation should not be greater than that expected from a Poisson distribution due to the statistical nature of the radiation field. Very high count rates from ore grade samples can induce an energy spectrum shift in the output. The spectrum shift range at high count rates can be experimentally determined. A set of reference gamma - emitting sources is used to facilitate the instrument energy calibration.

2.10 Radiometric Measuring Instruments

There are two main categories of radiation monitoring devices. They include gas filled detectors and scintillation detectors.

Gas detection instruments are based on the principle that ions are produced when radiation passes through a gas - filled chamber. Electrons liberated in the chamber are attracted to the centre electrode (anode) by a positive voltage potential, while positive ions are attracted towards the walls (cathode) of the chamber. This produces an electrical pulse or current which can then be detected and recorded by a scaler or ratemeter (Handloser, 1959; Price, 1964; Fenyves and Haiman, 1969; Ouseph, 1975). Gas filled detectors are of three types, namely ionization chambers, proportional counters, and Geiger - Mueller detectors. The primary difference between these detectors is the voltage applied to the chamber, and the

kind of detector to be used depends on the intensity and the type of radiation field encountered.

2.10.1 Ionization chambers

Ionization chambers operate at very low applied voltage. At very low voltages, ion pairs created by radiation passing through the chamber may recombine before they are collected and counted. As the voltage of a gas filled detector is increased, virtually every ion pair produced by the incident radiation will be captured. The current flowing through the meter is therefore directly proportional to the activity of the source. This feature makes ionization detectors very useful as radiation monitoring devices. Survey instruments operating at this voltage are called ionization chambers. Because almost all ion pairs are collected, this instrument is used when it is necessary to accurately determine exposures. Ionization chambers however, are relatively ineffective for measuring rates less than 1 mR/hr, and are slow to respond to changing fields. For this reason, ion chambers are not useful for detecting contamination. They are primarily used to determine exposures in areas of high radiation intensity.

2.10.2 Proportional counters

As the voltage of the tube is increased, electrons are accelerated faster and achieve sufficient energy to create secondary ionizations in the gas. This amplification is termed an avalanche and dramatically increases the size of the electrical pulse at the central anode. Gas multiplication can create millions of ion pairs per ionizing event, in contrast to the ionization chamber which creates one ion pair. Although an avalanche has occurred, gas amplification is proportional to the energy of the initiating event in this voltage region. Radiation monitoring devices operating in this region are therefore called proportional counters. With sufficiently thin windows, alpha particles which produce a large number of ions in the gas, can be

distinguished from beta particles. In addition, the counter can be used to measure the energies of incoming gamma rays.

2.10.3 Geiger-Mueller (GM) counters

The Geiger - Mueller counter is the most widely used area survey instrument for the detection of low - level radioactive contamination and exposure. It is very sensitive, relatively inexpensive, and rugged. Radiation passing into a Geiger-Mueller tube (typically containing helium, neon, or argon) creates ions that are accelerated by a high voltage potential of approximately 1200 volts. Secondary ionizations are created from collisions with the accelerated ions. These ions are also accelerated and achieve sufficient energy to form additional ions. This process eventually produces an avalanche of billions of ion pairs from the initial ionization and creates a large electrical pulse at the anode. The magnitude of the output pulse is independent of the nature of the particle or its energy because gas amplification has reached its maximum potential.

A major disadvantage of Geiger - Mueller counters is their limitation to low radiation fields, typically below 200 $mRhr^{-1}$. This is however within the expected values for radioactivity from natural sources. Once ionizations have been initiated in a Geiger - Mueller tube, it becomes insensitive for a short time, called the dead time, and will not respond to further ionizing events. As a result, the number of counts recorded will be less than the true count rate. This error is relatively very small at low radiation intensities.

2.10.4 Scintillation detectors

Scintillation detectors operate on the principle that certain materials scintillate or give off light when exposed to radiation. Scintillation detectors use a crystal that releases light when exposed to x-rays or gamma rays. There are two types of scintillation detectors namely solid and liquid. Most solid scintillation crystals are composed of sodium iodide with a small amount of thallium added as an "activator". The crystal is coupled to a photomultiplier tube

that converts the light flashes to amplified electrical pulses and amplification factors of a million or more are achieved. The number of pulses is directly proportional to the intensity, and the size of the pulse is directly proportional to the energy of the incident radiation. These pulses can then be analyzed by a counter, spectrometer, oscilloscope, or computer.

Because scintillation crystals are solid, rather than gaseous, their higher density and atomic number makes them very efficient and sensitive instruments for the measurement of x - rays and gamma rays. The crystal in a solid scintillation detector can be thin or thick. The thin crystal has an energy range of approximately 10 - 60 KeV, while the thick crystal has a range from about 50 KeV to 1 MeV. Scintillation detectors, however, are not as rugged as Geiger counters because the crystal is hygroscopic and can absorb water from the atmosphere.

Liquid scintillation detectors use organic compounds that give off light when radioactive materials are added to a liquid scintillation cocktail (LSC). Material from a swipe is dissolved or suspended in the solution, and almost all of the emitted radiation passes through some portion of the scintillator. The light is detected by photomultiplier tubes, analyzed and counted in a manner similar to solid scintillation detectors.

The major component of a gamma ray spectrometry is the detector crystal. The most widely used detectors for gamma ray spectrometry especially for in – situ radiometric surveys are Thallium activated sodium iodide crystals (NaI (TI)) (Lovborg *et al.*, 1971). Lithium drifted germanium, Ge (Li), has better energy resolution and is the most useful laboratory analyzer where high energy resolution and low energy measurements is required. In terms of efficiency of gamma ray detection, (NaI (TI)) detectors are better than Ge (Li) detectors. The second disadvantage of Ge (Li) as a gamma ray detector is that it must be cooled continually (even when not in use), to temperature of liquid nitrogen. Hyper Pure Germanium detectors (HPGe), however, have excellent resolution and are better than Ge (Li) detectors. They need to be cooled only when in use.

Heath (1969) and Smith and Wollenberg (1972) have described systems making use of Ge (Li) crystal for laboratory analyses of uranium samples. Also, their uses in car and truck – mounted systems for in – situ measurements have been reported. The use of plastic polyvin toluene (PVT) as detector for gross counting in airborne gamma ray survey has also been reported.

The crystal volumes for portable spectrometers are limited by size and weight of the whole system. The detector crystal (mainly cylindrical) is optically coupled to a photomultiplier tube. The voltage output pulse of the photomultiplier tube is directly proportional to the energy expanded in the crystal by the photons interacting with its atoms. A pulse height analyzer in the system then classifies the pulse according to their amplitudes.

2.11 Radiometric Data Processing

Gamma ray spectrometry is a strong technique from which guidance on the nature of radioactive anomalies obtained is required. It involves the detection, collection, sorting and classification of energy spectra by single, or multichannel pulse height analyzers, and the treatment of the spectral data, often by computers, to yield abundances of individual radioelements. The combination of aerial surveys, ground examinations of the detected anomalies, laboratory analysis of field samples and gamma – logging of drilled holes has been recognized as the most useful technique in uranium exploration (IAEA, 1976). However, since uranium and thorium are not gamma ray emitters themselves, and the gamma rays of their daughters are used to detect them; their activity determinations in rocks will be the true representative of their actual concentrations only when they are in secular equilibrium with their daughters (Ahmed, 1998).

Having obtained the spectrometric data, necessary corrections are then applied so as to obtain count rates, which are in proportion to the radio – element concentration (Ahmed, 1998). The results could then be expressed in terms of the concentration of the radioelements measured.

The procedure for estimating concentration of the three radio elements K, U and Th depends on the type of spectrometer used. Prior to calculation of the element concentrations, the readings have to be corrected for background effect. If the background is negligible, the concentration of the element is proportional to the counts recorded from the respective channels. For a threshold spectrometer, the relationship between the count rates and the element concentration is such that the concentrations are directly proportional to the background corrected count rate (Ahmed, 1998). For a "window spectrometer", suppose the count rates in count per second (c/s) in the thorium, uranium and potassium windows are Th_c, U_c and K_c respectively, then

$$Th\ (ppm) = (Th_c)\ K_1 \quad \text{.....2.5}$$

$$U\ (ppm) = (U_c)\ K_2 \quad \text{.....2.6}$$

and $$K\ (\%) = (K_c)\ K_3 \quad \text{.....2.7}$$

Where K_1, K_2 and K_3 are respectively the sensitivity constants of the spectrometer for the Th, U and K channels. However, where the background is significant, the readings (Th_c, U_c and K_c) must be corrected for this effect. Suppose the background readings in (c/s) in the thorium, uranium and potassium windows are Th_{bc}, U_{bc} and K_{bc} respectively, the above equations becomes

$$Th\ (ppm) = K_1\ (Th_c - Th_{bc}) \quad \text{.....2.8}$$

$$U\ (ppm) = K_2\ (U_c - U_{bc}) \quad \text{.....2.9}$$

And $$K\ (\%) = K_3\ (K_c - K_{bc}) \quad \text{.....2.10}$$

Also, because of the interference of thorium in the uranium counts and thorium and uranium in the potassium counts, other constants called stripping ratios have to be incorporated into the above equations. This is because in detecting potassium for example, the energy threshold used is 1.46 MeV which means that all gamma rays with energy above 1.46 MeV are counted. In this energy range, both gamma rays emitted by the decay chains of uranium and

thorium are present; hence a correction has to be made for their presence. Similarly, for detecting uranium, the threshold energy used is 1.76 MeV, so the only interference is from the gamma rays from thorium decay series and this must be accounted for. But in the detection of thorium, the energy threshold is 2.62 MeV hence there is no interference from any of the gamma rays from either potassium or uranium.

Suppose the stripped count rate (in counts per second) recorded in the U, Th and K windows for a U, Th and K standards are respectively S_u, per (ppm eU), S_{Th} per (ppm eTh) and S_K per (% K), then the element concentrations derived from the respective corrected count rates are given as

$$eTh\ (ppm) = \frac{K_1(Th_c - Th_{bc})}{S_{Th}} \quad \text{.....2.11}$$

$$eU\ (ppm) = \frac{K_2(U_c - U_{bc})}{S_u} \quad \text{..... ....2.12}$$

And $$K\ (\%) = \frac{K_3(K_c - K_{bc})}{S_K} \quad \text{.....2.13}$$

According to Uwah (1984), in the case of multichannel spectrometry the element contents are obtained by a least squares method as follows:

Let n = number of channels used

a_i = count rate of U standard in channel i

b_i = count rate of Th standard in channel i

c_i = count rate of K standard in channel i

d_i = count rate of sample in channel i

All counts are corrected for background effect

Let m_u = U in the sample in grams

m_{Th} = Th in the sample in grams

m_K = K in the sample in grams

M_u = U in U – standard in grams

M_{Th} = Th in Th – standard in grams

M_K = K in K – standard in grams and

W = weight in grams

Let $X = \frac{m_U}{M_U}$, $Y = \frac{m_{Th}}{M_{Th}}$, $Z = \frac{m_K}{M_K}$ 2.14

If a linear superposition of U, Th and K contributions to the counts in each channel is assumed, then the count rate in each channel can be written as follows:

$$d_1 = Xa_1 + Yb_1 + Zc_1$$

$$d_2 = Xa_2 + Yb_2 + Zc_2$$

$$\vdots$$

$$d_n = Xa_n + Yb_n + Zc_n$$

or $$\begin{pmatrix} d_1 \\ d_2 \\ \vdots \\ d_n \end{pmatrix} = \begin{pmatrix} a_1 & b_1 & c_1 \\ a_2 & b_2 & c_2 \\ \vdots & \vdots & \vdots \\ a_n & b_n & c_n \end{pmatrix} \begin{pmatrix} x \\ y \\ \vdots \\ z \end{pmatrix}$$ 2.15

or $D = Ax$ 2.16

x can be obtained from equation 2.12 by least squares as follows:

$$x = (A^T A)^{-1} A^T D$$ 2.17

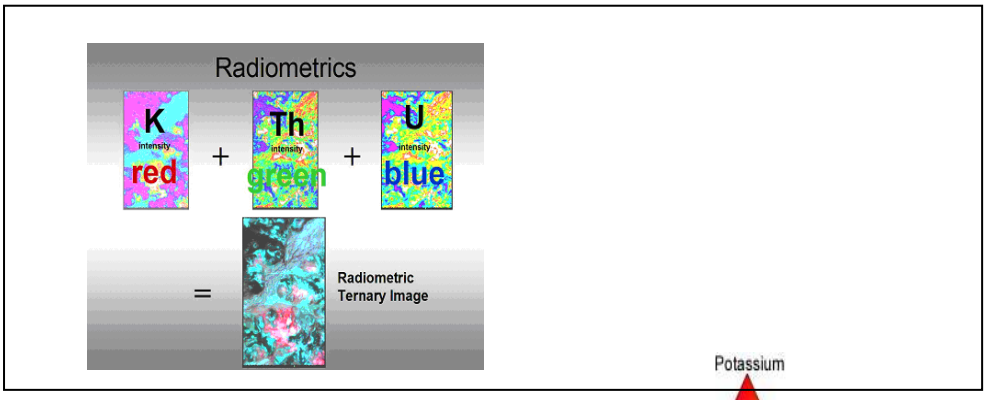
Then $eU\ (ppm) = \frac{XM_U}{W} x10^6$, $eTh\ (ppm) = \frac{YM_{Th}}{W} x10^6$, $K\ (\%) = \frac{ZM_K}{W} x10^6$ 2.18

This procedure is usually adopted for laboratory spectrometric measurements of eU and eTh of some rock samples.

2.12 Radiometric Data Presentation

Radiometric data is nowadays displayed as a "ternary image" by combining three datasets on one picture using a Red - Green - Blue (RGB) ratio. Each of the datasets are displayed using a different primary colour which when combined makes a colourful display with each shade representing different relative amounts of potassium, thorium and uranium. Usually the colours are displayed as follows:

Red = Potassium; Green = Thorium and Blue = Uranium. Fig. 2.3 illustrates how the three measured bands of radiation contribute to the ternary image.



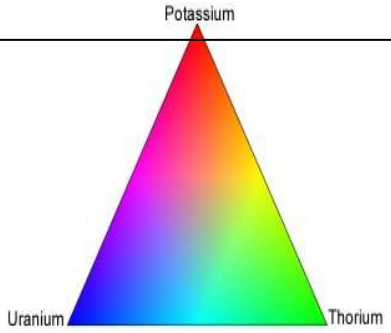


Fig. 2.3: Relative Proportion of Uranium, Potassium and Thorium on a Ternary Image Ratio (Source: Suzanne, 2011)

Using the above colour schemes, the following can be interpreted from the different colours on a ternary image map:

Red	=	high potassium with low uranium and thorium
Blue	=	high uranium with low potassium and thorium
Green	=	high thorium with low potassium and uranium

Cyan = high thorium and uranium with low potassium

Magenta = high potassium and uranium with low thorium

Yellow = high potassium and thorium with low uranium

Black = low potassium, thorium and uranium

White = high potassium, thorium and uranium

In order to recognize and understand radiometric signatures associated with the host rocks important to mineralization, enhancing techniques such as composite image maps, ratio maps as well as individual radioelement maps are produced. These are to help identify zones that have high activity concentrations of uranium, potassium and thorium.

A standard ternary image is normally plotted in RGB in which high concentrations of the 3 radioelements tend to white while low concentrations of the 3 radioelements tend to black.

In areas of high or low concentration, the dominant radioelement or combination of radioelements is obscure. Thus, another type of ternary image is constructed in which each of the radiometric grids is normalized as follows:

$$normK = \frac{K}{(K+Th+U)} \quad \text{.....2.1}$$

$$normTh = \frac{Th}{(K+Th+U)} \quad \text{.....2.2}$$

$$normU = \frac{U}{(K+Th+U)} \quad \text{.....2.3}$$

The resultant ternary image which is referred to as “normalized ternary” map has no black or white tones but pure colours showing the predominant radioelement or combination of the radioelements.

CHAPTER THREE

MATERIALS AND METHODOLOGY

3.1 Ground Scintillometric Survey

A scintillometer is used to detect gamma rays emitted from a variety of naturally occurring radioactive elements. Generally, total count values are acquired, which indicate the rate of gamma ray observations in counts per second. Recording the total count with a scintillometer does not distinguish between the radioactive elements.

3.1.1 Materials for the scintillometric survey

The ground scintillometric survey was carried out from 6 May, 2013 to 16 May, 2013 in an area of about 160 km^2 bounded approximately by latitudes 10º 00′ 35″ N to 10º 07′ 00″ N and longitudes 11º 00′ 36″ E to 11º 06′ 00″ E in the southwest of the Kerri - Kerri Formation. The purpose of this survey was to identify areas of more prominent radioactive anomalies within the study area for further ground spectrometric study.

Exploranium® portable gamma ray scintillometer; model GR - 101A, manufactured by Geometrics Inc. California was used for the survey. The (GR - 101A) scintillometer is an instrument that transforms incident gamma radiation into visual 'read out' of radioactive intensity as a function of the natural radioactive material present in the geologic formation (McDermott, 1977). A sodium iodide crystal converts gamma rays into flashes of light whose brilliance is proportional to the energy level of the gamma radiation measured (McDermott, 1977). These light flashes are detected by a high gain photomultiplier tube (PMT), amplified, and fed to a circuit which accepts signals above a certain energy level (McDermott, 1977). The accepted signals are averaged in a rate meter circuit as counts per second and continuously displayed on a 250^o meter on the instrument front panel. The frequency or signal count rate displayed is the intensity of all gamma ray energy above the present threshold. The detector crystal is a Sodium Iodide Thallium Activated (NaI) cylinder of

dimensions 38.1 mm x 38.1 mm, with a total crystal volume of 0.0431m^3 (McDermott, 1977) which records gross count only for all gamma rays of energies above 0.05 MeV. It also provides visual and audible indications of anomalous gamma radiation from local sources of radioactivity.

3.1.2 Methodology for the scintillometric survey

The Scintillometer (GR - 101A) was strapped at west height above the ground. Traversing the study area on foot, a total of three hundred and ninety four (394) total count readings were taken at random points and recorded with the scintillometer. The researcher and a field assistant taking readings with the scintillometer in the study area are shown in Plates I and II respectively. The locations of the random points were also recorded with a GPS. Rock samples were also collected at different locations within the study area for identification.

To estimate the cosmic ray contribution to the ground activity measured in the field, readings were taken in the middle of a Pond southwest of Tulmi located at 10^0 $12^{'}$ $09^{''}$ N and 11^0 $03^{'}$ $17.9^{''}$ E. The readings in the pond were taken first in the morning before the start of the survey and then in the evening, for each day of the survey. The background readings are taking in the morning and evening as cosmic rays from the sun are minimal at these periods of the day.

Two other sets of background readings were taken inside Dadin - Kowa Dam located east of Gombe town and about 60 km from the study area. This is to compare the background readings obtained in the dam with that obtained in the pond within the study area. The first set of background readings (i.e. morning and evening) were taken in the Dam on the first day of the survey while the second set of readings (i.e. morning and evening) were taken on the last day. The background readings taken in the Pond and Dadin - Kowa Dam are presented in Appendix I.

The data acquired with the scintillometer were corrected for background and presented in Appendix II. Golden Software "SUFER 9" was used to plot the contour map of count rates of the gamma ray energy of the study area.

3.2 Ground Spectrometric Survey

Unlike the scintillometer which records all the gamma rays coming from the source, the spectrometer can distinguish between the gamma rays emitted by the radioactive elements in separate windows. In line with the aim of this study, a ground gamma ray spectrometric survey was carried out in the area identified with more prominent radioactive anomaly identified in the scintillometric survey. The area is accessible by road from Mararaba to Tumu. The purpose of this investigation is to confirm the occurrence or otherwise of uranium, thorium and potassium mineralization in the rocks of the area.

3.2.1 Materials for the spectrometric survey

A Pico Envirotec Portable Ground Information System Gamma Ray Spectrometer (PGIS - SP), GIS - 15 Model - SN: GS 200510 - 5 was used for the spectrometric survey. The PGIS-SP is an advanced software driven instrumentation specifically designed for ground on foot environmental survey work (PEI, 2006). The PGIS - SP is a fully integrated system incorporating: a Gamma Ray Spectrometer (GRS2), an advanced Satellite (GPS) navigation, real - time path information that can be displayed over a map image (geo referenced BMP format) of an area, and a reliable data acquisition software package. Automatic synchronization of acquired data to the GPS position and time provides very close correlation between data and geographical position.

The PGIS - SP system consists of three units; a hand Held Computer (HHC), a GPS Receiver and an Intelligent Gamma Detector (IGD) as shown in Plate III. The IGD has a maximum of 15 crystal detectors, to provide real - time information on levels of radiation and uses NaI

(TI) detectors integrated with a fully automated detector control system. The NaI (TI) detector is 76 mm x 76 mm. The PGIS - SP and all other executable programs are installed in the HHC system.

The PGIS - SP program provides a multi - function system that is used to control data acquisition, display and navigation guidance. Acquired data, positional information and other reference data are stored in a compressed binary data format. The PGIS - SP data acquisition software performs a number of complex mathematical calculations in real time but the data collection and storage takes the highest priority. Collected data are retrieved from the storage media (Flash Card) via Personal Computer Memory Card International Association (PCMCIA) port and transferred into a Personal Computer (PC). The PGIS - SP has a self supporting software for spectrum calibration, hence no calibration is required (PEI, 2006).

3.2.2 Methodology for the spectrometric survey

The ground spectrometric survey in this study was carried out from 12 April, 2014 to 19 April, 2014. Prior to the commencement of the survey, the layout and orientation of the area was identified and marked out using a GPS. The area is 1.5 Km x 1.5 Km (2.25 Km^2) located north east of Tumu bounded by latitudes 10^o $00^{'}$ $47.2^{"}$ N to 10^o $01^{'}$ $19.4^{"}$ N and longitudes 11^o $00^{'}$ $57.5^{"}$ E to 11^o $01^{'}$ $29.7^{"}$E.

On arrival at the field, the HHC was connected to the IGD by a coiled interconnection cable. The GPS receiver was also connected to the IGD with an extension cable and mounted to the IGD. The IGD and GPS units were then mounted carefully on a backpack which was then strapped to the back of the operator. A routine check is then carried out on the equipment. This involves starting the PGIS-SP software which automatically initializes the communication mode between the IGD, GPS receiver and HHC. The system parameters such as: accumulation time (5 - 600 s), spectrum resolution (256 – 512 channels), fiducial, element library for defined regions of interest and auto recording are all set on the HHC. The ThPeak

is the tuning channel of the PGIS-SP for calibration which is to be checked on the HHC all the time during the survey. The range for proper tuning of the ThPeak should be 0.72 – 0.95 (PEI, 2006). In case the ThPeak is out of range, the PGIS-SP has to be calibrated. Sample of the data acquired with the PGIS-SP is presented in Appendix III for profiles 1 to 5. The data comprises of: profile Nos., marked station points, coordinates of station points (in UTM and latitude and longitude), total count (cps), U(cps), Th(cps), Cs(cps), K(%), eU(ppm), eTh(ppm), Dose($nGyph^{-1}$) and ThPeak. The ThPeak was observed to be in the acceptable tuning range throughout the survey.

A surveyor with another GPS walks ahead of the PGIS - SP operator on a bearing of 225^{o} (SW - NE) using the "*distance to go"* on the GPS and marks out the station points along each profile. This eliminates pegging of station points along the profiles. Measurements were then taken along the profiles at the station points marked by the surveyor. The survey parameters used were as follows:

- Profile spacing = 50 m
- Profile direction = SW – NE
- Station interval = 50 m
- Profile length = 1,500 m
- Baseline = 1,500 m
- Channels = 512
- Accumulation time = 5 s

A total of 961 data points were occupied along 31 profiles

The direction of the profiles is in a SW - NE across the strike of the anomaly identified in the scintillometric investigation as presented in Fig. 3.1.

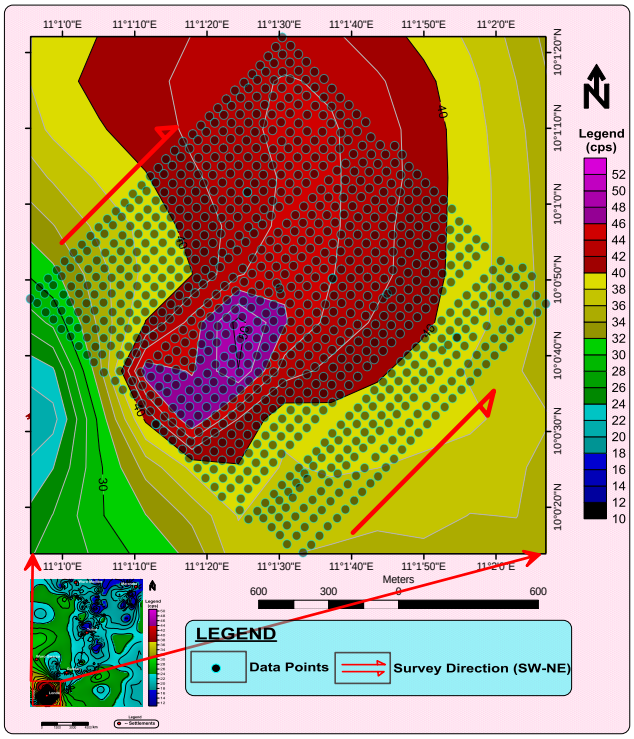


Fig. 3.1: Location of data points and direction of profiles for the spectrometric survey.

3.2.3 Spectrometric data processing

While data collection and storage takes the highest priority, the PGIS-SP data acquisition software also automatically computes the measured gamma ray activity of the radioelements in counts per second (cps) to elemental concentrations in parts per million (ppm). In addition to the three radionuclides ^{238}U, ^{232}Th and ^{40}K, the PGIS-SP also measures and records the Absorbed Dose Rate and Cesium (^{137}Cs).

The software used to process and enhance the data is the Geosoft ("Oasis Montaj") and Golden Software "Surfer 9". Quality control and processing of data generated with the PGIS-SP was done with "*PEIVIEW*" Software. The data was converted into Geosoft binary (gbn) file for processing *using* Microsoft Excel and Geosoft (Oasis Montaj) software. For statistical analysis and mathematical calculations of the data, "Microsoft Excel 2007" statistical extensions were used.

This survey was carried out at the peak of the dry season when all the streams and ponds were dry with no thick vegetation in and around the area hence no background readings were taken. The shielding of the crystals of the PGIS-SP also minimizes the effect of background radiations on the spectrometer.

Fully - processed Gamma ray survey data can be presented in a variety of ways to enable interpretation of radioelements along profiles and grids. The enhancement of gamma ray spectrometric data has benefited from digital image processing techniques over the years (IAEA, 2003). Nevertheless, the traditional presentation methods, such as profiles and contour maps, have their advantages, and are still in common use today. Although some visualization methods can be considered as routine in the presentation of gamma ray spectrometric data, none of the individual methods are universally applicable to all gamma ray mapping applications (IAEA, 2003). In general, one should experiment with different methods to find those that are optimally suited for a particular interpretation.

The processed data was gridded with Kriging method and color - shaded maps were produced with coloring of intervals between contour lines with range of colors from the natural color spectrum. The maps reveal at once the difference between highs and lows. This enhances the techniques to recognize and understand radiometric signatures associated with the host rocks important to mineralization.

Conventional Spectrometric surveys rely on visual inspection of plots, graphs or charts, to identify high radiometric points/areas. Such a visual interpretation is subjective and prone to the operator bias in determining what is high or low. Statistical analysis of the Gamma ray spectrometric data was therefore carried out to enhance the technique for visual interpretation. This includes: mean differencing, standard deviations and correlation coefficients which were used to enhance subtle variations in the data that otherwise would

remain unnoticed. Therefore applying both the statistical and mapping methods makes the interpretation objective and removes the operator's bias.

To make a better comparison between activity concentrations of the PGIS-SP data and that of the rock samples, the conversion factors given by the International Atomic Energy Agency (Abdul-Razek *et al.,* 2013) were used to calculate the values of ^{238}U and ^{232}Th in (Bq/kg) to ppm and ^{40}K in (Bq/kg) to (%) as given below.

1 ppm of ^{226}Ra = 11.1 (Bq/kg)…….3.1

1 ppm of ^{232}Th = 4.06 (Bq/kg) and……..3.2

1 % of ^{40}K = 313 (Bq/kg)……..3.3

Absorbed dose rates were also calculated from the activity concentrations of the radionuclides ^{238}U, ^{232}Th and ^{40}K in order to assess the risks associated with human exposure to these radiations. The conversion factors 0.462, 0.604 and 0.0417 for uranium, thorium and potassium, respectively as given by Ramasamy *et al. (*2010) were used to calculate the total dose rate (D) ($nGyh^{-1}$) for the rock samples using the equation:

$$D = (0.462C_U - 0.604C_{Th} - 0.0417C_K)nGyph^{-1} \quad \text{.....3.4}$$

Where: C_U, C_{Th} and C_K are the activity concentrations (Bq/kg) of ^{238}U, ^{232}Th and ^{40}K respectively. The values of eU and eTh as well as % K calculated from the activity concentrations of the radionuclides and the dose rate for the rock samples are presented in Appendix IV.

3.3 Collection and Preparation of Rock Samples

Rock samples were collected at thirty six (36) locations along grid points in the study area for laboratory gamma ray spectrometric analysis. The area was divided into nine cell units for the purpose of compositing. For each cell unit, four discrete rock samples collected were mixed into a single homogenized sample for the analysis. Thus, nine (9) composite samples were

formed. Fig. 3.2 shows the locations of the rock samples collected and the composite samples formed.

The composite rock samples were first dried in the sun for 5 days to remove any moisture, then crushed to grain size of about 1 mm, and placed into sample plastic containers. The sample containers were sealed so that no radon escapes and kept for 28 days in order to bring the rock samples into a state of secular equilibrium between the long-lived parent radionuclides (^{226}Ra and ^{228}Ra) and their short-lived progeny. Detection, counting and sorting of radionuclides was then carried out with a Laboratory Spectrometer at the Centre for Energy Research and Training (CERT), Ahmadu Bello University Zaria. Results of the laboratory gamma ray spectrometer analysis are presented in Appendix V.

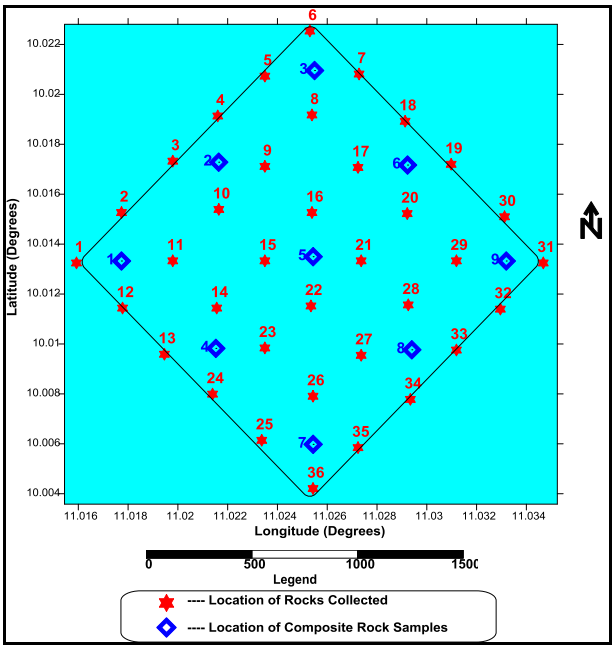


Fig. 3.2: Locations of rock samples collected and composite samples formed.

CHAPTER FOUR

RESULTS

4.1 Scintillometric Data Analysis

The average background reading taken in the Pond is 3.95 cps (Appendix 1). The average of the two sets of readings taken in Dadin - Kowa Dam is 3.75 cps. The two average sets of readings from the Dam and the Pond are close with that of the dam lower likely due to the larger volume of water. The average cosmic ray contribution from the Pond (i.e. 3.95 cps) was used for the background correction of the scintillometric data.

Figure 4.1 is the contour map of the corrected scintillometric data presented in Appendix II. The count rates of gamma ray energy are generally higher in the southwest of the study area located north east of Tumu and a prominent peak centered at (10^0 00' 38.6" N, 11^0 01' 32.9" E') is observed on the contour map.

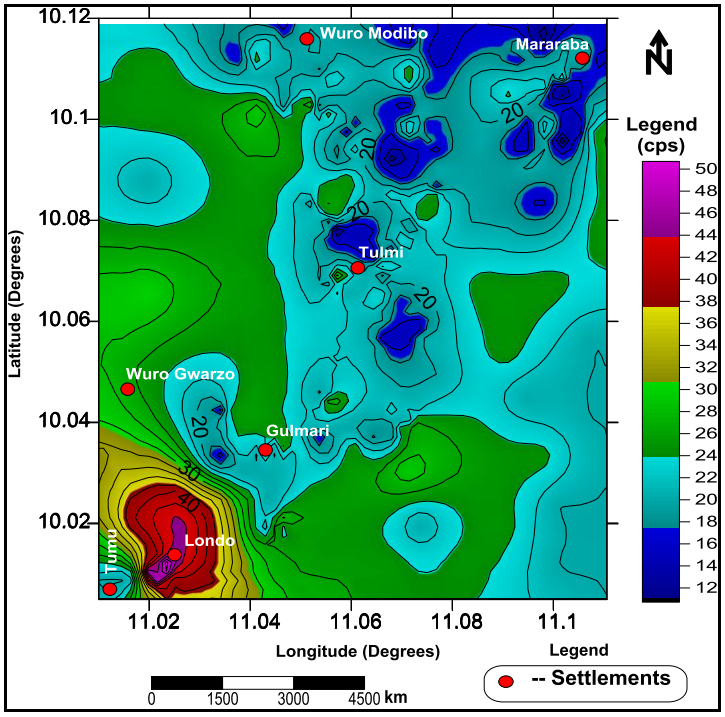


Fig.4.1: Contour map of count rates of gamma ray energy of the study area (Contour Interval = 2 cps)

Geologic formations are not necessarily uniform in radioactivity. As suggested by Ahmed (2006), an attempt has to be made in order to unify the errors that may arise in the

calculations of the average values of field activities and of standard deviations. Areas of radioactive anomalies can be delineated from the total count contour map.

According to Uwah (1984), a better method of determining the mean activity value for a geologic unit is to plot a frequency distribution curve of the gamma ray activity versus number of data points. The frequency distribution table is presented in Appendix VI while the frequency distribution curve of the scintillometric data is presented in Figure 4.2.

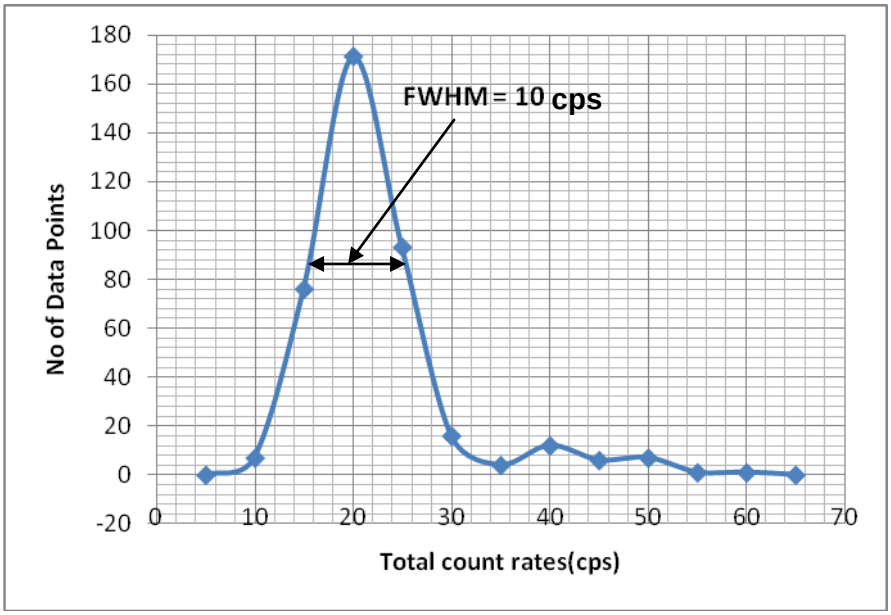


Fig. 4.2: Frequency Distribution of Total Count Rates of Gamma ray Energy of the Study Area

The *normal or expected mean activity* (EMA) is determined by using the *mode, standard deviation* (SD) and *full width half maximum* (FWHM). The mode is the value that appears most often in the set of data. The SD gives an idea of how close the entire set of data is to the mean value. The FWHM is an expression of the extent of a function, given by the difference between the two extreme values of the independent variable at which the dependent variable is equal to half of its maximum value.

The mean activity in Fig. 4.2 is the mode of the frequency distribution. The EMA value for the study area is obtained from the frequency curve (Fig. 4.2) as follows:

Mode = 20 cps

FWHM = 10

The SD is then given by Duval (1979) as:

SD = 10 x 0.75 = 7.5 cps ≈ 8 cps

The EMA value is then given by:

$$EMA = Mode \pm SD = (20 \pm 8) \text{ cps}$$

The threshold value (i.e. the highest activity) is therefore 28 cps. According to Uwah (1984), all other values above 28 cps in this case are considered anomalous.

According to Levinson (1974), for an activity to be of significance in terms of mineralization, it must be about twice the mean activity of the area. In this study, activities of more than twice the mode (i.e. 40 cps) were observed at the southwestern part of the study area. The area is located north east of Tumu village and bounded by latitudes 10^{o} $00^{'}$ $14^{''}$ N to 10^{o} $01^{'}$ $19^{''}$ N and longitudes 11^{o} $00^{'}$ $58^{''}$ E to 11^{o} $02^{'}$ $04^{''}$ E as shown in Fig. 4.1.

The scintillometric investigation has identified an area with more prominent radioactive anomaly situated north east of Tumu in the southwest of the study area (Fig. 4.1). A ground spectrometric survey was therefore carried out in the area identified with more prominent radioactive anomaly in the scintillometric survey to confirm the occurrence or otherwise of uranium, thorium and potassium mineralization in the study area.

4.2 Spectrometric Data Analysis

The analysis of the processed PGIS-SP data and that of the laboratory gamma spectrometer analysis of the rock samples were carried out by map analysis and statistical analysis.

4.2.1 Image maps for the PGIS-SP data

Human vision can distinguish approximately 32 grey - scale levels (Drury, 1992). This colour perception capability was used in the presentation of gamma ray spectrometric data. Single

radioelement channels were mapped in pseudo – colour which enabled better recognition of the distribution of radioelement concentrations as shown in most of the maps produced.

Figures 4.3, 4.4, 4.5 and 4.6 are respectively the total count (TC in cps), equivalent uranium (eU in ppm), equivalent thorium (eTh in ppm) and potassium (K in %) maps of the study area for the PGIS-SP data.

The total count map (Fig. 4.3) shows radiometric anomalies in the western, southwestern and around the central part of the area with values ranging from 120 cps to 150 cps while low values ranging from 55 cps to 70 cps are observed in the upper northwestern flank, north central and northeastern flank of the area.

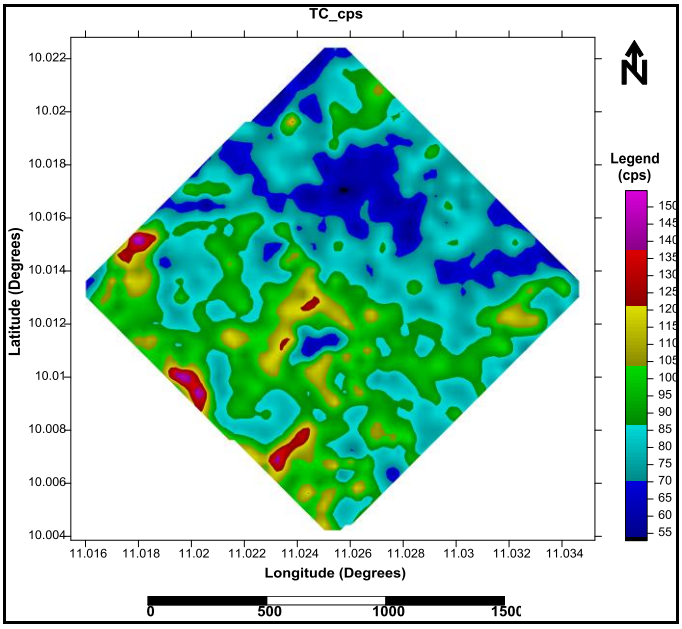


Fig. 4.3: Total count map of the study area for the PGIS-SP data

Uranium concentration is higher in the western, southern and northern end of the study area with values ranging from 8.5 ppm to 11.5 ppm (Figure 4.4) while lower concentration of uranium is observed in the north central, northeastern and southeastern parts of the study area with values ranging from 1.5 ppm to 8.0 ppm.

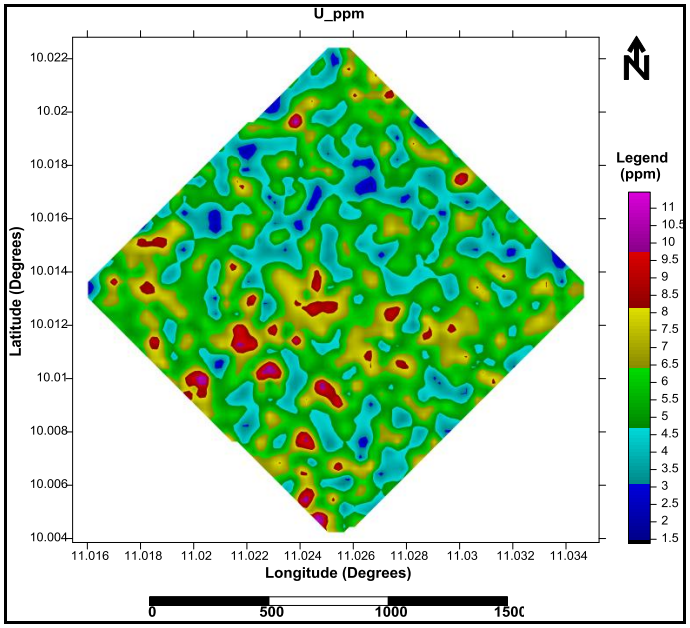


Fig. 4.4: Uranium concentration (eU) map of the study area for the PGIS-SP data

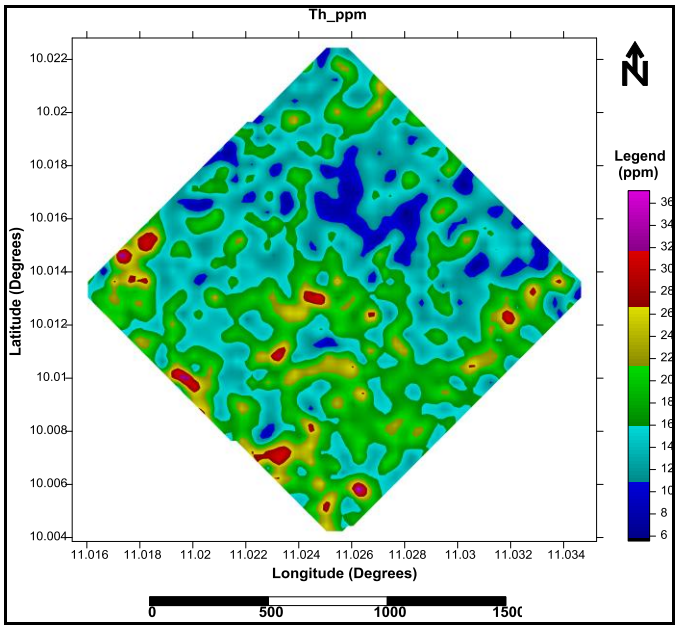


Fig. 4.5: Thorium concentration (eTh) map of the study area for the PGIS-SP data

The thorium map (Figure 4.5) shows anomaly in the: western end, southern, central and southeastern flank of the study area. High concentration of thorium ranges from 27 ppm to 36 ppm in the regions mentioned above. The northern part of the area has low concentration of thorium.

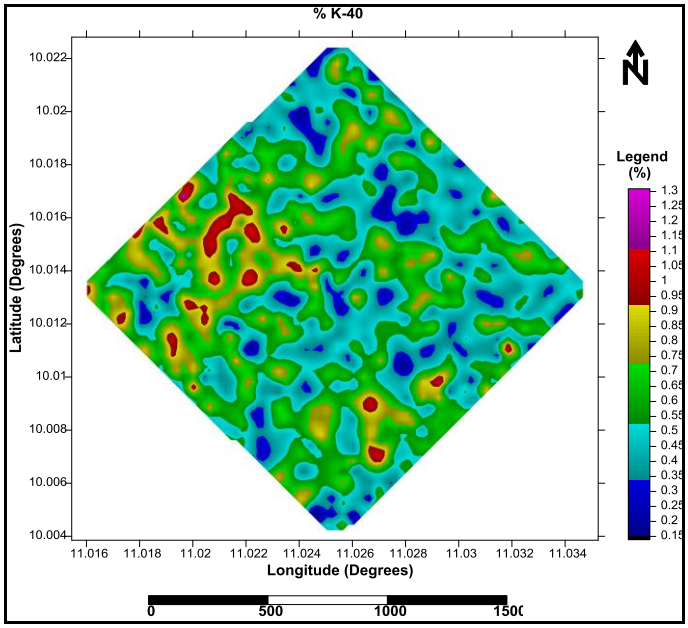


Fig. 4.6: Potassium concentration (%K) map of the study area for the PGIS-SP data

The potassium map (Figure 4.6) shows higher concentration of potassium in the western and southeastern regions of the study area with values ranging from 0.9 % to 1.3 % while lower concentration of potassium is observed in the rest of the area with values ranging from 0.15 % to 0.70 %.

Presented in Figure 4.7 is the absorbed dose rate map of the study area. Areas with higher and lower concentrations of the absorbed dose rate coincide with that of the total count image map (Figure 4.3). Low absorbed dose rates are observed in the northern parts of the study area.

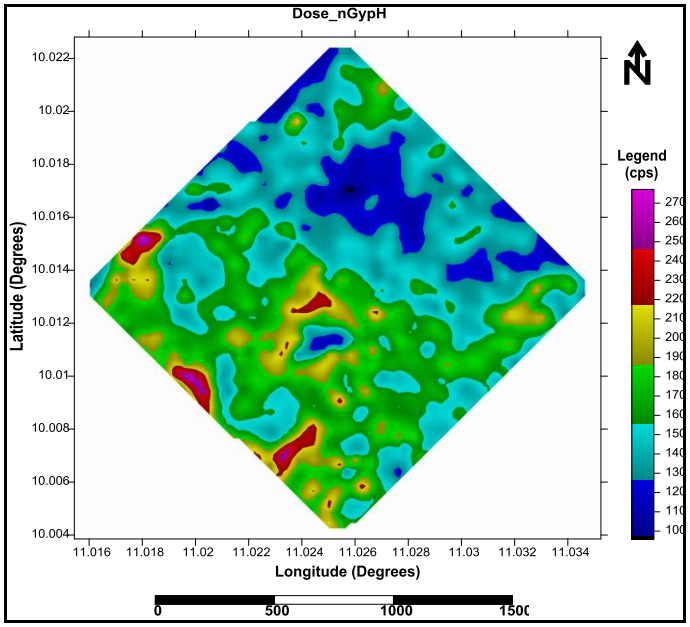


Fig. 4.7: Absorbed dose rate map of the study area

4.2.2 Image maps for the rock samples

From the results of the laboratory gamma spectrometer analysis of rock samples, image maps were produced for uranium (^{238}U), thorium (^{232}Th) and potassium (^{40}K) as presented in Figures 4.8, 4.9 and 4.10 respectively.

The uranium map for the rock samples (Figure 4.8) is characterized by closures of low uranium concentrations (1.2 ppm to 2.0 ppm) at the southwest, southeast and northern end of the study area while higher concentrations are observed at the southern end and eastern flank of the area with concentration values ranging from 3 ppm to 3.8 ppm.

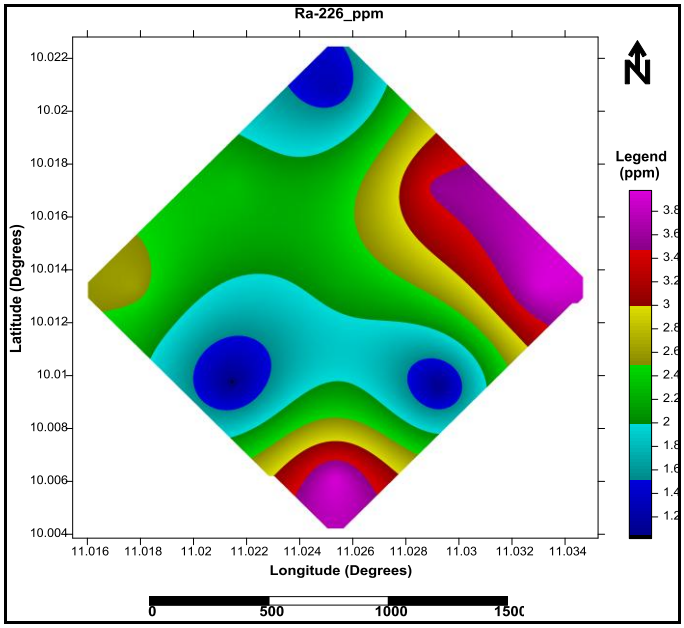


Fig. 4.8: Uranium (^{238}U) map of rock samples

In Figure 4.9, a thorium anomaly is observed in the southwestern part trending to the central part of the study area. Higher concentration of thorium ranges from 18.0 ppm to 25.0 ppm while lower thorium concentrations (10.0 ppm to 13.5 ppm) are observed in the north western and northeastern flanks of the study area.

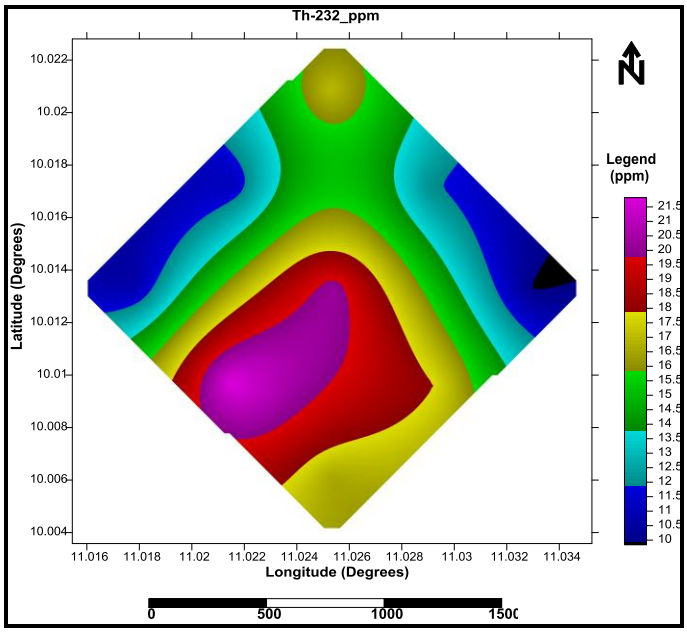


Fig. 4.9: Thorium (^{232}Th) map of rock samples

The concentration map of potassium (Figure 4.10) shows an anomaly trending from the central part to the north western part of the area with values ranging from 0.5 % to 0.9 %. The rest of the area has low concentration of potassium ranging from 0.1 % to 0.4 %.

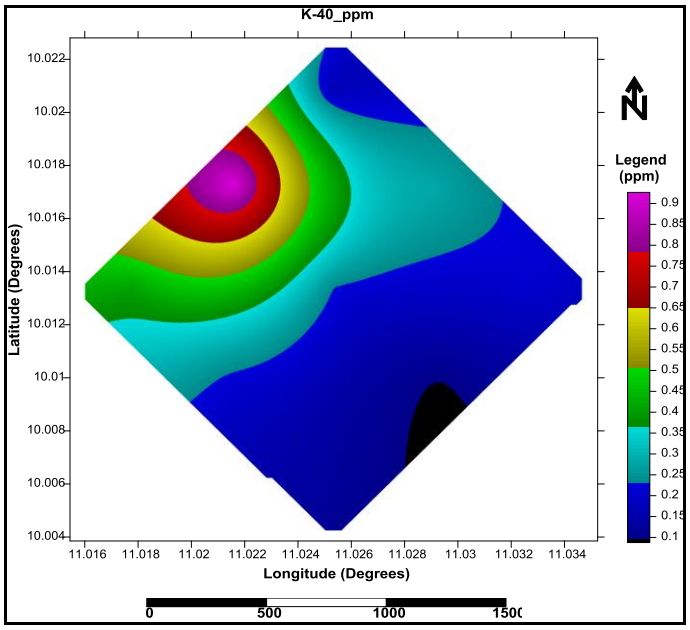


Fig. 4.10: Potassium (^{40}K) map of rock samples

4.2.3 Ternary maps for the PGIS-SP data

A standard ternary image map presented in Figure 4.11 for the PGIS-SP data shows high concentration of the three radioelements (i.e., the white portions) in the south, southwest and southeastern parts of the study area while low concentrations are observed in the northeast and northwestern parts of the study area.

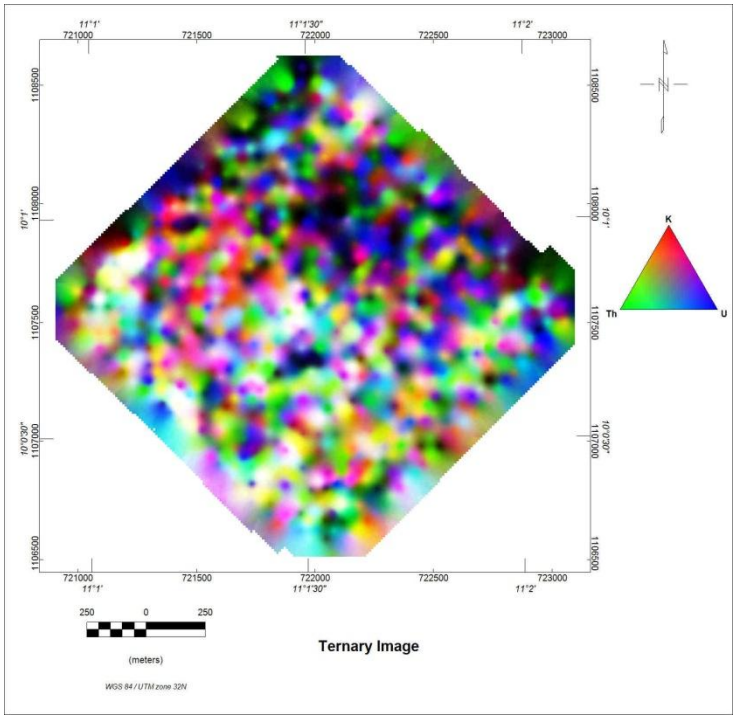


Fig. 4.11: Standard Ternary Map of the Study Area

Figure 4.12 is the normalized radiometric ternary image map of the study area. The resultant ternary image map has no black or white tones but pure colours showing the predominant radioelement or combination of the radioelements. Potassium is predominant in the western, central and northeastern parts of the study area. Thorium predominates in the southern, southeastern and northern parts of the study area while uranium is predominant in the central and northern parts of the study area.

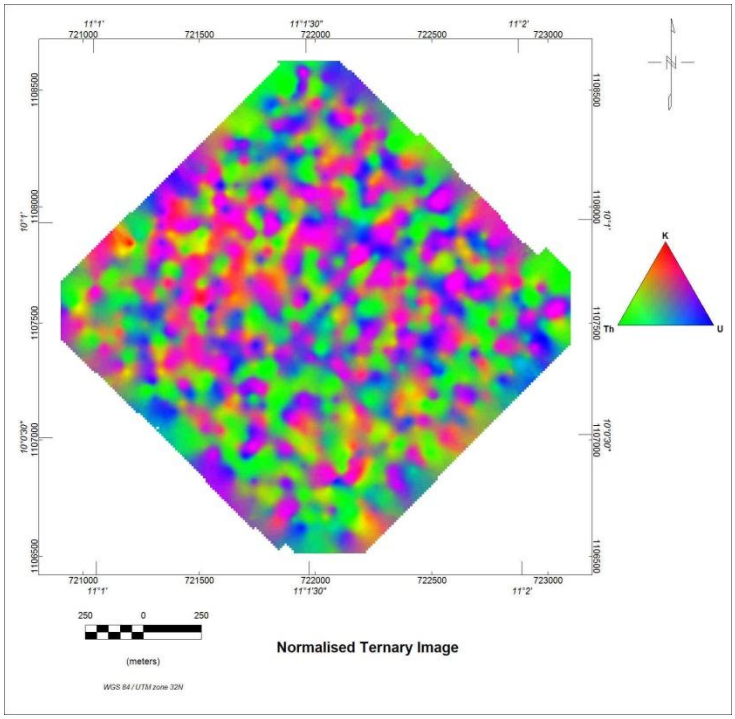


Fig. 4.12: Normalised Ternary Map of the Study Area

4.2.4 Ratio maps for the PGIS-SP data

The key to radiometric interpretation in uranium search is the use of ratios as the radioelements; potassium, uranium and thorium generally vary together (Wilkes, 1981). In areas of uranium mineralization, uranium is preferentially concentrated and, therefore, produces anomalously high uranium/thorium and uranium/potassium ratios (Wilkes, 1981). Radiometric ratios are often more reflective of lithological variation than the individual radiometric channels, hence a variety of radiometric ratio maps were produced. U/Th ratios have particular value in exploration for uranium deposits because it has been found to increase locally within regions containing uranium ores (Shives *et al.,* 1995).

Figure 4.13 is the Uranium to Thorium (eU/eTh) ratio map of the study area for the PGIS-SP data. The U/Th ratio map shows preferential enrichment of thorium to uranium in most parts of the study area. Enrichment of uranium to thorium is observed as spots in the northeast central and northwest central parts of the study area. The rocks in the northeast central and

northwest central parts were identified as shales while the rest of the study area consists of weathered ironstones (i.e., hematite).

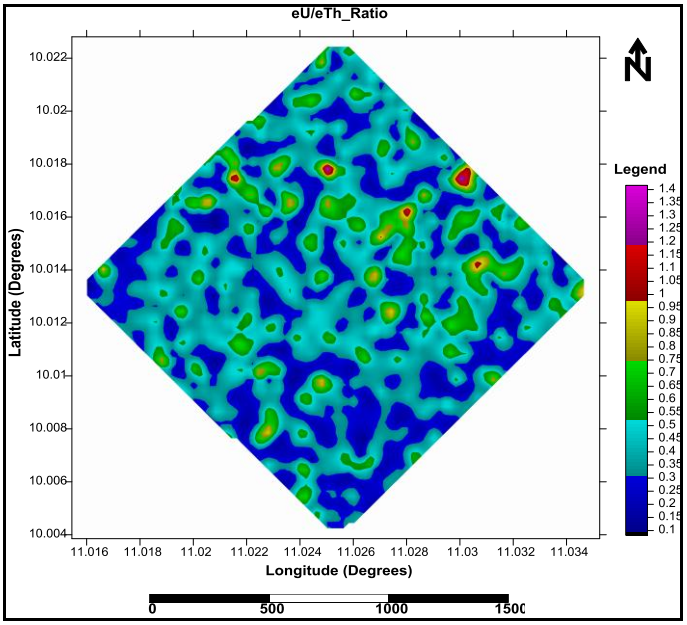


Fig. 4.13: U/Th Ratio Map of the Study Area for the PGIS-SP data

As thorium enrichment generally does not accompany potassium during hydrothermal alteration processes, Th/K ratio provides an excellent distinction between potassium associated with alteration and anomalies related to normal lithological variations. It has been established that in general, low Th/K ratios are excellent indicators of potassium alteration (Shives *et al.*, 1995).

Figures 4.14 and 4.15 are respectively the Thorium to Potassium (Th/K) ratio map and Uranium to Potassium (U/K) ratio map of the study area for the PGIS-SP data. High Th/K ratio signatures are observed in isolated spots in the: northwest, western, southern and southeastern parts of the study area. Regions with low Th/K ratio indicate preferential enrichment of potassium to thorium.

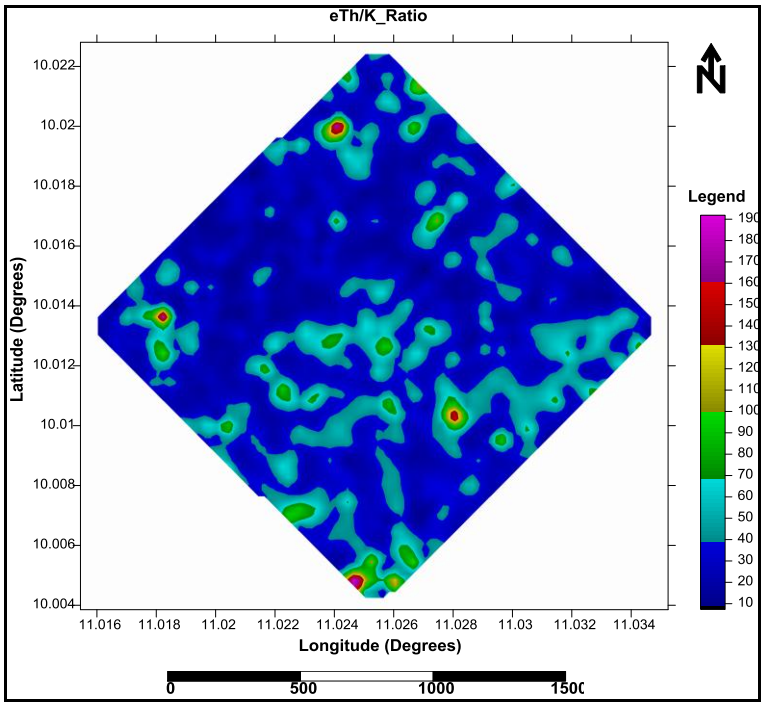


Fig. 4.14: Th/K ratio map of the study area for the PGIS-SP data

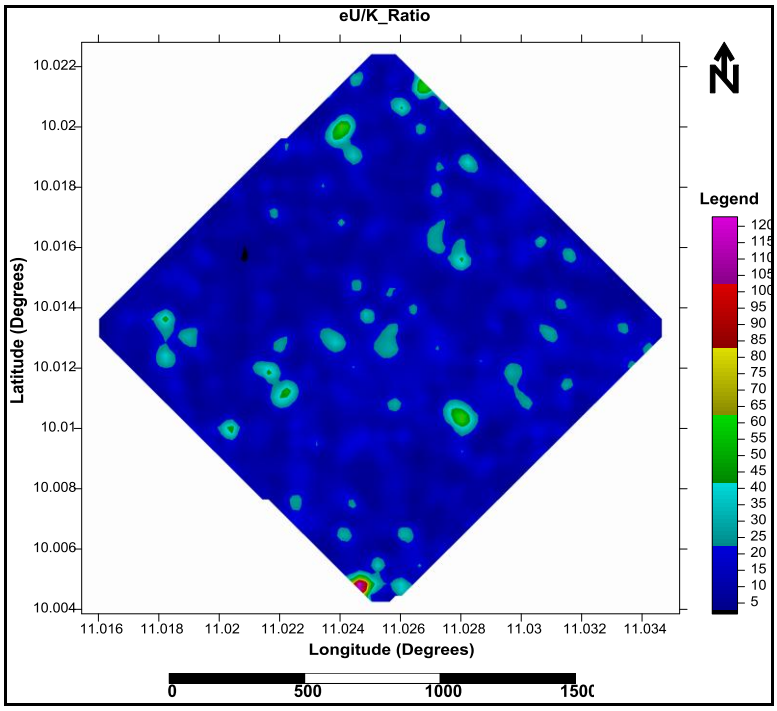


Fig. 4.15: U/K ratio map of the study area for the PGIS-SP data

In the U/K ratio map (Fig. 4.15), there is preferential enrichment of potassium to uranium as most of the area has low U/K ratio values while uranium enrichment is observed in the southern end of the study area.

Ratios of the radioelements can provide further constraints for identifying potential uranium deposits (Shives *et al.*, 1995).

A ratio of U^2/Th proved effective in highlighting uranium mineralization. The U^2/Th ratio is also effective in separating the primary uranium, associated with uranium - bearing rocks. High U^2/Th ratio values are associated with many uranium deposits and can be used to highlight new areas of potential mineralization. The U^2/Th ratio map (Figure 4.16) highlights areas that are both high in U and U/Th. The areas of high U^2/Th are shown as small isolated spots in the northern and southern parts of the area.

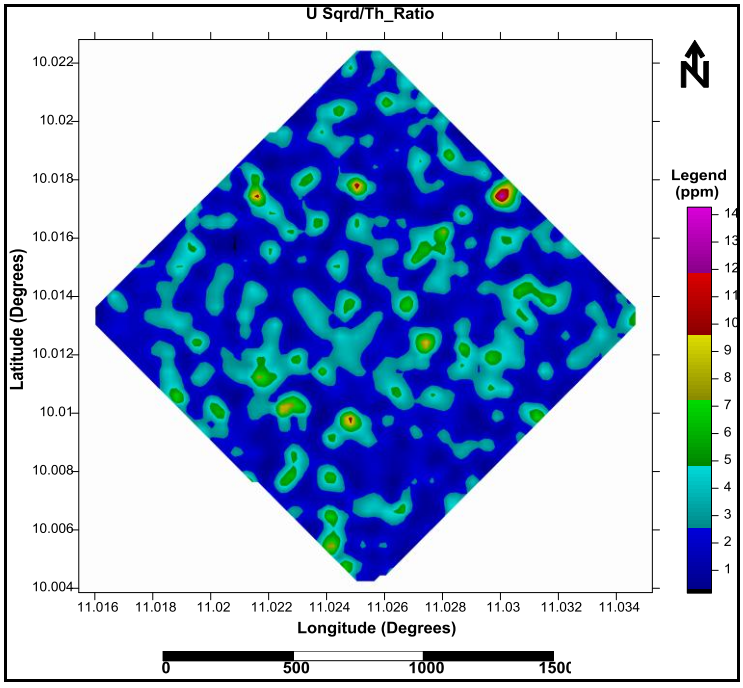


Fig. 4.16: U^2/Th Ratio Map of the Study area for the PGIS-SP data

4.2.5 Variation of concentration of radioelements with topography

A Shuttle Radar Topographic Map (SRTM) of the study area is presented in Figure 4.17. It is a digital representation of the terrain elevation modeled as a regular grid. The elevation of the study area ranges from 407 m to 465 m above sea level. The north western part of the study area is characterized by low elevation ranging from 415 m to 424 m. Interpretation of the radiometric maps was carried out in conjunction with the topography of the area.

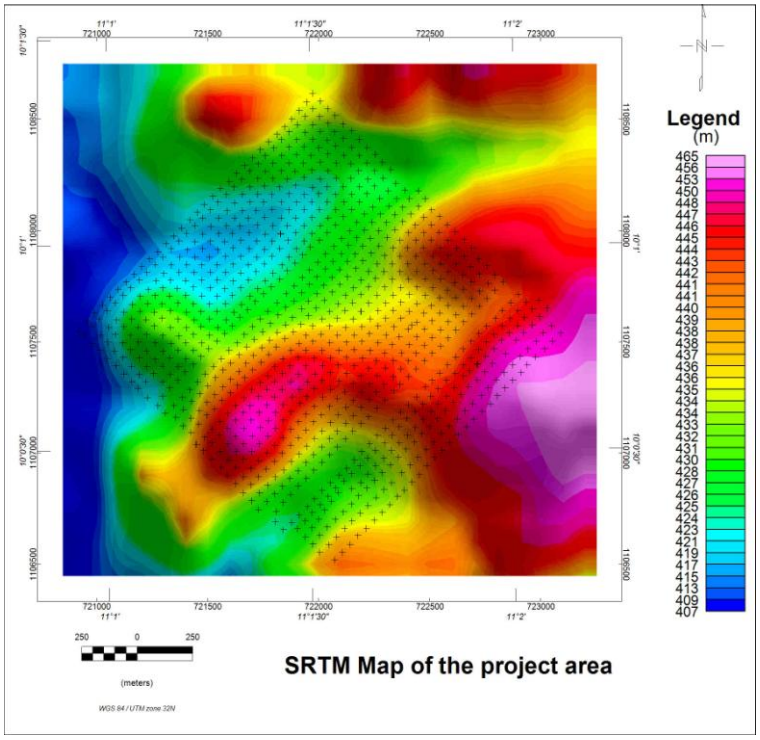


Fig. 4.17: Shuttle Rader Topographic Map of the study area (Inset is the data acquisition points)

The map can be used to assess the effect of weathering, because uranium oxidized to water in soluble form may be leached from primary source and deposited as sediment (Gana, 2011). The location of uranium occurrence can also be defined by low or high elevation areas (Gana, 2011).

To see the variation of concentrations of the radioelements (^{238}U, ^{232}Th and ^{40}K) with topography of the study area, their image maps were draped over the SRTM as presented in Figs. 4.18, 4.19 and 4.20. The distribution of the radioelements in the three maps draped over the SRTM shows their concentrations over the topography of the area. Uranium and thorium

are more concentrated in high elevated areas while potassium is concentrated on low level areas.

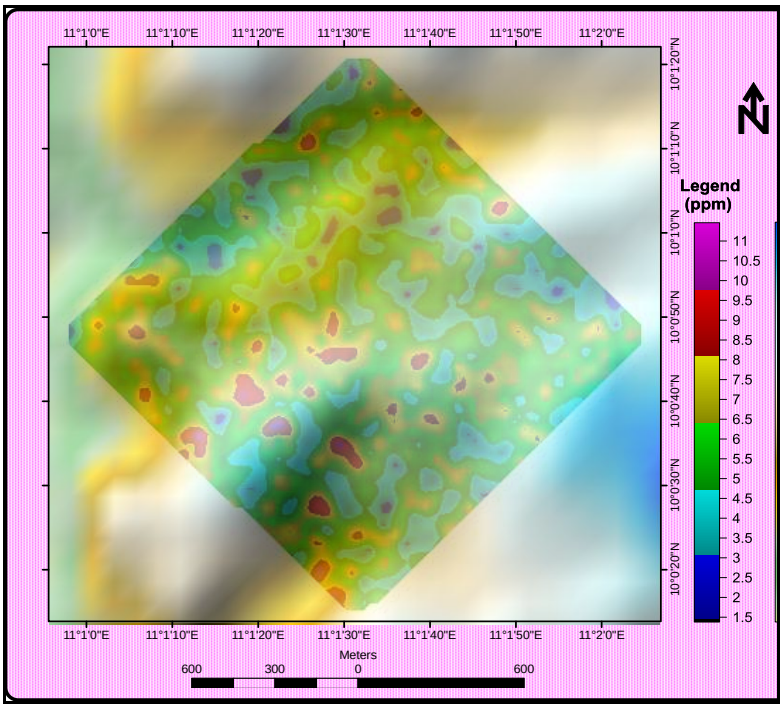


Fig. 4.18: Uranium map draped on SRTM for PGIS-SP data

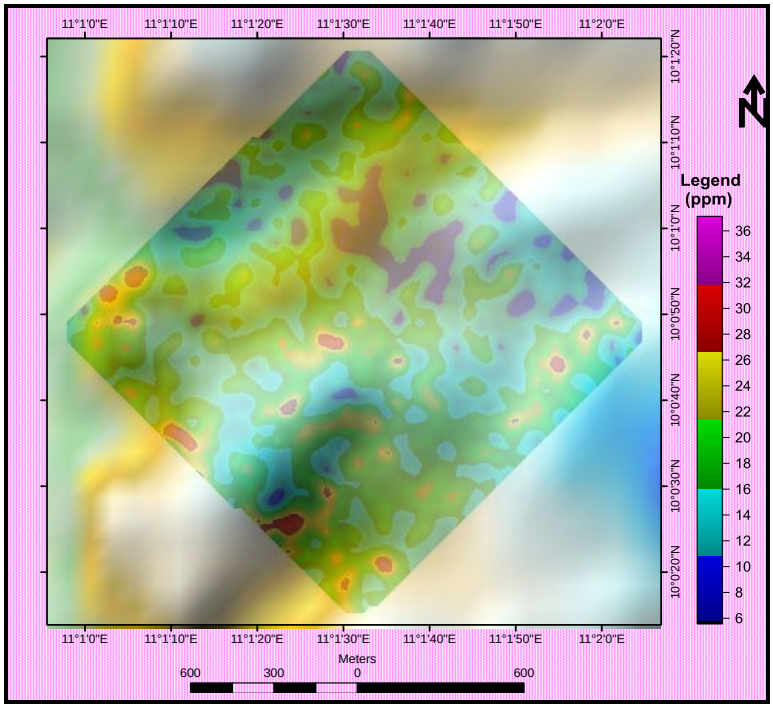


Fig. 4.19:Thorium map draped on SRTM for PGIS-SP data

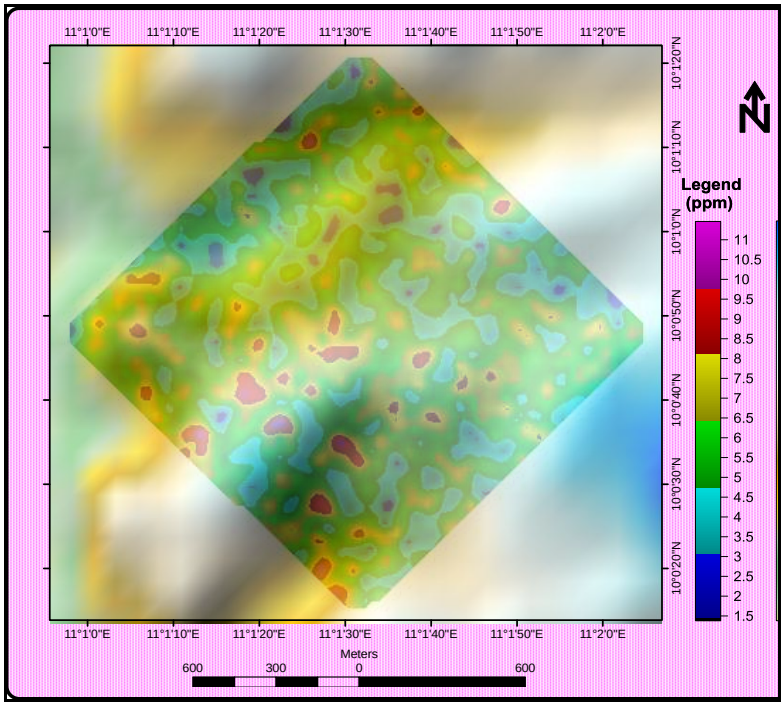


Fig. 4.20: Potassium map draped on SRTM for PGIS-SP data

4.2.6 Variation of concentration of radioelements with geology of the study area.

The geologic map of the spectrometric survey area derived from the geologic map of the study area (Fig. 1.3) is presented in Fig. 4.21.

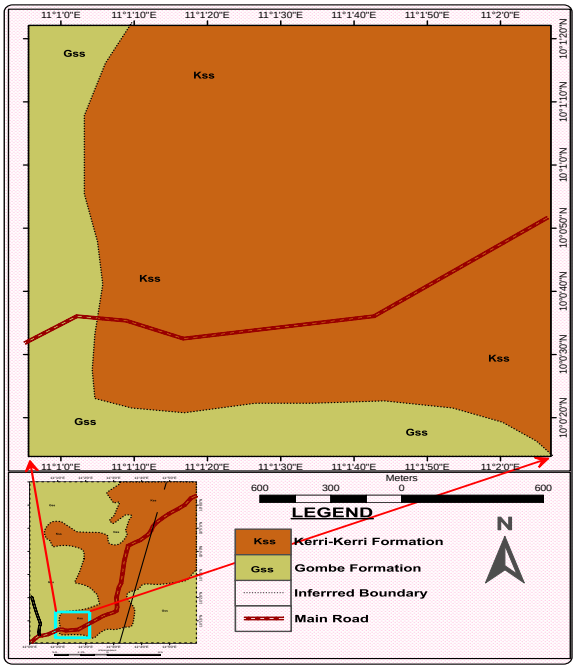


Fig. 4.21: Geologic map of the spectrometric survey area

Maps of the concentration of the radioelements ^{238}U, ^{232}Th and ^{40}K were also draped over the geologic map of the spectrometric survey area so as to see the variation of the concentrations of the radionuclides with geology as presented in Figs. 4.22, 4.23 and 4.24 respectively.

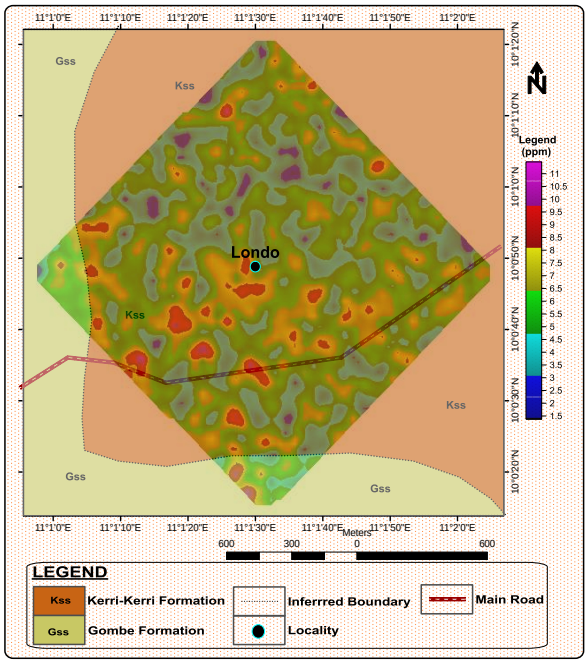


Fig. 4.22: Uranium map draped on geologic map of spectrometric survey area

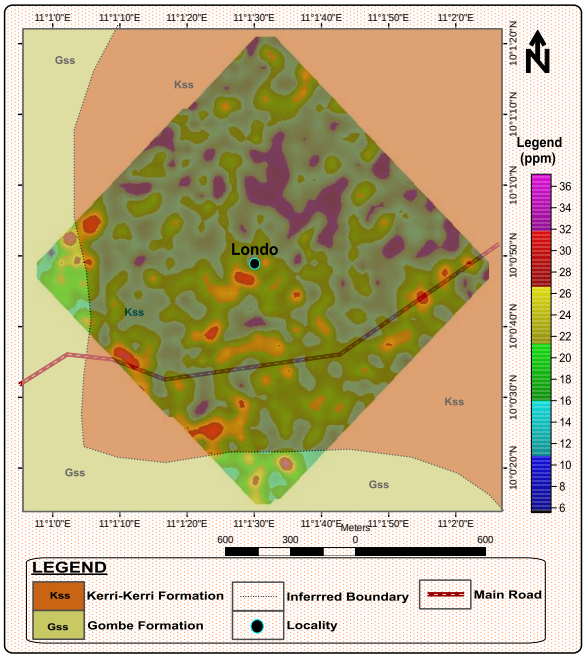


Fig. 4.23: Thorium map draped on geologic map of spectrometric survey area

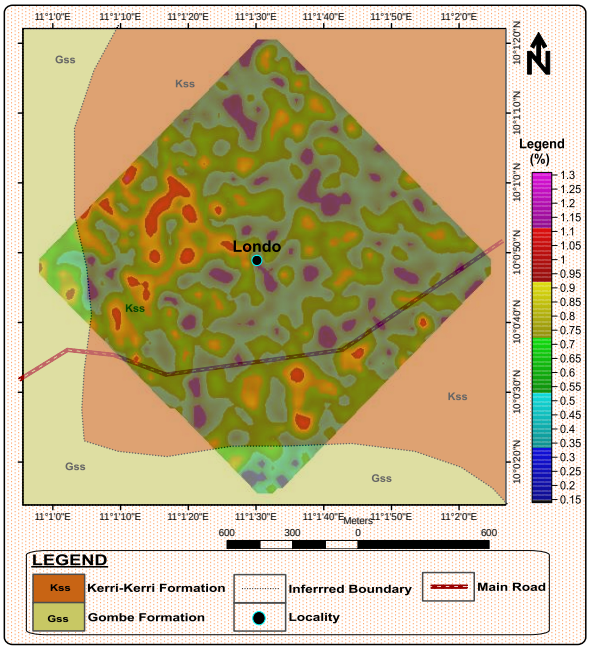


Fig. 4.24: Potassium map draped on geologic map of spectrometric survey area

The total count map of the study area (Fig. 4.3) is also draped over the geologic map of the area (Fig. 4.25) to see if the radiations are coming from the rocks or soils of the area.

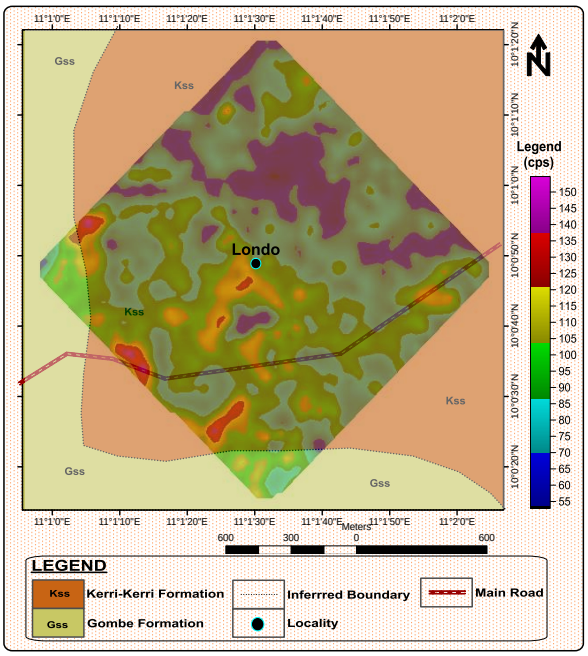


Fig. 4.25: Total count map draped on geologic map of the study area for the PGIS-SP data

4.3 Statistical Analysis of the Data

The methods of data analysis employed herein are the threshold, diagnostic ratio and average crustal radioelement concentration which involved the determination of the mean, minimum and maximum, standard deviation and coefficient of correlation of the radioelement concentrations. The purpose is to see if statistical correlations and mathematical relationships exist between the radiation parameter investigated in this study. Statistical extensions of "Microsoft Excel 2007" were used to compute the mean, standard deviation and correlation coefficients of concentrations of the radioelements. The statistical analysis of the concentrations of the radionuclides and dose rate for the PGIS-SP data and that of the rock samples are presented in tables 4.1 and 4.2 respectively.

Table 4.1: Statistical analysis of the PGIS-SP data

Radionuclide	Minimum	Maximum	Mean	Standard Dev.
eU (ppm)	0.740	12.760	5.534	2.062
eU (cps)	0.000	6.000	2.498	0.942
eTh (ppm)	5.574	41.210	16.299	5.574
eTh (cps)	0.200	6.000	2.170	0.876
K (%)	0.223	1.360	0.558	0.223
K (cps)	1.000	9.000	4.165	1.258
TC (cps)	2.000	162.000	85.316	7.138
Cs (cps)	10.800	41.200	21.054	4.625
Dose (nGyph-1)	7.849	28.777	15.646	3.029

Table 4.2: Statistical analysis of laboratory gamma spectrometer results of the rock samples

Radionuclide	Minimum	Maximum	Mean	Standard Dev.
Ra-226 (ppm)	0.996	3.988	2.432	1.207
Ra-226 (cps)	0.010	0.038	0.023	0.012
Ra-226 (Bq/Kg)	11.055	44.265	26.999	13.393
Th-232 (ppm)	9.878	21.963	15.250	4.464
Th-232 (cps)	0.035	0.078	0.054	0.016
Th-232 (Bq/Kg)	40.103	89.168	61.913	8.122
K-40 (%)	0.089	0.931	0.293	0.257
K-40 (cps)	0.018	0.188	0.059	0.052
K-40 (Bq/Kg)	27.745	291.527	91.704	80.371
Dose ($nGyph^{-1}$)	44.865	63.738	53.693	7.061

The mean concentrations of uranium, thorium and potassium for the PGIS-SP data (Table 5.1) are respectively 5.534 ppm, 16.299 ppm and 0.558 % while for the rock samples, the

mean concentrations of uranium, thorium and potassium (Table 5.2) are respectively 2.432 ppm, 15.250 ppm and 0.257 %.

4.3.1 Average crustal abundance of the concentration of the radioelements

The mean concentrations of uranium, thorium and potassium for the PGIS-SP data (Table 5.1) are respectively 5.534 ppm, 16.299 ppm and 0.558 % while for the rock samples, the mean concentrations of uranium, thorium and potassium (Table 5.2) are respectively 2.432 ppm, 15.250 ppm and 0.257 %.

4.3.2 Diagnostic ratio analysis of the data

Activity ratios (U/Th, U/K, Th/U, Th/K, K/U and K/Th) of the radionuclides for the PGIS–SP data and that of the rock samples were calculated and presented in Tables 4.3 and 4.4.

Table 4.3: Ratios of activity concentrations of the radionuclides for the PGIS-SP data

Ratio	Minimum	Maximum	Mean
U/Th	0.048	1.648	0.387
Th/K	0.063	2.286	0.560
U/K	0.042	3.667	0.643
Th/U	0.607	20.833	2.584
K/Th	0.438	15.873	1.786
K/U	0.273	23.810	1.555

Table 4.4: Ratios of activity concentrations of the radionuclides for the rock samples

Ratio	Minimum	Maximum	Mean
U/Th	0.124	1.098	0.510
Th/K	0.155	2.606	1.100
U/K	0.088	1.162	0.422
Th/U	0.917	8.065	3.310
K/Th	0.384	6.452	1.791
K/U	0.861	11.364	3.920

The average U/Th, Th/K and U/K values for the PGIS-SP data are 0.387, 0.560 and 0.643 respectively (Table 4.3) while for the rock samples, the U/Th, Th/K and U/K are respectively 0.510, 1.100 and 0.422 (Table 4.4).

4.3.3 Correlations between the concentrations of the radioelements

In order to determine any synergy of the ratios amongst the activity concentrations of the naturally radioelements in the rocks of the area, correlations between them were drawn up. The correlation between the activity concentrations of (^{238}U and ^{232}Th), (^{238}U and ^{40}K) and (^{232}Th and ^{40}K) for the PGIS-SP data are presented in Table 4.5 while Table 4.6 is for the rock samples. In all the cases, the correlation is found to be weak and positive for the PGIS–SP data (Table 4.5). For the rocks samples (Table 4.6), the correlation is also weak and positive except for the correlation between ^{238}U and ^{232}Th which is strong but negative.

Table 4.5: Correlations between U, Th and K for the PGIS-SP data

	^{238}U	**^{232}Th**	**^{40}K**
^{238}U	1.00		
^{232}Th	0.30	1.00	
^{40}K	0.31	0.24	1.00

Table 4.6: Correlations between ^{238}U, ^{232}Th and ^{40}K for the rock samples

	^{238}U	**^{232}Th**	**^{40}K**
^{238}U	1.00		
^{232}Th	-0.63	1.00	
^{40}K	0.05	0.50	1.00

To compare the gamma ray activity between the radioelements in the study area, the mean activity of each radioelement for each profile from the spectrometric data acquired with the PGIS-SP were calculated, the results presented as a bar chart (Figure 4.26). Another bar chart (Figure 4.27) is presented for the activity of the radioelements from the laboratory gamma ray results of the rock samples.

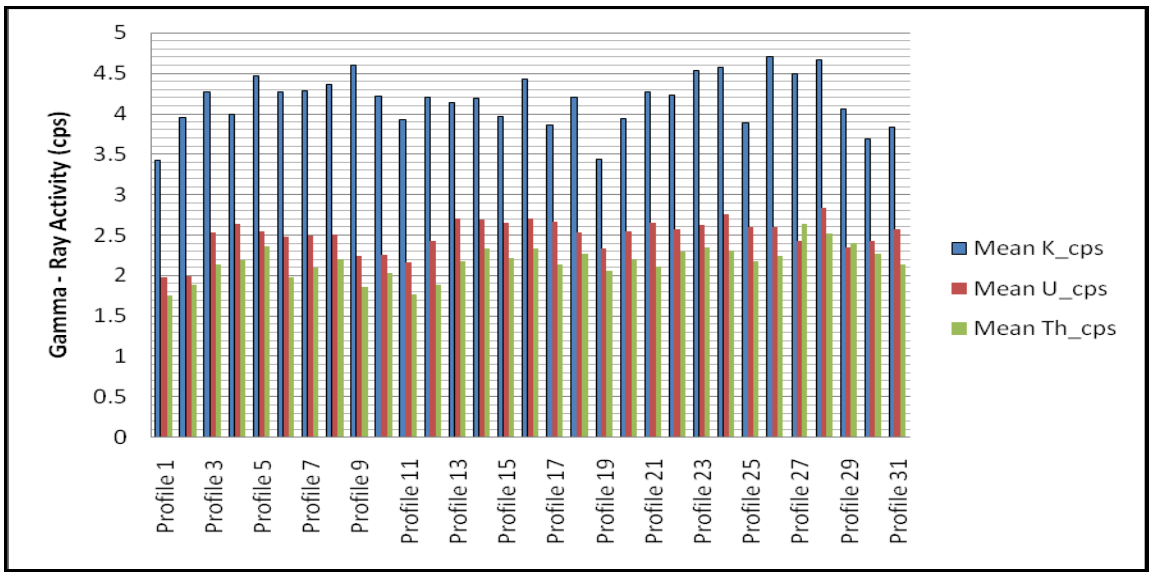


Fig. 4.26: Bar Chart of mean gamma ray activity of U, Th and K along profiles for PGIS-SP data

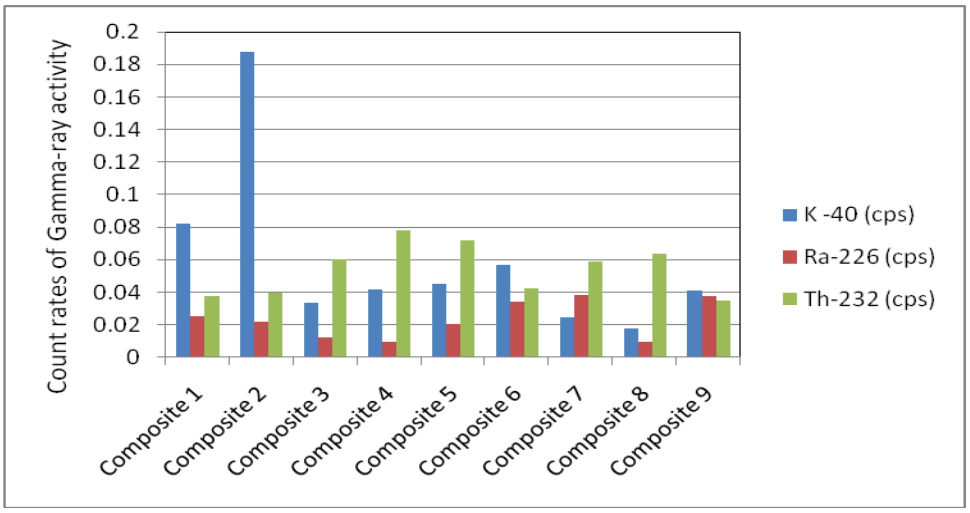


Fig. 4.27: Bar chart of gamma ray activity of U, Th and K of Rock Samples.

4.3.4 Threshold method of data analysis

In the threshold method, high and low activity concentrations are defined statistically as the threshold which is the sum of the mean and standard deviation (*i.e. threshold value = mean + standard deviation*) and any value above the threshold is considered anomalous (Mammoth Geophysical Inc., 2007).

To delineate areas of more prominent radiometric anomalies, the threshold method of analysis is employed as follows:

From table 4.1;

The threshold value for ***uranium*** = mean + Standard deviation.

= 5.534 ppm + 2.062 ppm

= 7.596 ppm

The threshold value (7.6 ppm) was separated from the uranium data and all values above this threshold value are regarded as anomalous. Fig. 4.28 is the map of concentration of uranium above the threshold value after the separation. Anomalous areas of uranium are shown in the upper northeastern ad southwestern parts of the study area.

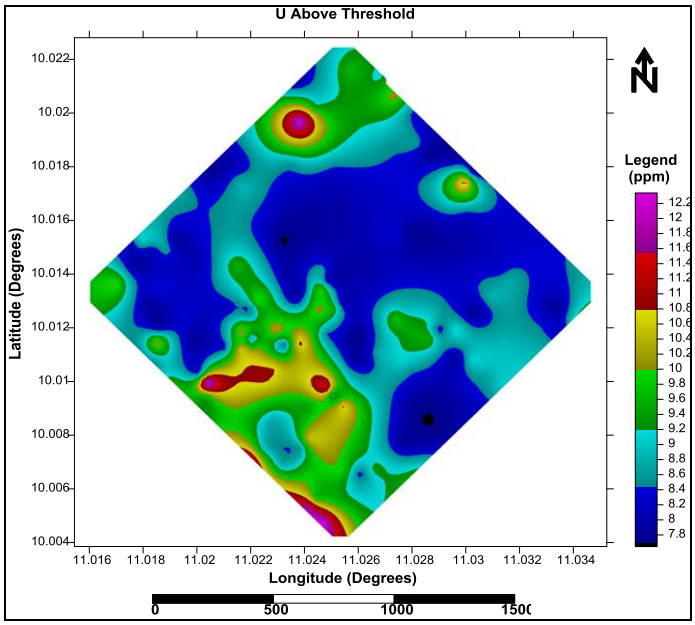


Fig. 4.28: Map of concentration of Uranium after separation of threshold value

Applying the same procedure, the threshold values for the concentrations of thorium and potassium are respectively 21.873 ppm and 0.781 % deduced from Table 4.1. Figs. 4.29 and 4.30 are respectively the maps of thorium and potassium concentrations after the separation

of their threshold values. Anomalous regions are distinctly shown in Figs. 4.28, 4.29 and 4.30.

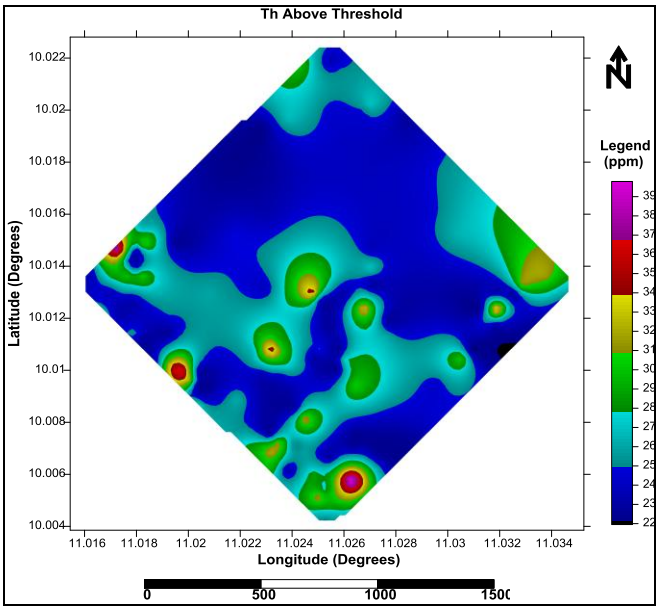


Fig. 4.29: Map of concentration of Thorium after separation of threshold value

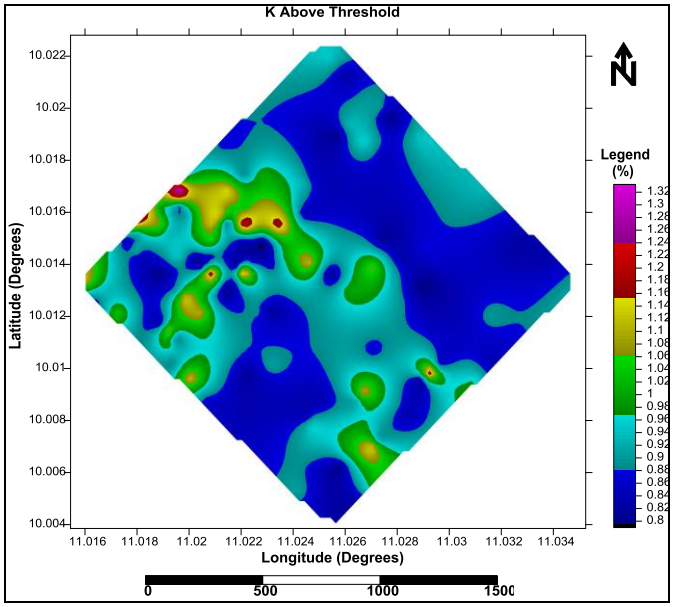


Fig. 4.30: Map of concentration of Potassium after separation of threshold value

According to Ahmed (2006), the most promising area/areas of uranium mineralization are areas of coinciding U above threshold and U/Th ratio. The map of U above threshold (Figure 4.28) and that of U/Th ratio (Figure 4.13) were combined to map out areas of coinciding anomalies. Areas of most promising uranium mineralization are shown in white polygons as presented in Fig. 4.31.

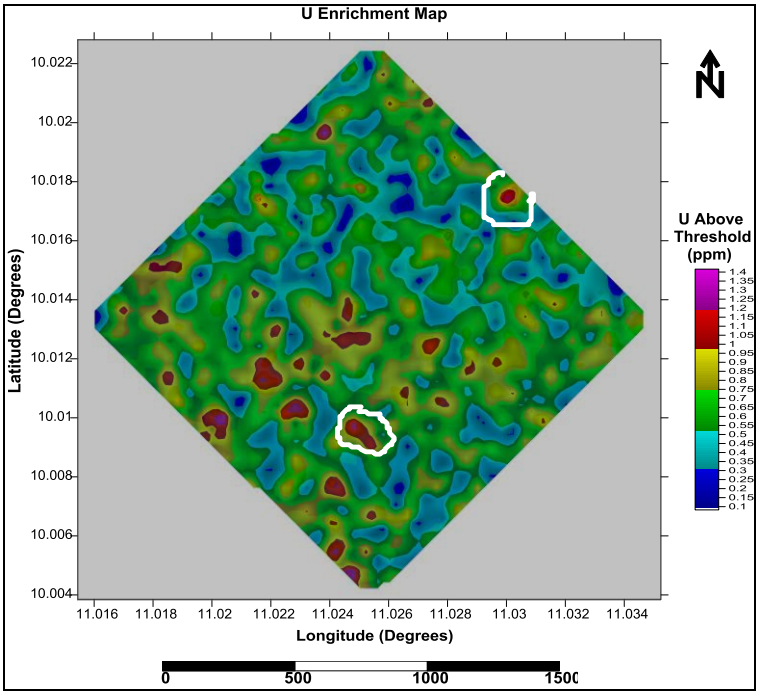


Fig. 4.31: Areas of most promising uranium mineralization

CHAPTER FIVE

DISCCUSSION OF RESULTS

5.1 Interpretation of Data

The task in radiometric interpretation is to interpret and understand the radiometric data in geological terms. This requires the study of geological maps together with radiometric data to establish correlations between the two. The interpretation of gamma ray surveys should therefore be directed towards applying knowledge on the processes that control the distribution of radioelements in rocks and soils to the enhancement and processing of the data (IAEA, 2003). The natural environmental radioactivity in a location depends primarily on its geological and geographical conditions. It is related to the composition of each lithologically separated area and the content of the rock from which the soil originates (Whicker, 1983; Wollenberg and Smith, 1990).

5.1.1 Map assessment

The maps of concentrations of Uranium, Thorium and Potassium after separation of their threshold values (Figs. 4.27, 4.28 and 4.29) have delineated areas of more prominent radioactive anomalies of the radioelements. The Uranium above threshold map (Fig. 4.27) shows concentration of uranium in the northwestern end, northeastern and southwestern parts of the study area. The rocks in the northwestern and southwestern parts were identified as highly weathered ironstones while those in the northeastern part consist of shales. The Thorium above threshold map (Fig. 4.28) shows the concentration of thorium in the southern, western, eastern and central part of the study area. Potassium is concentrated in the western and southeastern parts of the study area (Fig. 4.29).

Uranium distribution actually observed results from five main phenomena: partial melting, magmatic differentiation, and late magmatic processes, hydrothermal and meteoric alterations (Friedrich *et al.,* 1987). Uranium and thorium are generally enriched in the youngest, most

felsic and most potassic members of igneous rocks (Rogers and Adams, 1969). Uranium is a more mobile element than thorium, so if thorium is a very good indicator of the magmatic processes, uranium is a good indicator for the post-magmatic alteration processes (Hatem *et al.,* 2014). Uranium is easily oxidized to a water soluble form and can be readily leached from pegmatites and granites and be deposited in sediments at large distances from the source rock while thorium has no soluble ion and therefore tends to remain with the parent rock or transported over relatively short distances in the form of solid mineral grains (Bristow, 1979; Grasty, 1979 and Urquhart, 1988). The concentration of thorium is higher on high elevated areas as compared to that of uranium as shown in Figs. 4.18 and 4.19.

Thorium (Th) is more resistant to environmental leaching processes than uranium (U) and high Th concentrations are related to felsic minerals while low Th concentrations are related to mafic minerals (Shives *et al*., 1995). The concentration of thorium in the western, eastern, southern and upper southern parts may likely be due to deposition of mafic minerals in the study area during sedimentation.

Potassium radiation essentially comes from K feldspar, predominantly microcline and orthoclase or micas such as muscovite and biotite which are common in felsic igneous rocks (e.g. granite) and are low in mafic rocks (e.g. basalts and andesite) but virtually absent from dunite and peridotites (Manu, 1993). Potassium concentration is observed in the western and southeastern part of the area (Fig. 4.6). This could be associated with the deposition of materials highly rich in feldspar into the lowlands.

The ratio maps presented in Figs. 4.13, 4.14 and 4.15 have clearly revealed the preferential enrichment of thorium to uranium, potassium to thorium and potassium to uranium respectively in the study area.

The strong potassium anomaly is characterized by eTh/K ratio values as in Fig. 4.14. The low eTh/K ratios are excellent indicators of potassium alteration (Shives *et al.,* 1995). Unaltered

lithologies typically reflect the normal ratio of crustal abundances of K and Th. The resulting low eTh/K ratio, as observed in the project area (Fig. 4.14) is a good indicator of potassium anomalies that are of exploration significant from those related solely to lithological variation.

The minerals that carry uranium and thorium are generally associated with felsic intrusions - particularly with younger intrusion; they are found much less frequently in mafic rocks or in volcanic rocks (Grant, 1982). The uranium and thorium content of rock generally increases with acidity, with the highest concentrations found in pegmatites (Grant, 1982).

Unlike the K map, the eU and eTh maps (Figs. 4.4 and 4.5) could not clearly indicate distinct boundaries of the anomalies. The Th channel and Th/K ratio maps were used to assess the degree to which the source materials are weathered or leached since K response is associated with easily weathered minerals, whereas Th and U are typically associated with residual clay, oxides and accessory minerals (Wilford *et al.,* 1997).

The increase in K content and decrease in Th/K ratio observed in the western and southeastern regions is indicative of hydrothermal alterations. This is because K enrichments are not accompanied by Th during hydrothermal alteration processes (Dickson and Scott, 1997). Generally, K and other metal constituents are added to the host rock by hydrothermal solutions, and it is easily observed in mafic units or along lithologic contacts where hydrothermal alteration such as silicification is intensive (Dickson and Scott, 1997). The white portions in the standard ternary image (Fig. 4.11) are indications of high concentration of potassium, thorium and uranium resulting from felsic volcanic materials deposited into the Kerri- Kerri Formation.

There are no clear distinct lithological units in the study area; hence the total gamma ray activity as presented in Figs. 4.3 and 4.25 are radiations coming from the rocks of the area.

5.1.2 Statistical assessment

The mean concentration of U, Th and K for the PGIS–SP data (Table 4.1), are 5.534 ppm, 16.299 ppm and 0.558 % respectively while the mean concentrations of U, Th and K for the rock samples are respectively 2.432 ppm, 15.250 ppm and 0.293 % (Table 4.2). According to UNSCEAR (2000) report, the world average data for ^{238}U, ^{232}Th and ^{40}K in rocks are respectively (33 $Bqkg^{-1}$ = 2.973 ppm), (45 $Bqkg^{-1}$ = 11.084 ppm) and (420 $Bqkg^{-1}$ = 1.342 %). If one compares these values with the results in this study for the rock samples (Table 4.2), the mean concentrations for ^{238}U, and ^{40}K are lower than the world average values while that of ^{232}Th is higher than the world average value.

Ramasamy *et al. (*2004) have listed Th and U concentrations in ppm for some rock forming minerals and igneous rocks; they found that either in rock forming minerals such as quartz, feldspar, biotite, hornblende and olivine from dunite or igneous rocks, thorium levels are relatively higher than uranium levels. In this study, the average thorium concentration for the PGIS-SP data (16.299 ppm) is higher than the average uranium concentration (5.534 ppm). Similarly, the average thorium concentration for the rock samples (15.250 ppm) is higher than that of uranium (2.432 ppm). The bar charts (Figs. 4.25 and 4.26) shows that the activity concentration of the radionuclides are in the order (U < Th < K) for both the PGIS-SP data and rock samples.

The average content of ^{238}U, ^{232}Th and ^{40}K in sedimentary rocks (Table 1.3) ranges from (0.1 to 1.7 ppm), (0.4 to 11.2 ppm) and (0.1 to 2.7%) respectively (Galbraith and Saunders, 1983). In this study, the average content of ^{238}U and ^{232}Th for the PGIS-SP data are above the values stated by Galbraith and Saunders (1983) while that of ^{40}K is within the reported range. A similar trend is obtained for the average content of the radionuclides for the rock samples.

According to Gupta (2001), the standard deviation indicates low degree of uniformity if it is higher than the mean and vice versa. The standard deviation of the concentrations of the radionuclides ^{238}U, ^{232}Th and ^{40}K in this study for both the PGIS-SP data and rock samples

presented in Tables 4.1 and 4.2 are lesser than their mean activity concentrations which indicates a high degree of uniformity.

5.1.3 Activity ratios of the concentrations of the radioelements

The activity ratios (U/Th, Th/K, U/K, Th/U, K/Th and K/U) were calculated and tabulated in Table 4.3 for the PGIS-SP data and Table 4.4 for the rock samples. In this study, U/Th ratio varied from 0.048 to 1.468 with an average of 0.387 for the PGIS-SP data while that for the rock samples varied from 0.124 to 1.098 with an average of 0.510. Powel *et al. (*2007) reported that the average value of U/Th ratio of the upper crust value is 0.8 which is higher than the values obtained in this study. This shows that the concentration of uranium and thorium in the present study are lesser than the normal concentration of uranium and thorium in the upper crust.

Th/U ratio according to Orgun *et al. (*2007) is an indication of the relative depletion or enrichment of the radioisotopes. According to El-Bahi (2003), there is low geochemical mobility of thorium compared to uranium when Th/U ratio is higher than unity which explains a preferential accumulation of ^{232}Th by sediments than ^{238}U. In this study, the mean Th/U ratios for the PGIS-SP data and rock samples are respectively 2.584 and 3.310 which indicates preferential accumulation of ^{232}Th by sediments than ^{238}U in the Kerri - Kerri Formation.

Dheenathayalu *et al. (*2000) and Ramasamy *et al. (*2002; 2004) calculated K/U and K/Th for crustal rocks and obtained K/U to be higher than K/Th. A similar trend is obtained for the rock samples (Table 4.4) in this work with mean values of K/U and K/Th to be 3.920 and 1.791 respectively.

5.1.4 Correlations between activity concentrations of the radionuclides

From the statistical analysis, the correlation coefficients between (^{238}U and ^{232}Th), (^{238}U and ^{40}K), and (^{232}Th and ^{40}K) are all weak for both the PGIS-SP data (Table 4.5) and rock samples (Table 4.6). It is expected that the correlation between (^{238}U and ^{232}Th) should be very good since both ^{238}U and ^{232}Th came from natural decay series whereas ^{40}K, although a naturally occurring radionuclide, is not part of any such decay series (Rajesh *et al.,* 2013).

Lima *et al. (*2005) have obtained a strong correlation (r = 0.9) between ^{238}U and ^{232}Th for rock samples. Also, they reported that, this strong correlation indicates the presence of significant amount of radioactive accessory minerals such as zircon, monazite, thorite and garnet. In this study, the weak correlation (0.30) between ^{238}U and ^{232}Th for the PGIS-SP (Table 4.5) and negative correlation (-0.63) between ^{238}U and ^{232}Th (Table 4.6) indicates the absence of these accessory minerals. However, a positive correlation may still be attributed to the property of the rock in retaining these radionuclides under varying weather conditions.

Weak correlations exists between (^{232}Th and ^{40}K) and (^{238}U and ^{40}K) with correlation coefficients of 0.24 and 0.31 respectively (Table 4.5). This indicates that ^{40}K concentrations may not be related with the presence of ^{232}Th and ^{238}U bearing minerals. The same type of weak correlations between these radionuclides was also reported by Mohanty *et al. (*2004).

5.1.5 Absorbed dose rate

It is of great importance to assess the hazards to human beings due to radiation of radionuclides in the environment. The statistics of the absorbed dose rates which were automatically computed and recorded by the PGIS-SP from the concentrations of the radioelements and that calculated using the conversion factor given by Ramasamy *et al. (*2010) for the rock samples as earlier discussed in section 4.4 were presented in Tables 4.1 and 4.2 respectively.

The absorbed dose rate in the study area varied from 7.849 nGyph^{-1} to 28.777 nGyph^{-1} with an average value of 15.646 nGyph^{-1} for the PGIS data while that of the rock samples varied

from 44.865 $nGyph^{-1}$ to 63.738 $nGyph^{-1}$ with an average value of 53.693 $nGyph^{-1}$. The average absorbed dose rate for the study area is lower than the world average value of 60 $nGyph^{-1}$ (UNSCEAR, 2000).

CHAPTER SIX

CONCLUSIONS AND RECOMMENDATIONS

6.1 Conclusions

From the analysis of the maps, the most promising areas of uranium mineralization are revealed as presented in Fig. 4.30 which is located in the northeastern end and upper southern part of the study area. The correlation between topography and the concentration of the radioelements presented in Figs. 4.18, and 4.19 have shown a trend of higher concentrations of ^{232}Th at higher elevations.

The potassium concentration map (Fig. 4.10) for the rock samples collected has a better correlation with the potassium concentration map (Fig. 4.6) for the PGIS-SP as compared to that of U and Th. Even though the correlation coefficient between the concentrations of the radioelements is weak, there seems to be a correlation in the concentration of the radio – elements uranium, thorium, potassium and the absorbed dose rate with topography of the area. On the basis of low levels of natural radioactivity, the study area which is part of the Kerri–Kerri Formation can be considered as a less natural background radiation hazard area. It is concluded that the activity of the rocks of the study area has no harmful radiation effects to people and environment. Results from statistics and map analysis have shown that the concentration of potassium is higher compared to uranium and thorium which is of great advantage to agriculture in the study area.

For an activity to be of significance in terms of radioelement mineralization, it must be higher than the observed mean activity of the area (Uwah and Ajakaiye, 1992), and the most probable area of uranium mineralization is the area of coinciding eU and eU/eTh anomalies. These two quantities are the major indices in the interpretation of radiometric data in an area of high potassium concentration as in the present area of study.

For any of the radio - elements to be extracted economically, they have to be located where they have already been concentrated by geological processes to many times the average figures given in Table 1.3. According to Darnley (1972), this must be about 250 times the average content in normal rock and in addition their ratios must reflect preferential enrichment of the particular element to the others (Uwah, 1984). Results of the data analysis and interpretation in this study have shown that the enrichment of uranium, thorium and potassium did not satisfy the condition for the radio-elements to be extracted economically.

This investigation has revealed that:

i. The mean concentrations of the radionuclides uranium (U), thorium (Th) and potassium (K) in the Study area are respectively 5.534 ppm, 16.299 ppm and 0.558 % for the PGIS-SP while that for the rock samples collected are respectively 2.432 ppm, 15.250 ppm and 0.293 % which are within the world average values.

ii. Areas of most promising uranium mineralization are in the northeastern edge of the study area consisting of shales and upper southern part consisting of highly weathered ironstones.

iii. The concentration of the radionuclides ^{238}U, ^{232}Th and ^{40}K in the study area are in the order (U < Th < K) which indicates preferential enrichment of potassium to both uranium and thorium.

iv. The average absorbed dose rate obtained in this study is below the world average value. On the basis of low levels of natural radioactivity, the study area can be considered as a less natural background radiation hazard area. The radioactivity of the rocks of the study area are therefore not harmful to human beings and the environment.

v. There is occurrence of uranium, thorium and potassium in the study area as suggested by Oshin (1986) and observed on the Ternary image map of Gombe Sheet 152 SW. (NGSA, 2007) but of no economic value.

6.2 Recommendations

Results of this investigation have confirmed the occurrence of uranium mineralization in the Kerri–Kerri Formation which is of no economic value and that potassium is the major source of radioactivity in the area.

Other geophysical methods, such as radiological logging, ground magnetics, mineralogical and geochemical analysis of the rocks of the area can be carried out to complement the findings from this work and give a complete account of uranium and allied mineral potentials of the area.

With the dwindling fall in oil price globally, the Federal Government of Nigeria, State Governments and all stake holders in mining and exploration of solid minerals need to gear up. There is need for more research in the exploration of solid mineral resources in all the states of the federation to boost our economy.

Radiometric surveys are expensive hence government should provide more funding to institutions and other agencies for conducting radiometric investigations so as to provide credible and reliable data for investors.

REFERENCES

Adegoke, O. S., Agumanu, A. E. and Ajayi, P. O. (1986). New Stratigraphic, sedimentologic and structural data on the Kerri - Kerri Formation, Bauchi and Borno States, Nigeria. *Journal of African Earth Sciences, Vol. 5, pp 249-277.*

Abdul-Razek, Y. A., Abu-Diab, A. A. and Bakhit, A. F. (2013). Correlation between the Concentrations of the Heavy Minerals and the Terrestrial Radioactivity at El Massaid and El Kharrouba, Sinai, Egypt. Retrieved from *http://www.rphysp.com/presentation11/session1/correlation.pdf*.

Abdullahi M. (2013). Gamma ray spectrometry of naturally radioactive materials for Birrnin Gwari. Artismal Goldmine of Kaduna State. *Unpublished M.Sc Thesis, Department of Physics, Ahmadu Bello University, Zaria.*

Ahmed, A. L. (1998). Gamma ray Spectrometry and Radon Emanometry in the Detection of Groundwater Associated with Fault Zones. *A Seminar Paper Presented to the Department.of Physics, Ahmadu Bello University, Zaria.*

Ahmed, A. L. (2006). Detailed Radiometric Surveys of the Albite Riebeckite Granites of Dutsen - Wai Ring Complex, Kaduna State Northern Nigeria. *Unpublished Ph.D. Thesis, Department of Physics, Ahmadu Bello University, Zaria.*

Arabi A. S., Funtua I. I., Dewu, B. B. M., Alagbe, S. A., Kwaya, M. Y., Garba, M. I. and Baloga, A. D. (2012). Activity concentration of uranium in groundwater from uranium mineralized areas and its neighbourhood. *Journal of radiological and nuclear chemistry. DOI 10.10007/s1096-012-1957-x*

Arabi A. S., Funtua, I. I., Dewu, B. B. M. and Muhammad A. M. (2015). Background radiological hazard associated with local building materials around Zaria, Nigeria. *Radiochemistry*, Vol. 57, No. 2, pp 207-212.

Ayodeji, A., Adetayo, A., Dauda, A., Omowumi, O., Isiaka, O. O. and Pascal, T. (2011). Basement data of the Terrestrial Radionuclide level of Abuja, Federal Capital Territory (FCT), Nigeria. *Journal of Environmental Protection*, Vol. 2, pp 359-364.

Baretta, P. M. (1981). Recent Development in Uranium Exploration. *International Atomic Energy Agency (IAEA) Bulletin, Vol. 23, No. 2;* pp 15 – 20.

Bowden, P., Van=Breeman, O., Hutchison, J. and Turner, D. C. (1981). Paleozoic and Mesozoic Age trends for Some Ring Complexes in Niger and Nigeria. Reprinted from *Nature. Vol. 259, No 5541;* pp 297 – 299.

Bowie, S. U. H. (1970). Some Geological Concepts for Consideration in the Search for Uranium Provinces and Major Uranium Deposits. *Uranium Exploration Geology,* International Atomic Energy Agency *(IAEA), Vienna;* pp 16 – 39.

Bowie, S. H. U. and Cameron, J. (1976). Existing and New Techniques in Uranium Exploration. In Exploration for Uranium Ore Deposits. *IAEA, Vienna;* pp 3 – 13.

Bristow, Q. (1979). Gamma Ray Spectrometric Methods in Uranium Exploration - Airborne Instrumentation in Geophysics and Geochemistry in the Search for Metallic Ores (P.J. Hood, ed.), *Geological Survey of Canada, Economic Geology Report 31*, pp 135-146.

Bute, S. I. (2013). Uranium ore deposits in Northeastern Nigeria: Geology and Prospect. *Continental Journal of Earth Science 01/2013; 8(1)*:21-28. DOI: 10.5707/cjearthsci.2013.8.1.21.28.

Carter, J. D., Barber, W., Tait, E. A. and Jones, G. P. (1963). The Geology of Parts of Adamawa, Bauchi and Bornu Provinces in Northeastern Nigeria. *Geological Survey of Nigeria, Bulletin No. 50.*

Crossley, D. J. and Reid, A. B. (1982). Inversion of Gamma Ray Data for Element Abundances. *Geophysics Vol. 47. No 1;* pp 117 -126.

Dada, S. S., Dandume, S. G. and Binyoti, F. (1982). Central Nigeria Mineral Exploration Project. *Nigerian Mining Corporation Report No.10,* pp 6-23.

Darnley, A. G. (1972). Airborne Gamma Ray Survey Techniques. In Bowie *et al. (*Editors), Institute of Mining and Metallurgy, London. *Uranium Prospecting Handbook;* pp 174 – 211.

Darnley, A. G. (1973). Airborne Gamma Ray Survey Techniques - Present and Future. *Uranium Exploration Methods. IAEA, Vienn,;* pp 67 – 108.

Dewu, B. B. M. (1986). A geophysical Ground Follow – up to an Aeroradiometric Anomaly at Bisichi Area of Plateau State, Nigeria. *Unpublished M.Sc. Thesis, Department of Physics, Ahmadu Bello University, Zaria;* pp 1 - 85

Dewu, B. B. M. (1989). Distribution of Uranium in Granites and Mobility of Uranium during Low Temperature Alteration Processes. *Unpublished Ph.D. Thesis, University of Exeter, U.K.;* pp 63-98.

Dheenathayalu, M., Arumugam, M. and Ramasamy, V., (2000) *ActaCienc. Indica*, XXVII p 179. [In Rajesh, P., Joseph, S. V., Ramasmy, V. and Meenakshisundaram, V. (2013)].Measurement of level of natural gamma emitting radionuclides in charnockite rocks of Kalrayan Hills, India. *Archives of Applied Science Research, Vol. 5 (2),* pp278-286.

Dickson, B. L., Christianson, E. M. and Luborg, L. (1982). Reference Material for Calibration of Laboratory Gamma ray Analysis. *Uranium Exploration Methods. IAEA, Vienna;* pp 682 – 698.

Dickson, B. L. and Scott, K. M. (1997). Interpretation of Aerial Gamma ray Surveys - adding the Geochemical Factors. *AGSO Journal of Australian Geology and Geophysics,* 17 (2); pp 187 - 200.

Dike, E. F. C. (1993). Stratigraphy and structure of the Kerri - Kerri Basin, Northeastern Nigeria. *Journal of Mining and Geology, Vol.29, pp 77-93.*

Dodd, P. H. (1977). Uranium Exploration Technology. *Institute of Mining and Metallurgy Symposium, London;* p 158.

Doig, R. (1968). The natural Gamma ray flux: In – Situ Analysis. *Economic Geology, Vol. 33,* pp 311 – 330.

Duval, J. S. (1979). Aerial Gamma ray Survey in Duval. Liveok, Texas. *United States Geological Survey Professional Paper 1122D.*

Drury, S. A. (1992). Image interpretation in Geology 2nd Edition, *Allen and Unwin, London,* p 253.

El-Bahi, S. M. (2003).-Assessment of radioactivity and radon exhalation rate in Egyptian cement. *Applied Radiation and Isotopes,* 58(1), 143-148.

Evans, R. D (1955). The Atomic Nucleus. *McGraw Hill Book Comp, USA.*pp 83-87.

Fenyves, E. and Haiman, O. (1969). The Physical Principle of Nuclear Radiation Measurements. *Academic, New York;* p 256.

Friedrich, M, Cuney, M. and Poty, B. (1987). Uranium Geochemistry in Peraluminous Leucogranites. *Uranium Vol. 3;* pp. 353 – 385.

Gana, J. S. (2011). Detailed Radiometric Survey of Igboho/Igbope Area in 1:100,000 Sheet 200 (Igboho), of Oyo State. Nigerian Geological Survey Agency (NGSA) Survey Report: pp 21 – 22.

Galbraith, J. H. and Saunders, D. F. (1983). Rock Classification by Characteristics of Serial Gamma Ray Measurements. *Journal of Geochemical Exploration. Vol. 18, No. 1;* pp 49-73.

Gascoyne, M. (1977). A Simple Method of Uranium Extraction from carbonate Ground Water and its Application to U^{234}/U^{238} Disequilibrium Studies. *Geochemical Exploration Vol. 14;* pp 199 – 207.

Grant, F. S (1982). Gamma Ray Spectrometry for Geological Mapping and for Prospecting, in Mining Geophysics. *Workshop by Paterson Grant and Watson Limited*

.

Grasty, R. L. (1975). Uranium Measurements by Airborne Gamma ray Spectrometry. *Geophysics, Vol. 40, No. 3;* pp 503 – 519.

Grasty, R. L. (1979). Gamma Ray Spectrometric Methods in Uranium Exploration - Theory and Operational Procedures; in Geophysics and Geochemistry in the Search for Metallic Ores (P.J. Hood, ed.), *Geol. Survey of Canada, Economic Geology Report* 31, pp 147-161.

Gupta, S.P. (2001). "Statistical methods", *Sultan Chand and Sons, Educational Publishers,* New Delhi, pp 54-61.

Handloser, J. S. (1959). Health Physics Instrumentation. *Pergamon, New York;* p 338.

Hansen, D.A (1980). Radiometric Ch. 1 in Practical Geophysics for the Exploration Geologist, R. Van Blairicom, Ed., *Northwest Mining Association, Spokane, Washington., U.S.A.*, p 1038.

Haq B. U., Hardenbol J. and Vail P. R. (1988). Mesozoic and Cenozoic Chronostratigraphy and Cycles of Sea Level Change, in Sea Level Change: an Integrated Approach to Social Economics (C. K. Wilgus *et al.*, Ed.), *Paleontologists and Mineralogists Special Publication*. 42; 71–108.

Hatem A., Emad H. and Haytham S. (2014). Mapping of Structurally Controlled Uranium Mineralization in Kadabora Granite, Central Eastern Desert, Egypt Using Remote Sensing and Gamma Ray Spectrometry Data. *The Open Geology Journal, 8, (Suppl 1: M4),* pp. 54-68.

Hayashi, S. (1970). Uranium Occurrences in Small Sedimentary Basin in Japan. *Uranium Exploration Geology, IAEA, Vienna;* pp 235 – 241.

Heath, R. L. (1969). Gamma Ray Spectrometry and Automated Data Analyses System for Activation Analysis. *National Bureau of Standards (U.S.A.) Special Publication;* p 312.

IAEA Technical Report Series (1979). Gamma ray surveys in Uranium Exploration. *IAEA Report No.186.*

IAEA Technical Report Series (2003). Guidelines for Radioelement Mapping Using Gamma Ray Spectrometry Data. *IAEA – Technical Document No.* 1363.

Kehinde, L. O., Oluwole, A. R., Oshin, I. O. and Fleming, R. (1983). Assay of Nigerian Uranium by passive gamma ray spectrometry. *International journal of Applied Radiation and Isotopes, Vol. 34, No. 6,* pp 936-937.

Lenntech (2013). Chemical Properties and Applications of Uranium. Retrieved from *http://www.lenntech.com/index.htm on 11/09/2013*

Levinson, A.A. (1974). Introduction to Exploration Geochemistry. *Applied Publishing Ltd: Maywood Illinois;* p 614.

Lima, A., Albanese, S. and Cicchella, D. (2005). Background and baseline concentration values of harmful elements in the volcanic soils of metropolitan and provincial areas of Napoli (Italy). *Applied Geochemistry*, Vol. 20, pp 611-625.

Lovborg, L., Wollenberg, H., Sorensen, P. and Rose–Hansen, J. (1971). Field Determination of Uranium and Thorium by Gamma ray Spectrometry. Exemplified by Measurements in the Ilimaussag Alkaline Intrusive, South Greenland. *Economic Geology, Vol. 66;* pp68 – 378.

Mammoth Geophysical Incorporated (2007). Geophysical Exploration, Oil and Gas Field, Barraackville, West Virginia. *Technical Report,* (304) 355-1810

Manu, J. (1993). Gold deposits of Birimian Greenstone Belts in Ghana: Hydrothermal Alteration and Thermodynamics. *Verlag Mainz Susterfeld Str.Vol.* 83, p 52072 Aachen.

McDermott, A. (1977). "Field Experiments with Exploration Model GR- 101A". *Geometrics Exploranium Model GR-101A Users Manual;* p 10.

Mohanty, A. K., Sengupta, D., Das, S. K., Saha, S. K., and Van, K. V. (2004). Natural radioactivity in the newly discovered high background radiation area on the eastern coast of Orissa, India, *Journal of Environmental Radioactivity*, Vol. 38, pp 153–165.

Morce, J. G. (1977). Nuclear Methods in Mineral Exploration and Production. *Elsevier Scientific Publishing Company, Amsterdam, Oxford, New York.*

NGSA (2004). Geological map of Nigeria. A compilation by Nigerian Geological Survey Agency, 2004 Edition.

NGSA (2006). Lineaments map of Nigeria. A compilation by Nigerian Geological Survey Agency. 2006 Edition.

NGSA (2007). Airborne radiometric image map of Gombe Sheet 152 SW. *A progress report by* Nigerian Geological Survey Agency, 2006.

OECD and IAEA (1979). "Uranium Resources, Production and Demand". *A Joint Report by Organisation for Economic Cooperation and Development (OECD) and* International Atomic Energy Agency *(IAEA),* pp 63-69.

Odedede O. and Adaikpoh E. O. (2011). Sequence Stratigraphic Analysis of the Gombe Sandstone and lower Kerri–Kerri Formation Exposed Around Fika-Potiskum, Upper Benue Trough, Nigeria: A Consideration for Petroleum Reservoir Indicators. *Indian Journal of Science and Technology, Vol. 4*; *pp 492 – 498.*

Olabode, S. O., Adekoya, J. A. and Ola, P. S. (2015). Distribution of sedimentary formations in the Borno Basin, Nigeria. *Petroleum Exploration and Development, Vol. 42 (5), pp. 674-682.*

OnlineNigeria.com (2015) Physical Setting of Gombe State Retrieved October 20th 2015 from *http://links.onlinenigeria.com/gombeadv.asp?blurb=262*

Orgun, Y., Altinsoy, N., Sahin, S.Y., Gungor, Y., Gultekin, A.H., Karaham, G. and Karaak, Z. (2007). Activity Concentrations of Natural Radionuclides in Soils of Rainforest Sites in Western Ghats. *Applied Radiation and Isotopes, Vol.* 65, pp 739-747.

Oshin, I. O. (1986). Uranium Favourability Study in Nigeria. *Journal of African Earth Sciences, Vol. 2;* pp 175-175.

Ouseph, P. J. (1975). Introduction to Nuclear Radiation Detectors. *Plenum Press, New York, Vol.2.*

Parker, A. and Ruziicka, V. (1979). A Genetic Classification of Uranium Deposits. *International Geological Congress Report, Montreal,* pp 42 – 87.

.

PEI (2006). Pico Envirotec Inc. - Portable Ground Information System–Spectrometer (PGIS-SP). *User Manual Version 1.1.6.*

Powell, B.A., Hughes, L.D., Soreefan, M. A., Deborah F., Michaal W. and Devol, T. A. (2007). Elevated concentrations of primordial radionuclides in sediments from the Reedy River and surrounding creeks in Simpsonville, South Carolina. *Journal of Environmental Radioactivity*, Vol. 94 (3), pp 121-128.

Price, W. J. (1964). Nuclear Reaction Detection. (2nd ed), *McGraw-Hill, San Francisco,* pp 25-31.

Rajesh P., Joseph S. V., Ramasamy V. and Meenakshisundaram V. (2013). Measurement of level of natural gamma emitting radionuclides in charnockite rocks of Kalrayan Hills, India.*Archives of Applied Science Research*, No. 5 (2):278-286.

Ramasamy V., Dheenathayalu M., Meenakshisundaram V. and Ponnusamy V. (2002). Gamma ray spectroscopic analysis of biotite granites. *Current Science*, 83(9), pp 1124 – 1128.

Ramasamy V., Dheenathayalu, M., Ravisankar, R., Ponnusamy, V., Victor, R. G., DajKumar, S., Meenakshisundaram, V. and Gajendran, V. (2004). Natural radioactivity measurements in beach-rock samples of southeast coast of Tamilnadu, India. *Radiation Protection Dosimetry*, 111 (2), 229-235.

Ramasamy, V., Suresh, G., Meenakshisundaram, V. and Ponnusamy, V. (2010). Distribution and characterization of minerals and naturally occurring radionuclides in river sediments of Ponnaiyar, India. *Carpathian Journal of Earth and Environmental Sciences,* 5 (1), pp 41- 48.

Reedman, J. H. (1979). Techniques in Mineral Exploration. *Applied Science Publishers Ltd., Ripple Road, Barking, Essex, England,* pp 42 – 154.

Rich, R. A., Holland, H. D. and Peterson, U. (1972). Hydrothermal uranium Deposits. *Elsevier;* pp 26 – 30.

Robert D. N. (1954). The Uranium Ore Minerals. *Van Nostrand Company, Inc., New York;* pp 10 – 11.

Roberts, W.L., Rapp, G. R. (Jr) and Webber, J. (1974). Encyclopedia of Minerals, *Van Nostrand Reinhold Company;* p 63.

Rogers, J. W. and Adams, J. A. S. (1969). Uranium. *Handbook of Geochemistry, Springer - Verlag: Berlin (4).*

Rosholt, J. N. (1959). Natural Radioactive Disequilibrium of the Uranium Series. *U.S. Geological Survey Bulletin 1084;* pp 73 – 81.

Shives, R. B. K., Ford, K. L. and Charbonneau, B. W. (1995). Applications of Gamma ray Spectrometry/Magnetic/VLF–EM Surveys, Workshop Manual; *Geological Survey of Canada, 3061,* p 82.

Smith, A. R. and Wollenberg, H. A. (1972). High Resolution Gamma ray Spectrometry for Laboratory Analysis of the Uranium and Thorium decay Series. *U.S. ERDA Conference Report 20805;* pp 2 – 10.

Soonawalla, N. M. (1974). Data Processing Techniques for the Radon Method of Uranium Exploration. *Canadian Institute of Mining Bulletin, Vol. 67;* pp 110 – 116.

Stanley, H. W. (1990). Geotechnical and Environmental Geophysics. (Ed) *Society of Exploration Geophysics, Vol. 1,* pp 219-261.

STI/PUB (Scientific and Technical Publications) (2001). "Analysis of Uranium Supply to 2050". *Technical Report Series, 1104*, pp 1-7.

Suzanne H. (2011). A Review on Ternary Image Maps; Retrieved from *(http://spatial.agric.wa.gov.au/geophysics/radiometrics.asp)*

Taiwo A. O., Adeyemo D. J., Sadiq U. and Bappah I. A. (2014). Determination of external and internal hazard indices from natural occurring radionuclides around a superphosphate fertilizer factory in Nigeria. *Archives of Applied Science Research, 2014, 6 (1):23-27.*

Titayeva, N. A, Taskayev, A. I, Ovchenkov, V, Aleksakin, R. M. and Shirktomova, I. I. (1973). Behaviour of Uranium and Thorium isotopes in Crystalline Rocks and Surface Waters in a Cold Climate. *Geochemical Internet. No. 10;* pp 1146 – 1151.

Tukel A. Karakus, Y. and Kahriman, A. (2009). Importance of Thorium as Alternative Energy Source and the Role of Turkey. 9th International Multidisciplinary Scientific GeoConference. *SGEM 2009 Conference Proceedings, ISBN 10: 954-91818-1-2, Vol. 2;* pp 429 – 430.

UMMC (2013). Importance of potassium. Retrieved from University of Maryland Medical Centre (UMMC): website: *http://medschool.umaryland.edu/*

UNSCEAR (2000). United Nations Scientific Committee on Effect of Atomic Radiation. Sources and Effects of Ionizing Radiation. *Report to General Assembly, with Scientific Annexes, United Nations, New York.*

Urquhart, W. E. S. (1988). Airborne Gamma Ray Spectrometry Surveys. A Paper presented at the 55th *Annual Meeting of SEG, Anaheim*, October, 1988.

Urquhart, W. E. S. (2009). Airborne Gamma ray Spectrometry Surveys. *Geo Exploration Ltd., Santiago, Chile.*

Uwah, J.E. (1984). "Investigation of Radiometric Anomalies by Nuclear and Other Methods: A Case Study of the Sokoto Basin of Nigeria". *Unpublished Ph.D. Thesis, Department of Physics, Ahmadu Bello University, Zaria.*

Uwah, J. E. and Ajakaiye, D. E (1992). Ground Radiometric Reconnaissance Survey in Sokoto Basin of Nigeria *Journal of Mineral .and Geology, Vol.28, No 1 pp 135-140*

Whicker, F.W. (1983). Radionuclide Transport Processes in Terrestrial Ecosystems, *Radiation Research*, Vol.94, pp.135-150.

Wilford, J. R., Bierwirth, P. N. and Craig, M. A. (1997). Application of Airborne Gamma Ray Spectrometry in Soil/Regolith Mapping and Applied Geomorphology. *Journal of Australian Geology and Geophysics, 17(2)*, pp 201–216.

Wilkes, P. G. (1981). Acquisition, Processing and Interpretation of Airborne Gamma ray Spectrometry Data. *Bureau of Mineral Resources and Mining, Geology and Geophysics, Report 186*, pp 48 – 49.

Wollenberg, H.A. and Smith, R.A. (1990). A Geochemical Assessment of Terrestrial Gamma Ray Absorbed Dose Rates. *Health Physics,* Vol.58, pp 183-189.

Wooley, A. (1978). (Editor). The Illustrated Encyclopedia of the Mineral Kingdom, *Hamlyn Publication Company,* p 240.

Zaborski P., Ugoduluwa F., Idornigie A., Nnabo P. and Ibe K. (1997). Stratigraphy and Structure of the Cretaceous Gongola Basin, Northwest Nigeria. Bulletin De Centre des Recherché Exploration Production Elf–Aquitaine, 21, pp 153–186.

APPENDICES

Appendix I: Background readings taken in the Pond and Dadin - Kowa Dam

Day/Date of Survey	Background Readings (cps)					
	Pond in the Study Area			Dadin-Kowa Dam		
	Morning	Evening	Average	Morning	Evening	Average
Mon. 06/05/2013	4.0	4.0	4.00	3.50	4.00	3.75
Tue. 07/05/2013	4.0	5.0	4.50	-	-	-
Wed. 08/05/2013	5.0	3.0	4.00	-	-	-
Thur.09/05/2013	4.0	3.0	3.50	-	-	-
Fri. 10/05/2013	3.0	4.0	3.50	-	-	-
Sat. 11/05/2013	4.0	4.0	4.00	-	-	-
Mon. 13/05/2013	4.0	5.0	4.50	-	-	-
Tue. 14/05/2013	5.0	3.0	4.00	-	-	-
Wed. 15/05/2013	5.0	3.0	4.00	-	-	-
Thur.16/05/2013	3.0	4.0	3.50	4.00	3.50	3.75
Average	4.1	3.8	3.95	3.75	3.75	3.75

Appendix II: Corrected Scintillometric Data

S/No	Longitude				Latitude				Tot. Count.
	(Deg.)	(Min.)	(Sec)	Converted	(Deg.)	(Min.)	(Sec)	converted	(cps)
1	10	1	8.0	10.0188889	11	2	36.8	11.04355556	20
2	10	1	3.6	10.0176667	11	2	37.7	11.04380556	25
3	10	1	7.4	10.0187222	11	2	40.8	11.04466667	30
4	10	1	8.5	10.0190278	11	2	45.7	11.04602778	20
5	10	1	13.6	10.0204444	11	2	47.4	11.04650000	30
6	10	1	19.4	10.0220556	11	2	44.6	11.04572222	25
7	10	1	23.9	10.0233056	11	2	39.8	11.04438889	20
8	10	1	31.6	10.0254444	11	2	33.3	11.04258333	20
9	10	1	31.7	10.0254722	11	2	26.2	11.04061111	25
10	10	1	46.4	10.0295556	11	2	17.8	11.03827778	20
11	10	1	54.0	10.0316667	11	2	10.9	11.03636111	20
12	10	1	59.7	10.0332500	11	2	4.5	11.03458333	15
13	10	2	0.0	10.0333333	11	2	0.5	11.03347222	15
14	10	2	6.3	10.0350833	11	2	58.4	11.04955556	25
15	10	2	5.1	10.0347500	11	2	57.0	11.04916667	30
16	10	2	4.4	10.0345556	11	2	54.9	11.04858333	20
17	10	2	3.3	10.0342500	11	2	51.3	11.04758333	20
18	10	2	2.6	10.0340556	11	2	50.1	11.04725000	20
19	10	2	1.3	10.0336944	11	2	45.9	11.04608333	25
20	10	2	1.1	10.0336389	11	2	43.3	11.04536111	20
21	10	2	1.7	10.0338056	11	2	41.1	11.04475000	20
22	10	2	1.1	10.0336389	11	2	38.7	11.04408333	20
23	10	2	1.1	10.0336389	11	2	36.8	11.04355556	25
24	10	2	2.2	10.0339444	11	2	34.4	11.04288889	25
25	10	2	2.4	10.0340000	11	2	31.2	11.04200000	20
26	10	2	2.6	10.0340556	11	2	23.0	11.03972222	20
27	10	2	2.7	10.0340833	11	2	22.8	11.03966667	25
28	10	2	5.1	10.0347500	11	2	19.6	11.03877778	25
29	10	2	6.7	10.0351944	11	2	16.8	11.03800000	25
30	10	2	7.6	10.0354444	11	2	13.3	11.03702778	20
31	10	2	10.5	10.0362500	11	2	9.9	11.03608333	25
32	10	2	14.2	10.0372778	11	2	5.9	11.03497222	20
33	10	2	26.9	10.0408056	11	2	0.8	11.03355556	20
34	10	2	26.9	10.0408056	11	2	1.7	11.03380556	20
35	10	2	32.6	10.0423889	11	2	3.3	11.03425000	15
36	10	2	34.9	10.0430278	11	2	4.2	11.03450000	20
37	10	2	35.1	10.0430833	11	2	4.8	11.03466667	20
38	10	2	31.2	10.0420000	11	2	9.6	11.03600000	25

Tot.

S/No	Longitude				Latitude				Count.
	(Deg.)	(Min.)	(Sec)	Converted	(Deg.)	(Min.)	(Sec)	converted	(cps)
39	10	2	15.3	10.0375833	11	2	23.2	11.03977778	25
40	10	2	11.1	10.0364167	11	2	23.4	11.03983333	20
41	10	2	5.3	10.0348056	11	2	33.1	11.04252778	25
42	10	2	6.8	10.0352222	11	2	42.4	11.04511111	20
43	10	2	6.7	10.0351944	11	2	43.7	11.04547222	30
44	10	2	41.6	10.0448889	11	3	19.3	11.05536111	20
45	10	2	40.8	10.0446667	11	3	18.0	11.05500000	20
46	10	2	39.9	10.0444167	11	3	20.8	11.05577778	30
47	10	2	2.5	10.0340278	11	3	13.6	11.05377778	20
48	10	2	2.4	10.0340000	11	3	21.8	11.05605556	20
49	10	1	52.0	10.0311111	11	3	30.6	11.05850000	25
50	10	2	5.0	10.0347222	11	3	34.8	11.05966667	25
51	10	2	7.9	10.0355278	11	3	38.9	11.06080556	25
52	10	2	10.7	10.0363056	11	3	44.1	11.06225000	20
53	10	2	10.4	10.0362222	11	3	48.4	11.06344444	20
54	10	2	12.8	10.0368889	11	3	50.3	11.06397222	20
55	10	2	14.9	10.0374722	11	3	53.6	11.06488889	15
56	10	2	15.8	10.0377222	11	3	57.4	11.06594444	20
57	10	2	17.4	10.0381667	11	4	2.8	11.06744444	15
58	10	2	20.6	10.0390556	11	4	9.5	11.06930556	25
59	10	2	24.3	10.0400833	11	4	13.5	11.07041667	20
60	10	2	25.7	10.0404722	11	4	16.6	11.07127778	15
61	10	2	25.2	10.0403333	11	4	16.8	11.07133333	25
62	10	2	28.9	10.0413611	11	4	18.3	11.07175000	30
63	10	2	30.7	10.0418611	11	4	19.1	11.07197222	20
64	10	2	32.1	10.0422500	11	4	14.4	11.07066667	25
65	10	2	32.2	10.0422778	11	4	13.4	11.07038889	15
66	10	2	32.0	10.0422222	11	4	9.7	11.06936111	25
67	10	2	31.5	10.0420833	11	4	7.9	11.06886111	20
68	10	2	31.4	10.0420556	11	4	6.6	11.06850000	25
69	10	2	29.6	10.0415556	11	4	1.9	11.06719444	20
70	10	2	25.8	10.0405000	11	3	57.5	11.06597222	20
71	10	2	23.5	10.0398611	11	3	55.5	11.06541667	20
72	10	2	22.9	10.0396944	11	3	52.4	11.06455556	20
73	10	2	27.8	10.0410556	11	3	48.6	11.06350000	20
74	10	2	24.8	10.0402222	11	3	34.2	11.05950000	20
75	10	2	24.7	10.0401944	11	3	31.0	11.05861111	20
76	10	2	20.6	10.0390556	11	3	20.0	11.05555556	20
77	10	2	19.5	10.0387500	11	3	16.8	11.05466667	25
78	10	2	19.1	10.0386389	11	3	15.3	11.05425000	20
79	10	2	19.1	10.0386389	11	3	13.9	11.05386111	20

	Longitude	Latitude	Tot.

S/No									Count.
	(Deg.)	(Min.)	(Sec)	Converted	(Deg.)	(Min.)	(Sec)	converted	(cps)
80	10	2	13.1	10.0369722	11	3	12.3	11.05341667	15
81	10	3	57.4	10.0659444	11	3	29.0	11.05805556	20
82	10	3	56.7	10.0657500	11	3	25.6	11.05711111	25
83	10	4	0.5	10.0668056	11	3	19.9	11.05552778	20
84	10	4	2.7	10.0674167	11	3	22.6	11.05627778	20
85	10	4	4.2	10.0678333	11	3	21.9	11.05608333	20
86	10	4	5.5	10.0681944	11	3	19.9	11.05552778	20
87	10	4	9.6	10.0693333	11	3	16.8	11.05466667	20
88	10	4	16.8	10.0713333	11	3	12.4	11.05344444	20
89	10	4	19.1	10.0719722	11	3	11.3	11.05313889	20
90	10	4	20.2	10.0722778	11	3	12.5	11.05347222	20
91	10	4	18.7	10.0718611	11	3	15.0	11.05416667	20
92	10	4	15.9	10.0710833	11	3	21.1	11.05586111	20
93	10	4	7.7	10.0688056	11	3	26.3	11.05730556	30
94	10	4	0.4	10.0667778	11	3	31.5	11.05875000	20
95	10	6	44.4	10.1123333	11	6	24.9	11.10691667	20
96	10	6	44.9	10.1124722	11	6	13.3	11.10369444	20
97	10	6	48.3	10.1134167	11	6	12.7	11.10352778	20
98	10	6	50.5	10.1140278	11	6	5.6	11.10155556	20
99	10	6	56.5	10.1156944	11	5	58.5	11.09958333	15
100	10	6	0.0	10.1000000	11	6	0.0	11.10000000	20
101	10	6	57.3	10.1159167	11	5	53.7	11.09825000	10
102	10	6	54.3	10.1150833	11	5	43.6	11.09544444	15
103	10	6	51.8	10.1143889	11	5	39.0	11.09416667	20
104	10	6	49.7	10.1138056	11	5	35.1	11.09308333	20
105	10	6	43.3	10.1120278	11	5	32.8	11.09244444	15
106	10	6	35.1	10.1097500	11	5	30.0	11.09166667	20
107	10	6	18.1	10.1050278	11	5	28.5	11.09125000	25
108	10	6	7.8	10.1021667	11	5	29.7	11.09158333	20
109	10	6	2.5	10.1006944	11	5	30.5	11.09180556	20
110	10	5	59.1	10.0997500	11	5	31.9	11.09219444	20
111	10	5	59.3	10.0998056	11	5	33.8	11.09272222	20
112	10	5	56.1	10.0989167	11	5	38.7	11.09408333	15
113	10	5	55.3	10.0986944	11	5	42.6	11.09516667	15
114	10	5	1.5	10.0837500	11	5	50.9	11.09747222	15
115	10	6	15.1	10.1041944	11	5	54.3	11.09841667	15
116	10	6	20.6	10.1057222	11	5	55.3	11.09869444	25
117	10	6	24.1	10.1066944	11	6	2.8	11.10077778	10
118	10	6	28.7	10.1079722	11	6	7.3	11.10202778	25
119	10	6	31.8	10.1088333	11	6	12.6	11.10350000	15

S/No	Longitude				Latitude				Tot. Count.
	(Deg.)	(Min.)	(Sec)	Converted	(Deg.)	(Min.)	(Sec)	converted	(cps)

120	10	6.0	39.4	10.1109444	11	6	21.3	11.1059167	20
121	10	6.0	43.1	10.1119722	11	6	27.9	11.1077500	15
122	9	56.0	36.6	9.9435000	10	59	22.6	10.9896111	25
123	9	56.0	38.1	9.94391667	10	59	24.0	10.9900000	20
124	9	56.0	38.2	9.94394444	10	59	20.4	10.9890000	30
125	9	56.0	37.5	9.94375000	10	59	18.3	10.9884167	30
126	9	56.0	36.0	9.94333333	10	59	17.5	10.9881944	25
127	9	56.0	35.0	9.94305556	10	59	20.3	10.9889722	25
128	9	56.0	35.4	9.94316667	10	59	21.6	10.9893333	20
129	9	57.0	16.6	9.95461111	10	58	53.3	10.9814722	20
130	9	57.0	18.4	9.95511111	10	58	55.3	10.9820278	30
131	9	57.0	14.3	9.95397222	10	58	50.6	10.9807222	20
132	9	57.0	16.0	9.95444444	10	58	52.0	10.9811111	20
133	10	0.0	34.2	10.0095000	11	0	59.5	11.0165278	20
134	10	4.0	21.4	10.0726111	11	3	53.5	11.0648611	15
135	10	4.0	15.3	10.0709167	11	3	55.5	11.0654167	25
136	10	4.0	8.0	10.0688889	11	3	59.8	11.0666111	15
137	10	4.0	3.7	10.0676944	11	3	56.5	11.0656944	20
138	10	4.0	0.2	10.0667222	11	3	53.1	11.0647500	25
139	10	3.0	59.9	10.0666389	11	3	50.9	11.0641389	20
140	10	3.0	52.1	10.0644722	11	3	54.4	11.0651111	25
141	10	3.0	44.4	10.0623333	11	3	57.9	11.0660833	20
142	10	3.0	36.3	10.0600833	11	3	59.0	11.0663889	20
143	10	3.0	23.7	10.0565833	11	3	57.0	11.0658333	15
144	10	3.0	21.5	10.0559722	11	3	56.0	11.0655556	20
145	10	3.0	20.4	10.0556667	11	4	3.8.0	11.0677222	15
146	10	3.0	19.9	10.0555278	11	4	10.5	11.0695833	15
147	10	3.0	21.9	10.0560833	11	4	17.3	11.0714722	15
148	10	3.0	21.8	10.0560556	11	4	23.8	11.0732778	20
149	10	3.0	26.4	10.0573333	11	4	26.3	11.0739722	20
150	10	3.0	31.1	10.0586389	11	4	24.8	11.0735556	15
151	10	3.0	36.7	10.0601944	11	4	21.3	11.0725833	15
152	10	3.0	44.0	10.0622222	11	4	18.3	11.0717500	20
153	10	3.0	48.7	10.0635278	11	4	13.0	11.0702778	15
154	10	4.0	1.4	10.0670556	11	4	7.0	11.0686111	20
155	10	4.0	6.6	10.0685000	11	4	4.6	11.0679444	20
156	10	4.0	14.1	10.0705833	11	4	2.1	11.0672500	25
157	10	4.0	22.3	10.0728611	11	3	58.1	11.0661389	20
158	10	4.0	26.5	10.0740278	11	3	53.8	11.0649444	15
159	10	4.0	29.5	10.0748611	11	3	52.9	11.0646944	20
160	10	4.0	39.6	10.0776667	11	3	50.4	11.0640000	15

Appendix III: PGIS-SP Data for Profiles 1 to 10

Profile	RECE_fid	MarkSpot	StationPt	Xco_m	Yco_m	Lat_deg	Lon_deg	TC_cps	K_cps	U_cps	Th_cps	Cs_cps	cK_PCT	cU_PPM	cTh_PPM	Dose_nGypH	ThPeak1
1	53	A	A-1	720918	1107546	10.0132	11.0154	67	3.4	2.4	1.4	17.6	0.6	6.53	10	124.04	0.83549
1	189	B	A-2	720957	1107594	10.0136	11.0158	72	2.2	2	3.2	15.2	0.29	3.54	19.61	131.25	0.83472
1	239	C	A-3	720992	1107629	10.0139	11.0161	83	5.6	2.6	2.8	19.2	0.51	4.1	22.61	153.62	0.83539
1	288	D	A-4	721028	1107664	10.0142	11.0165	76	3.4	2	2.2	18.8	0.59	4.14	17.28	140.52	0.83596
1	337	E	A-5	721062	1107700	10.0146	11.0168	73	4.4	2	1.2	17.4	0.43	4.87	12.43	128.09	0.83633
1	390	F	A-6	721099	1107735	10.0149	11.0171	86	4.6	2.6	2.2	23.6	0.48	6.32	15.78	151.1	0.83625
1	439	G	A-7	721134	1107768	10.0152	11.0174	102	5	3.6	1.8	21.6	0.44	7.9	19.77	182.03	0.83705
1	485	H	A-8	721170	1107804	10.0155	11.0178	102	5	1	1.8	25.6	1.19	1.33	16.85	180.61	0.83595
1	531	I	A-9	721204	1107839	10.0158	11.0181	69	4.6	0	0.4	14.8	1.27	1.39	5.95	124.72	0.83593
1	579	J	A-10	721240	1107873	10.0161	11.0184	65	1.8	2.8	2.2	13.6	0.32	5.73	17.46	125.96	0.83544
1	661	K	A-11	721277	1107905	10.0164	11.0187	63	2.8	2.4	2.6	13.6	0.5	4.12	17.61	120.04	0.83516
1	762	L	A-12	721313	1107940	10.0167	11.0191	67	4.2	2	1.2	16	0.74	3.87	13.75	128.95	0.83582
1	819	M	A-13	721347	1107976	10.017	11.0194	77	3.8	2.6	1.2	20.2	0.45	8.76	11.63	147.32	0.83596
1	874	N	A-14	721384	1108011	10.0174	11.0197	70	5	1.4	1	19.2	0.92	3.24	8.24	124.4	0.83534
1	927	O	A-15	721420	1108048	10.0177	11.02	58	3.2	2.4	1.6	14.4	0.62	6.01	12.84	121.35	0.83515
1	976	P	A-16	721454	1108082	10.018	11.0204	64	2.6	2.4	1.6	15.4	0.35	5.19	10	117.99	0.83573
1	1023	Q	A-17	721486	1108118	10.0183	11.0207	67	2.6	1.8	0.2	17.4	0.47	4.3	5.57	116.63	0.83617
1	1074	R	A-18	721522	1108153	10.0186	11.021	77	3.4	2.6	2.2	20	0.38	5.36	14.53	139.23	0.83611
1	1123	S	A-19	721557	1108189	10.019	11.0213	68	4	1.8	1.6	15	0.59	4.37	10.25	122.59	0.83711
1	1173	T	A-20	721598	1108220	10.0192	11.0217	86	4.4	3	3	22.8	0.41	4.69	20.05	151.38	0.83813
1	1218	U	A-21	721632	1108256	10.0196	11.022	83	4.6	2.2	1.2	17.2	0.54	6.42	10.42	148.65	0.83815
1	1268	V	A-22	721668	1108294	10.0199	11.0223	55	1.2	1.2	1	13.6	0.17	3.04	8.99	103.85	0.83814
1	1317	W	A-23	721703	1108327	10.0202	11.0227	73	4.6	2	2.4	18.6	0.52	2.65	20.46	132.92	0.83839
1	1368	X	A-24	721738	1108363	10.0205	11.023	57	3.6	1.4	2.2	13.4	0.41	2.64	17.76	117.1	0.83866
1	1423	Y	A-25	721775	1108399	10.0209	11.0233	51	2.2	0.6	1.6	13.8	0.53	3.04	9.69	103.94	0.83895
Profile	RECE_fid	MarkSpot	StationPt	Xco_m	Yco_m	Lat_deg	Lon_deg	TC_cps	K_cps	U_cps	Th_cps	Cs_cps	cK_PCT	cU_PPM	cTh_PPM	Dose_nGypH	ThPeak1

1	1503	Z	A-26	721813	1108432	10.0211	11.0237	76	1.4	3.2	2.2	19.6	0.2	7.81	12.14	134.94	0.83866
1	1549	a	A-27	721848	1108466	10.0215	11.024	67	3.8	1.6	1.8	15.4	0.54	4.12	12.3	123.39	0.83825
1	1598	b	A-28	721880	1108502	10.0218	11.0243	69	2.6	1.4	3.2	18.4	0.34	2.61	30.32	139.81	0.8389
1	1647	c	A-29	721914	1108539	10.0221	11.0246	54	1.6	1.6	1.4	12.4	0.24	2.93	12.35	109.46	0.83909
1	1695	d	A-30	721946	1108578	10.0225	11.0249	63	3.2	1.8	0.2	16.2	0.46	5.72	5.34	114.25	0.83807
1	1745	e	A-31	721972	1108617	10.0228	11.0251	46	1.2	0.8	1.6	13.4	0.22	2.47	12.87	92.9	0.83779
2	1793	f	A-32	722008	1108583	10.0225	11.0254	74	3.2	3	2	20.4	0.25	4.89	15.54	133.27	0.83795
2	1887	g	A-33	721974	1108548	10.0222	11.0251	64	2.2	1.4	1.6	18.4	0.25	2.57	9.89	110.25	0.83821
2	1937	h	A-34	721939	1108512	10.0219	11.0248	52	2.8	1.8	0.6	12.8	0.3	6.62	6.57	104.77	0.83773
2	1985	i	A-35	721904	1108476	10.0215	11.0245	58	2.8	2.6	1.4	14.2	0.15	5.94	13.14	104.19	0.83753
2	2040	j	A-36	721868	1108443	10.0212	11.0242	55	3	1	1	14.2	0.47	3.43	10.28	104.66	0.83721
2	2089	k	A-37	721832	1108409	10.0209	11.0238	69	2.2	1.4	2.6	18.6	0.33	3.12	16.72	121.74	0.83761
2	2135	l	A-38	721799	1108371	10.0206	11.0235	59	3.2	1.2	1.2	15.2	0.62	4.1	12.06	111.05	0.83726
2	2184	m	A-39	721761	1108337	10.0203	11.0232	57	1.8	1.2	0.8	14	0.38	2.95	10.55	96.95	0.83674
2	2307	n	A-40	721728	1108300	10.02	11.0229	61	1.6	1	0.8	17.2	0.48	2.6	11.14	111.44	0.83652
2	2358	o	A-41	721690	1108268	10.0197	11.0225	66	3.2	2	1.2	15.8	0.51	6.27	7.7	120.27	0.83726
2	2405	p	A-42	721655	1108230	10.0193	11.0222	87	3.4	2.8	2.6	22.2	0.26	7.19	19.3	159.49	0.83864
2	2448	q	A-43	721620	1108196	10.019	11.0219	73	2.8	1.8	2.2	13.8	0.3	5.59	16.31	137.96	0.83797
2	2494	r	A-44	721585	1108162	10.0187	11.0216	64	3.2	0.8	0.8	14.8	0.67	3.05	8.19	120.36	0.83788
2	2542	s	A-45	721548	1108127	10.0184	11.0212	64	4.2	2	0.4	16.4	0.88	4.48	5.51	114.93	0.8376
2	2589	t	A-46	721513	1108092	10.0181	11.0209	74	3.6	1.6	1.8	17.4	0.46	2.86	12.16	132.63	0.83725
2	2637	u	A-47	721477	1108058	10.0178	11.0206	85	4.2	3	2	19.8	0.4	7.73	14.01	147.05	0.83722
2	2684	v	A-48	721443	1108023	10.0175	11.0203	73	3.4	1.8	2	16.2	0.76	2.84	11.25	123.64	0.83668
2	2736	w	A-49	721405	1107988	10.0172	11.0199	105	8.2	3.6	2.2	23.4	1.06	5.96	19	193.37	0.83785
2	2799	x	A-50	721373	1107952	10.0168	11.0196	81	7	2	1.4	16.8	1.36	4.33	11.21	153.58	0.83859
2	2861	y	A-51	721335	1107918	10.0165	11.0193	68	3.4	1.6	1.2	15.4	0.49	6.86	10.4	128.8	0.83842
2	2935	z	A-52	721301	1107882	10.0162	11.019	77	4.8	1.2	1.8	17.4	0.97	3.24	12.78	136.76	0.83873

Profile	RECE_fid	MarkSpot	StationPt	Xco_m	Yco_m	Lat_deg	Lon_deg	TC_cps	K_cps	U_cps	Th_cps	Cs_cps	cK_PCT	cU_PPM	cTh_PPM	Dose_nGypH	ThPeak1
2	2987	1	A-53	721264	1107848	10.0159	11.0186	95	4.4	2.2	2.2	23.8	1.11	5.06	18.3	168.28	0.83882

2	3039	2	A-54	721228	1107813	10.0156	11.0183	102	4.4	2.4	3.6	24.4	0.61	3.86	25.77	181.17	0.83854
2	3089	3	A-55	721193	1107777	10.0153	11.018	162	7.2	5.4	4.2	38.4	0.93	9.26	28.23	287.77	0.83697
2	3140	4	A-56	721156	1107743	10.015	11.0176	120	4.6	2	2.4	34	0.82	7.23	20.65	224.3	0.83724
2	3188	5	A-57	721122	1107708	10.0146	11.0173	132	7	3.2	6	33	0.67	5.87	39.29	252.76	0.83842
2	3240	6	A-58	721086	1107674	10.0143	11.017	101	4.2	2.4	2.6	22.6	0.57	4.37	20.85	181.12	0.839
2	3293	7	A-59	721049	1107639	10.014	11.0166	73	4.2	1.6	0.4	19.8	0.74	5.07	5.16	137.44	0.83894
2	3353	8	A-60	721014	1107603	10.0137	11.0163	62	4.2	1.2	1	14.2	0.72	4.1	13.25	120.66	0.83852
2	3404	9	A-61	720979	1107568	10.0134	11.016	64	4	0.6	2.4	14.2	1.13	0.74	14.49	120.2	0.83806
2	3457	A	A-62	720947	1107529	10.013	11.0157	62	4.2	1.8	2	15	0.73	4.77	14.47	115.86	0.83933
3	92	A	A-1	720983	1107492	10.0127	11.016	87	4.6	2.2	1.2	19.6	0.88	5.34	11.36	155.38	0.83844
3	157	B	A-2	721021	1107528	10.013	11.0164	97	5.2	2.4	2.8	24.2	0.73	5.46	19.5	176.07	0.83893
3	227	C	A-3	721057	1107565	10.0133	11.0167	101	3.2	2.2	2.4	23.8	0.46	5.31	16.51	179.12	0.83989
3	284	D	A-4	721090	1107598	10.0136	11.017	118	6.6	5.2	4.8	29	0.46	10.17	28.61	228.68	0.83973
3	343	E	A-5	721125	1107633	10.014	11.0173	85	4	1.8	2.4	17.8	0.54	4.49	18.94	168.92	0.83935
3	413	F	A-6	721162	1107669	10.0143	11.0177	124	7	4.4	3	27.6	0.7	7.79	24.48	225.62	0.83952
3	485	G	A-7	721197	1107704	10.0146	11.018	112	5.8	1.6	2.6	27.8	0.93	6.17	22.41	209.71	0.83897
3	551	H	A-8	721233	1107736	10.0149	11.0183	127	5.8	4.8	4	32.8	0.46	8.04	31.77	237.57	0.83924
3	630	I	A-9	721269	1107774	10.0152	11.0187	129	7	5.4	3.6	29	0.52	8.87	28.23	241.48	0.83955
3	774	J	A-10	721305	1107807	10.0155	11.019	87	7	2.8	1	19.8	1.07	6.92	13.99	162	0.83998
3	830	K	A-11	721337	1107845	10.0159	11.0193	78	3.6	3.6	1.8	20.4	0.42	8.22	12.72	141.57	0.83936
3	908	L	A-12	721374	1107882	10.0162	11.0196	69	5.2	1	2.2	14.8	0.86	1.81	15.16	129.02	0.83873
3	1002	M	A-13	721410	1107913	10.0165	11.0199	58	3	2	0.8	13.6	0.49	5.54	6.51	112.87	0.83818
3	1159	N	A-14	721444	1107949	10.0168	11.0203	87	4.4	2.2	1.4	23.2	0.57	5.11	13.21	153.38	0.83932
3	1209	O	A-15	721480	1107984	10.0171	11.0206	97	5	2.8	3.2	25	0.59	6.07	21.1	164.13	0.83931
3	1259	P	A-16	721515	1108019	10.0174	11.0209	82	2.8	1.4	2	22	0.46	3.93	15.54	151.81	0.83858
3	1323	Q	A-17	721550	1108056	10.0178	11.0212	84	5.4	2.8	3	20.6	0.76	3.45	22.22	147.75	0.83892
Profile	RECE_fid	MarkSpot	StationPt	Xco_m	Yco_m	Lat_deg	Lon_deg	TC_cps	K_cps	U_cps	Th_cps	Cs_cps	cK_PCT	cU_PPM	cTh_PPM	Dose_nGypH	ThPeak1
3	1367	R	A-18	721588	1108089	10.0181	11.0216	64	2.2	3	1.4	15.2	0.35	8.06	8.75	118.46	0.84002
3	1417	S	A-19	721622	1108124	10.0184	11.0219	70	3.2	1	2.2	17.6	0.62	1.64	17.4	121.64	0.84008

3	1465	T	A-20	721656	1108161	10.0187	11.0222	67	3.4	1.2	1.8	15.8	0.45	2.03	18.43	131.36	0.84049
3	1520	U	A-21	721690	1108197	10.019	11.0225	71	4.2	1.8	0.6	14.8	0.63	4.62	8.01	116.75	0.84046
3	1572	V	A-22	721726	1108233	10.0194	11.0229	72	3.8	3.4	2	20.6	0.28	6.8	22.04	138.76	0.84108
3	1620	W	A-23	721761	1108267	10.0197	11.0232	65	3.4	2.2	1.2	15.8	0.49	4.9	13.25	120	0.84066
3	1669	X	A-24	721796	1108303	10.02	11.0235	69	2.4	1.8	2.6	18.6	0.33	3.67	18.46	131.31	0.84093
3	1717	Y	A-25	721833	1108338	10.0203	11.0238	74	3.8	3.2	1.4	20	0.55	6.39	9.22	133.14	0.84059
3	1764	Z	A-26	721867	1108375	10.0206	11.0241	73	3.6	2.6	1.2	17	0.43	5.6	11.95	139.83	0.84033
3	1813	a	A-27	721903	1108409	10.0209	11.0245	73	2.8	2.2	2.8	16.2	0.5	4.46	16.52	137.41	0.84099
3	1866	b	A-28	721939	1108442	10.0212	11.0248	71	3.4	2	1.4	18	0.39	3.49	13.5	124.51	0.84018
3	1918	c	A-29	721975	1108476	10.0215	11.0251	79	3.4	1.6	1.2	21.6	0.75	2.93	14.98	140.92	0.84035
3	1969	d	A-30	722005	1108515	10.0219	11.0254	74	4	1.4	2.8	17.8	0.95	1.81	23.22	150.82	0.84016
3	2018	e	A-31	722041	1108549	10.0222	11.0257	63	3.4	2.4	1.4	16.2	0.54	7.06	10.29	125.73	0.84088
4	2060	f	A-32	722075	1108518	10.0219	11.026	74	3.4	2.8	1.6	17	0.46	6.12	14.56	137.65	0.84237
4	2113	g	A-33	722042	1108482	10.0216	11.0257	90	4	4.6	3.4	23	0.41	9.73	25.01	171.84	0.84079
4	2164	h	A-34	722007	1108447	10.0213	11.0254	80	5	1.8	1.2	18.6	0.83	4.94	8.54	153.01	0.84021
4	2216	i	A-35	721972	1108412	10.021	11.0251	79	3.4	2.4	1.4	17.8	0.44	5.08	12.04	137.96	0.83976
4	2270	j	A-36	721935	1108377	10.0206	11.0248	69	2	1.6	1.6	18.4	0.43	5.44	10.2	129.02	0.83943
4	2314	k	A-37	721900	1108342	10.0203	11.0244	66	3.6	2.4	1.2	16.2	0.48	9.11	11.01	126.69	0.83887
4	2360	l	A-38	721866	1108305	10.02	11.0241	65	3	2.8	2.8	17.2	0.08	6.34	17.75	120.99	0.83933
4	2406	m	A-39	721832	1108269	10.0197	11.0238	132	4	5.2	4.4	32.4	0.24	12.49	26.86	229.24	0.83876
4	2453	n	A-40	721795	1108236	10.0194	11.0235	97	3.6	3.6	2.6	25	0.58	7.12	17.45	178.99	0.83916
4	2507	o	A-41	721758	1108202	10.0191	11.0231	67	2	2	1.8	15.8	0.41	4.67	10.01	129.03	0.83912
4	2558	p	A-42	721728	1108163	10.0187	11.0229	74	3.4	2.4	2.6	19.6	0.56	3.7	18.03	137.31	0.83936
4	2606	q	A-43	721692	1108128	10.0184	11.0225	77	4.6	1.6	2.8	17.6	0.75	4.74	18.5	139.17	0.83931
4	2706	r	A-44	721656	1108091	10.0181	11.0222	67	2.6	2	1.2	19.4	0.29	4.26	8.93	117.33	0.83976
Profile	RECE_fid	MarkSpot	StationPt	Xco_m	Yco_m	Lat_deg	Lon_deg	TC_cps	K_cps	U_cps	Th_cps	Cs_cps	cK_PCT	cU_PPM	cTh_PPM	Dose_nGypH	ThPeak1
4	2757	s	A-45	721621	1108057	10.0178	11.0219	60	3.6	1.4	1.6	14.8	0.65	1.55	14.37	111.78	0.83965
4	2803	t	A-46	721586	1108023	10.0175	11.0216	78	5.6	2.8	1	17.8	0.76	8.71	5.74	138.84	0.83849
4	2851	u	A-47	721551	1107986	10.0171	11.0212	91	4.6	1.8	2.8	19.8	0.77	2.49	18.86	158.54	0.83904

4	2917	v	A-48	721513	1107952	10.0168	11.0209	91	4.2	2.4	1.8	23.4	0.51	5.44	13.85	159.88	0.839
4	3016	w	A-49	721478	1107918	10.0165	11.0206	42	2.4	1.8	0.4	12.8	0.39	4.33	3.66	78.49	0.83936
4	3083	x	A-50	721445	1107881	10.0162	11.0203	79	3.6	2.2	1.2	23	0.68	3.85	12	136.21	0.83948
4	3157	y	A-51	721408	1107847	10.0159	11.0199	89	5.6	2.4	2.6	20.4	0.91	3.61	19.22	158.72	0.84007
4	3224	z	A-52	721371	1107813	10.0156	11.0196	93	5.4	3.6	2	22.4	0.38	8.21	12.63	167.37	0.84013
4	3279	1	A-53	721334	1107777	10.0153	11.0193	86	4	3.2	2	17.4	0.92	7.63	12.98	155.9	0.84009
4	3339	2	A-54	721298	1107742	10.0149	11.0189	74	4.4	3.4	1.8	15.2	0.45	8.69	12.63	133.5	0.83958
4	3408	3	A-55	721264	1107708	10.0146	11.0186	85	4	3.4	2.4	22	0.65	5.75	16.35	152.07	0.8398
4	3475	4	A-56	721230	1107672	10.0143	11.0183	105	5	3.4	2.2	28.4	0.83	6.9	13.53	181.57	0.8404
4	3531	5	A-57	721194	1107637	10.014	11.018	99	5.2	2.4	2.4	23.6	0.7	4.68	23.11	196.37	0.83971
4	3600	6	A-58	721159	1107602	10.0137	11.0176	123	3.8	3.6	4.8	37.2	0.35	7.18	30.27	223.51	0.84002
4	3673	7	A-59	721123	1107569	10.0134	11.0173	87	2.8	2	1.4	22.2	0.55	4.57	17.3	160.9	0.83943
4	3736	8	A-60	721086	1107534	10.0131	11.017	107	5.2	2.8	3.4	29	0.93	7.47	23.8	194.91	0.83989
4	3780	9	A-61	721050	1107498	10.0127	11.0166	107	5.2	3	3	30	0.54	6.91	19.05	200.36	0.83955
4	3837	A	A-62	721016	1107463	10.0124	11.0163	88	4.8	1	2.4	21.6	0.82	3.34	19.1	169.7	0.84007
5	3887	B	A-63	721049	1107424	10.0121	11.0166	102	4.4	3	4.4	25	0.52	5.78	27.4	197.94	0.84127
5	3999	C	A-64	721083	1107459	10.0124	11.0169	91	6.2	2	2.6	25.2	0.78	4.98	18.86	164.5	0.842
5	4093	D	A-65	721120	1107494	10.0127	11.0173	85	5	2.2	3	21.6	0.71	6.18	21.4	159.74	0.8414
5	4161	E	A-66	721154	1107530	10.013	11.0176	103	5.8	3.2	2.2	21.6	0.7	5.86	19.23	184.11	0.84178
5	4243	F	A-67	721188	1107566	10.0134	11.0179	116	4.4	3.4	1.8	30	0.48	8.24	17.87	202.81	0.84113
5	4295	G	A-68	721224	1107600	10.0137	11.0182	118	4.8	4	4.4	30.8	0.15	8.25	30.58	220.45	0.84158
5	4370	H	A-69	721260	1107634	10.014	11.0186	105	6.2	3.6	2.2	26.4	0.85	7.3	15.44	190.22	0.84196
5	4444	I	A-70	721297	1107669	10.0143	11.0189	61	3.8	1.4	1.4	17.8	0.55	5.58	11.9	118.41	0.84169
5	4514	J	A-71	721328	1107707	10.0146	11.0192	76	3.6	3.4	2.6	19.8	0.27	5.98	17.28	143.36	0.84166
Profile	RECE_fid	MarkSpot	StationPt	Xco_m	Yco_m	Lat_deg	Lon_deg	TC_cps	K_cps	U_cps	Th_cps	Cs_cps	cK_PCT	cU_PPM	cTh_PPM	Dose_nGypH	ThPeak1
5	4583	K	A-72	721365	1107740	10.0149	11.0195	84	4.2	0.6	3.2	21.4	0.95	1.8	22.19	146.42	0.84238
5	4641	L	A-73	721401	1107776	10.0152	11.0199	81	5.4	2.2	1.8	20	0.75	4.84	13.52	141.62	0.84201
5	5004	M	A-74	721439	1107813	10.0156	11.0202	86	3.4	2	2.8	20.4	0.48	3.62	20.15	169.28	0.84215
5	5054	N	A-75	721473	1107846	10.0159	11.0205	90	5.4	2.6	2.2	22.8	0.72	3.67	20.9	166.04	0.84282

5	5135	O	A-76	721508	1107882	10.0162	11.0208	79	4	2	3.6	17.4	0.72	1.64	23.13	145.82	0.84178
5	5239	P	A-77	721546	1107914	10.0165	11.0212	63	3.4	2.8	1.8	15.4	0.59	5.65	13.45	122.64	0.84147
5	5326	Q	A-78	721579	1107951	10.0168	11.0215	86	6	2.4	1	20.4	1.16	5.93	12.89	151.95	0.84256
5	5393	R	A-79	721612	1107987	10.0171	11.0218	85	3.8	4	2.6	20.2	0.26	8.88	16.71	159.75	0.84247
5	5438	S	A-80	721646	1108021	10.0174	11.0221	84	5.8	3.2	2.6	21	0.88	6.39	18.27	157.21	0.84274
5	5491	T	A-81	721683	1108056	10.0177	11.0225	66	3	1.8	1.6	16	0.46	3.53	16.62	123.31	0.84271
5	5587	U	A-82	721720	1108091	10.0181	11.0228	79	3.8	2	2	20	0.7	5.87	14.23	139.71	0.84234
5	5664	V	A-83	721754	1108127	10.0184	11.0231	84	4.4	2.2	2.2	20.8	0.71	4.65	15.69	150.33	0.84224
5	5720	W	A-84	721789	1108161	10.0187	11.0234	81	4.2	2.6	2.4	19.2	0.63	4.18	16.24	148.71	0.84306
5	5779	X	A-85	721824	1108196	10.019	11.0237	84	4.2	2.4	1.8	16.8	0.47	3.73	14.65	150.93	0.84381
5	5830	Y	A-86	721860	1108232	10.0193	11.0241	75	3.6	2.2	1.8	17.8	0.3	6.32	11.43	142.33	0.84373
5	5879	Z	A-87	721895	1108267	10.0197	11.0244	77	3.8	2.2	2.4	20.4	0.32	4.34	17.21	146.91	0.84308
5	5929	a	A-88	721931	1108303	10.02	11.0247	60	4.2	2	2	12.2	0.63	3.34	13.59	115.06	0.84343
5	5980	b	A-89	721968	1108336	10.0203	11.0251	80	4.8	2.8	1.8	20.4	0.48	6.52	15.9	149.27	0.84312
5	6028	c	A-90	722002	1108371	10.0206	11.0254	85	4.6	2.6	2.4	19.2	0.49	5.33	17.04	155.71	0.84339
5	6090	d	A-91	722040	1108406	10.0209	11.0257	80	3.4	3.6	2.4	20.4	0.24	5.58	18.39	144.44	0.84428
5	6167	e	A-92	722073	1108444	10.0212	11.026	88	4.8	1.6	2.4	20.6	0.82	4.56	18.37	162.71	0.84386
5	6235	f	A-93	722109	1108478	10.0215	11.0264	89	4.2	2.8	1.8	20.2	0.59	5.27	14.28	160.27	0.84291
6	6318	g	A-94	722149	1108449	10.0213	11.0267	90	4	4.6	2.2	20.8	0.12	9.08	14.86	162.29	0.84315
6	6365	h	A-95	722111	1108414	10.021	11.0264	88	5	1.6	2	21.8	0.67	4.62	14.39	168.26	0.84292
6	6409	i	A-96	722076	1108380	10.0207	11.0261	85	3.8	3.6	1.6	22.6	0.18	9.3	11.01	148.45	0.84271
6	6456	j	A-97	722041	1108344	10.0203	11.0257	81	3	1.6	2	21.8	0.67	4.12	15.1	153.19	0.84225
6	6503	k	A-98	722007	1108308	10.02	11.0254	102	5.8	2.6	4.2	26.2	0.61	3.94	24.5	176.92	0.84239
Profile	RECE_fid	MarkSpot	StationPt	Xco_m	Yco_m	Lat_deg	Lon_deg	TC_cps	K_cps	U_cps	Th_cps	Cs_cps	cK_PCT	cU_PPM	cTh_PPM	Dose_nGypH	ThPeak1
6	6574	l	A-99	721970	1108272	10.0197	11.0251	70	1.4	1.8	2.8	19.6	0.25	2.74	17.21	135.73	0.8418
6	6635	m	A-100	721934	1108239	10.0194	11.0248	73	4.4	2.2	1.4	18.2	0.49	6.44	11.26	136.09	0.84193
6	6683	n	A-101	721899	1108203	10.0191	11.0244	75	2	3.4	2	18.6	0.18	7.58	13.19	145.73	0.84204
6	6727	o	A-102	721866	1108166	10.0187	11.0241	89	5.2	2.2	3	22.4	0.7	6.22	19.18	163.01	0.84228
6	6773	p	A-103	721831	1108129	10.0184	11.0238	78	3.4	2	1.2	19.2	0.55	4.61	10.71	140.74	0.84192

6	6840	q	A-104	721791	1108095	10.0181	11.0234	77	2.4	3.4	1.6	17.2	0.31	8.54	10.98	133.88	0.84266
6	6905	r	A-105	721758	1108062	10.0178	11.0231	88	3.8	1.4	1.2	22.8	0.57	6.05	6.22	147.71	0.84251
6	6970	s	A-106	721724	1108025	10.0175	11.0228	69	5.6	2	1.8	11.6	1.01	4.47	12.36	127.42	0.8422
6	7047	t	A-107	721688	1107991	10.0172	11.0225	62	3.8	2.4	1.4	15.6	0.51	4.98	11.21	122.2	0.84224
6	7125	u	A-108	721650	1107955	10.0168	11.0221	72	5.4	3	0.6	19	0.55	6.66	7.48	129.95	0.84279
6	7192	v	A-109	721616	1107921	10.0165	11.0218	72	5	1.6	1	18	1.08	3.89	10.84	134.76	0.84359
6	7262	w	A-110	721580	1107885	10.0162	11.0215	80	5.6	2.6	1.6	21.2	1.05	4.58	12.7	142.06	0.84355
6	7361	x	A-111	721544	1107847	10.0159	11.0212	94	6.2	1.6	1.4	24.8	1.15	4.16	15.28	178.35	0.84356
6	7428	y	A-112	721511	1107814	10.0156	11.0209	84	4.2	0.6	2.4	22.2	1.13	1.53	15.87	150.72	0.84295
6	7495	z	A-113	721474	1107778	10.0153	11.0205	85	5.8	1.6	1.2	19.6	1.04	5.25	11.16	161	0.8438
6	7573	1	A-114	721438	1107746	10.015	11.0202	84	3.8	1.8	1.4	22.4	0.78	5.38	11.05	149.14	0.84428
6	7629	2	A-115	721403	1107709	10.0146	11.0199	79	2.2	2.2	2.2	19.6	0.37	4.46	17.1	142.72	0.84401
6	7699	3	A-116	721366	1107674	10.0143	11.0195	73	6	2.6	1.4	19	0.96	4.86	11.08	133.94	0.8429
6	7772	4	A-117	721332	1107640	10.014	11.0192	73	2.8	1.8	1.8	18.6	0.43	3.35	15.72	136.98	0.84327
6	7847	5	A-118	721297	1107605	10.0137	11.0189	83	3.8	1.6	1.2	23.8	0.79	2.95	10.32	140.64	0.84325
6	7906	6	A-119	721261	1107570	10.0134	11.0186	100	4.4	3.4	2.8	20	0.54	8.49	16.38	185.95	0.84236
6	7957	7	A-120	721226	1107533	10.013	11.0183	101	4	4.4	2.6	26.2	0.33	7.86	20.54	195.71	0.84245
6	8025	8	A-121	721189	1107500	10.0128	11.0179	97	2.6	3.6	3.8	21.8	0.31	5.24	23.33	180.36	0.84295
6	8188	9	A-122	721154	1107464	10.0124	11.0176	100	6.2	1.8	2.4	22.8	0.96	4.89	15.37	171.15	0.84408
6	8253	A	A-123	721119	1107429	10.0121	11.0173	104	5.2	3.4	3.6	26	1.05	5.47	23.12	184.5	0.84447
6	8330	B	A-124	721088	1107394	10.0118	11.017	97	5.8	4.4	1.4	25.4	0.67	7.15	13.54	167.92	0.84445
7	8350	C	A-125	721123	1107355	10.0114	11.0173	82	3.6	1.6	1.8	19.2	0.47	5.22	14.1	150.81	0.84603

Profile	RECE_fid	MarkSpot	StationPt	Xco_m	Yco_m	Lat_deg	Lon_deg	TC_cps	K_cps	U_cps	Th_cps	Cs_cps	cK_PCT	cU_PPM	cTh_PPM	Dose_nGypH	ThPeak1
7	10170	D	A-126	721158	1107390	10.0118	11.0176	89	4.4	2.2	2	26.8	0.72	4.66	14.68	158.55	0.84545
7	10246	E	A-127	721194	1107425	10.0121	11.018	91	3.4	2.8	1.4	23.4	0.31	6.38	14.56	165.23	0.84481
7	10342	F	A-128	721228	1107458	10.0124	11.0183	95	3.6	3.8	2.4	25.6	0.18	7.86	20.21	161.95	0.84624
7	10404	G	A-129	721265	1107494	10.0127	11.0186	95	3.6	2.2	2.2	23	0.65	4.16	15.63	173.93	0.84843
7	10466	H	A-130	721299	1107529	10.013	11.0189	75	3.2	2.8	2.2	17.8	0.23	8.17	13.52	143.83	0.8484
7	10525	I	A-131	721335	1107564	10.0133	11.0193	71	3	3.2	2	16.8	0.27	6.7	13.88	136.41	0.84757

7	10592	J	A-132	721367	1107601	10.0137	11.0195	94	4	1.8	3	24.2	0.55	5.27	15.71	163.18	0.84787
7	10656	K	A-133	721407	1107633	10.0139	11.0199	78	2.8	2.8	1.6	21.6	0.39	6.15	14.26	140.88	0.84714
7	10714	L	A-134	721438	1107671	10.0143	11.0202	79	6.4	3.2	2.6	22	0.83	8.02	16.99	148.17	0.84742
7	10775	M	A-135	721475	1107707	10.0146	11.0205	79	5.6	2.2	1.8	18.4	0.95	6.72	11.3	149.39	0.84789
7	10836	N	A-136	721511	1107742	10.0149	11.0209	101	6	2.2	1.8	24.8	1.06	5.67	13.71	186.89	0.84819
7	10906	O	A-137	721545	1107778	10.0152	11.0212	90	4.8	2.8	1.6	25.2	0.56	6.57	14.19	154.85	0.84737
7	10968	P	A-138	721580	1107812	10.0156	11.0215	80	4.4	1.6	1.8	19.8	0.85	4.59	14.06	148.11	0.84778
7	11036	Q	A-139	721615	1107848	10.0159	11.0218	95	4.6	3	1.8	22	0.58	6.33	16.19	168.29	0.84716
7	11097	R	A-140	721651	1107884	10.0162	11.0221	85	5.2	1.6	2.2	19.6	1.02	4.1	17.64	169.74	0.84622
7	11235	S	A-141	721688	1107918	10.0165	11.0225	81	5.2	3.4	1.8	17.8	0.76	6.6	12.13	148.35	0.84681
7	11294	T	A-142	721724	1107952	10.0168	11.0228	70	4	2	2.4	18.6	0.59	2.35	19.21	133.12	0.84694
7	11358	U	A-143	721761	1107985	10.0171	11.0232	75	2.6	3.6	2.2	19.2	0.49	7.05	15.68	148.62	0.84723
7	11415	V	A-144	721795	1108022	10.0174	11.0235	88	4.6	2	2.6	21	0.65	3.82	15.99	155.94	0.84664
7	11468	W	A-145	721832	1108057	10.0178	11.0238	79	4.6	2.4	2.8	21.4	0.57	4.98	20.63	139.4	0.84644
7	11538	X	A-146	721867	1108093	10.0181	11.0241	72	4	1	1.6	20.4	0.56	3.93	11.71	127.82	0.8477
7	11621	Y	A-147	721902	1108126	10.0184	11.0245	71	3.6	2.8	1.8	19.4	0.42	6.99	17.57	142.62	0.84693
7	11680	Z	A-148	721937	1108161	10.0187	11.0248	77	2.2	1.8	1.8	21	0.22	3.23	14.24	141.01	0.84718
7	11744	a	A-149	721973	1108194	10.019	11.0251	72	3	1.8	3.2	19	0.35	3.59	20.42	130.79	0.84751
7	11808	b	A-150	722008	1108231	10.0193	11.0254	93	3.8	2.4	1.6	25	0.42	7.12	11.2	161.47	0.84717
7	11875	c	A-151	722043	1108267	10.0196	11.0257	93	5.6	2.6	2.6	23.6	0.67	5.56	19.21	161.79	0.84739
7	11939	d	A-152	722080	1108303	10.02	11.0261	86	4.4	3	2.2	20.4	0.61	6.13	18.9	160.84	0.84792

Profile	RECE_fid	MarkSpot	StationPt	Xco_m	Yco_m	Lat_deg	Lon_deg	TC_cps	K_cps	U_cps	Th_cps	Cs_cps	cK_PCT	cU_PPM	cTh_PPM	Dose_nGypH	ThPeak1
7	12003	e	A-153	722113	1108339	10.0203	11.0264	83	3	2.4	1.6	20.4	0.54	5.43	12.75	156.22	0.84781
7	12062	f	A-154	722149	1108373	10.0206	11.0267	101	7.4	3.2	1.2	25.2	0.89	7.16	12.04	179.53	0.84832
7	12115	g	A-155	722183	1108410	10.0209	11.027	108	6.2	3	3.4	26.8	0.63	5.32	27.57	204.3	0.84885
8	3482	B	A-63	721158	1107320	10.0111	11.0176	101	5.2	3.8	1.6	22.2	0.48	8.15	14.81	176.83	0.83963
8	3541	C	A-64	721193	1107353	10.0114	11.0179	111	3.4	2.8	3.4	26.8	0.54	5.19	25.6	200.87	0.83923
8	3611	D	A-65	721228	1107388	10.0117	11.0183	91	4	2.2	1.8	23.4	0.5	5.11	15.94	171.24	0.83977
8	3667	E	A-66	721264	1107423	10.0121	11.0186	85	3	2.6	1.8	20.6	0.41	7.71	12.86	161.59	0.84044

8	3725	F	A-67	721299	1107457	10.0124	11.0189	92	3	2	1.2	22.8	0.47	5.03	15.74	167.49	0.84085
8	3799	G	A-68	721336	1107492	10.0127	11.0193	74	4	3.2	3.6	20.2	0.33	7.5	21.14	144.68	0.841
8	3862	H	A-69	721370	1107527	10.013	11.0196	105	6.2	2.8	2.4	25.6	0.91	5.31	18.96	190.31	0.84029
8	3910	I	A-70	721404	1107564	10.0133	11.0199	81	4.8	2	2	20.8	0.49	5.26	15.42	151.82	0.84123
8	3966	J	A-71	721440	1107598	10.0136	11.0202	74	4.6	1.4	1	18	0.72	5.71	7.31	128.24	0.84053
8	4024	K	A-72	721472	1107635	10.014	11.0205	87	4.6	1.6	1.6	22.4	0.79	4.8	10.29	148.4	0.84037
8	4093	L	A-73	721510	1107669	10.0143	11.0208	73	4	1.6	2.4	17	0.85	2.96	20.63	139.9	0.84011
8	4172	M	A-74	721544	1107705	10.0146	11.0212	96	4	2.8	1.8	24	0.62	5.44	15.12	168.61	0.8406
8	4250	N	A-75	721579	1107739	10.0149	11.0215	87	4	3	3	20.6	0.36	3.84	21.42	159.06	0.84078
8	4304	O	A-76	721615	1107773	10.0152	11.0218	96	4.8	3.6	3.2	21.4	0.52	6.33	24.98	194.56	0.84177
8	4363	P	A-77	721649	1107810	10.0155	11.0221	102	7	3	1.4	23.6	1.26	8.39	10.45	182.83	0.8418
8	4411	Q	A-78	721685	1107846	10.0159	11.0225	99	5.4	2.2	2.2	25.8	0.77	5.35	19.1	173.97	0.84129
8	4464	R	A-79	721722	1107881	10.0162	11.0228	83	4.6	2.8	0.6	20.4	0.48	7.51	8.15	145.52	0.84181
8	4547	S	A-80	721758	1107916	10.0165	11.0231	62	2.8	1.6	2.2	13.2	0.35	2.21	15.74	117.15	0.8405
8	4598	T	A-81	721793	1107952	10.0168	11.0234	65	3.2	2	0.6	15.4	0.38	4.71	6.38	114.64	0.84061
8	4647	U	A-82	721829	1107985	10.0171	11.0238	74	3.6	1.2	1.6	16.8	0.57	2.32	12.58	129.73	0.84044
8	4654	V	A-83	721830	1107986	10.0171	11.0238	71	3.8	2.6	1.8	19	0.54	6.67	14.17	134.42	0.84046
8	4707	W	A-84	721860	1108023	10.0174	11.0241	78	3.6	1.2	2.6	19.2	0.67	4.28	20.74	143.94	0.8399
8	4765	X	A-85	721896	1108058	10.0178	11.0244	88	5.8	3	2.4	20	0.73	7.38	17.34	159.99	0.84076
8	4939	Y	A-86	721935	1108096	10.0181	11.0248	67	2.8	2.8	1.6	15	0.34	5.81	10.88	120.63	0.84059
Profile	RECE_fid	MarkSpot	StationPt	Xco_m	Yco_m	Lat_deg	Lon_deg	TC_cps	K_cps	U_cps	Th_cps	Cs_cps	cK_PCT	cU_PPM	cTh_PPM	Dose_nGypH	ThPeak1
8	5132	Z	A-87	721969	1108129	10.0184	11.0251	65	3	1.6	3	15.2	0.42	2.83	21.6	127.65	0.84079
8	5361	a	A-88	722001	1108166	10.0187	11.0254	103	4.6	2.6	2.2	26.2	0.7	5.76	14.52	188.03	0.84196
8	5563	b	A-89	722040	1108196	10.019	11.0257	81	5.6	2.2	2.6	20.2	0.8	3.65	18.19	146.13	0.8423
8	5995	c	A-90	722079	1108236	10.0194	11.0261	86	5	1.8	2.6	21.6	0.93	3.52	17.88	146.47	0.84111
8	6086	d	A-91	722147	1108301	10.0199	11.0267	94	4	4	3.6	24	0.21	7.1	24.59	178.5	0.84087
8	6139	e	A-92	722182	1108336	10.0203	11.027	97	4.2	2.8	3.8	23.2	0.56	4.64	27.3	177.02	0.84221
8	6188	f	A-93	722218	1108373	10.0206	11.0273	102	6.8	4.8	2.6	23.4	0.37	10.29	18.63	179.41	0.84137
9	6204	g	A-94	722255	1108343	10.0203	11.0277	79	3.2	1.8	2	19	0.42	3.78	13.54	134.52	0.8415

9	6281	h	A-95	722218	1108304	10.02	11.0273	86	6.6	2.8	0.8	21	0.9	6.09	12.59	163.88	0.84145
9	6331	i	A-96	722181	1108268	10.0196	11.027	95	4.6	2.4	1.8	21.4	0.63	7.1	13.36	164.11	0.84167
9	6384	j	A-97	722144	1108234	10.0193	11.0267	88	3.6	2.4	2.8	23	0.56	4.45	16.31	158.85	0.84104
9	6656	k	A-98	722112	1108198	10.019	11.0264	82	5.2	2.8	1.4	19.6	0.69	6.72	14.67	150.97	0.84178
9	6706	l	A-99	722075	1108163	10.0187	11.026	64	4	1.4	1	15.2	0.61	4.35	9.12	117.75	0.84158
9	6754	m	A-100	722040	1108129	10.0184	11.0257	71	3.2	2	0.8	18.8	0.75	5.65	10.14	129.59	0.84096
9	6803	n	A-101	722004	1108095	10.0181	11.0254	68	3.8	1.6	1.6	14.4	0.65	3.48	13.94	133.73	0.84033
9	6852	o	A-102	721971	1108059	10.0178	11.0251	56	3.8	3.6	0.8	13.8	0.61	8.19	4.97	101.04	0.84103
9	6903	p	A-103	721935	1108023	10.0174	11.0247	82	4.4	1.4	2.4	20	0.85	3.12	15.81	146.56	0.84139
9	6955	q	A-104	721897	1107992	10.0172	11.0244	61	3.8	1.6	1.8	17	0.93	3.36	12.19	116.33	0.84126
9	7004	r	A-105	721862	1107955	10.0168	11.0241	61	2.2	2.4	2.6	15.4	0.22	6.75	20.31	130.18	0.8417
9	7050	s	A-106	721826	1107919	10.0165	11.0237	77	4.6	2.8	1	18.6	0.72	7.36	7.41	145	0.84199
9	7097	t	A-107	721790	1107885	10.0162	11.0234	69	3	2.4	1.4	17.4	0.56	5.18	7.43	129.49	0.84142
9	7245	u	A-108	721755	1107851	10.0159	11.0231	82	4.4	1	3	18.6	0.77	2.18	23.37	150.88	0.84273
9	7292	v	A-109	721719	1107817	10.0156	11.0228	81	4.6	1.8	1.4	20	0.61	4.12	16.39	153.07	0.84248
9	7343	w	A-110	721685	1107778	10.0152	11.0225	72	5.8	0.8	1.4	17	1.02	3.3	13.19	131.77	0.84216
9	7393	x	A-111	721649	1107743	10.0149	11.0221	89	6.2	2.6	1.6	20.8	0.84	5.55	13.04	157.03	0.84188
9	7445	y	A-112	721611	1107710	10.0146	11.0218	85	5	0.6	1.6	19.6	0.84	2.5	13.52	151.44	0.84208
9	7498	z	A-113	721580	1107672	10.0143	11.0215	111	5.2	5	2.6	26.4	0.46	9.66	18.09	192.36	0.84217
Profile	RECE_fid	MarkSpot	StationPt	Xco_m	Yco_m	Lat_deg	Lon_deg	TC_cps	K_cps	U_cps	Th_cps	Cs_cps	cK_PCT	cU_PPM	cTh_PPM	Dose_nGypH	ThPeak1
9	7562	1	A-114	721543	1107638	10.014	11.0211	82	5.2	1.8	1.6	17.4	0.72	5.95	11.53	157.8	0.84249
9	7629	2	A-115	721508	1107604	10.0137	11.0208	84	8.2	2.2	1.8	18.2	1.23	3.77	12.5	147.57	0.84254
9	7694	3	A-116	721471	1107569	10.0134	11.0205	80	4.2	1.8	3	21.6	0.63	4.95	17.23	141.92	0.84304
9	7747	4	A-117	721437	1107532	10.013	11.0202	84	4.6	2	1.2	17.6	0.67	5.34	12.53	149.16	0.84279
9	7799	5	A-118	721402	1107496	10.0127	11.0199	81	5.6	2.6	1.6	22.2	1.15	5.8	13.91	150.27	0.84371
9	7852	6	A-119	721366	1107461	10.0124	11.0195	72	3.8	2.4	1.2	17.4	0.45	8.38	9.22	128.87	0.84392
9	7923	7	A-120	721330	1107428	10.0121	11.0192	80	3.4	1.6	3.6	20.4	0.73	3.44	24.96	150.5	0.84382
9	7981	8	A-121	721297	1107391	10.0118	11.0189	90	4.4	1.8	1.6	22	0.81	3.95	13.53	176.41	0.84342
9	8035	9	A-122	721259	1107357	10.0115	11.0185	117	5	5.2	3	27.4	0.43	10.51	21.28	212.4	0.84329

9	8083	A	A-123	721222	1107322	10.0111	11.0182	105	6.6	4	3.2	27	0.88	6.97	22.54	193.3	0.84405
9	8150	B	A-124	721187	1107290	10.0109	11.0179	80	4.4	1	2	19.2	0.88	1.82	15.62	150.27	0.84313
10	47	A	A-1	721230	1107249	10.0105	11.0183	107	5.2	4	2.8	23.6	0.72	7.87	21.79	197	0.845
10	187	B	A-2	721298	1107320	10.0111	11.0189	92	3.8	2.6	1.2	22.4	0.61	6.69	12.5	163.85	0.84535
10	242	C	A-3	721333	1107354	10.0114	11.0192	98	6.2	2.6	3.4	22.4	1.13	3.9	22.29	176.66	0.84602
10	348	D	A-4	721368	1107390	10.0118	11.0195	89	6	3	3.2	21.8	0.75	6.04	18.73	163.67	0.84802
10	406	E	A-5	721404	1107425	10.0121	11.0199	79	2.8	2	1.4	18.6	0.71	4.64	14.39	138.33	0.84801
10	455	F	A-6	721438	1107461	10.0124	11.0202	92	4.8	2.4	2.4	24.8	0.77	5.49	18.7	164.15	0.84847
10	500	G	A-7	721473	1107495	10.0127	11.0205	89	4.6	2.4	1.2	21.2	1	5.22	14.43	167.52	0.84824
10	544	H	A-8	721510	1107528	10.013	11.0208	90	3.8	2	3.8	21.4	0.65	2.08	26.01	168.73	0.84854
10	592	I	A-9	721545	1107565	10.0133	11.0212	92	3.2	4	1.6	25	0.65	8.7	13.18	156.67	0.84871
10	651	J	A-10	721583	1107598	10.0136	11.0215	91	5	2.6	2.8	22.2	0.6	6.86	19.73	167.77	0.84893
10	708	K	A-11	721619	1107634	10.0139	11.0218	90	5.4	2.4	1.8	22.2	0.8	6.96	12.74	164.65	0.84992
10	760	L	A-12	721654	1107669	10.0143	11.0222	81	6.2	2.2	2.2	18	0.85	4.81	15.95	152.74	0.84918
10	807	M	A-13	721690	1107704	10.0146	11.0225	77	3.8	1.4	1.4	17.6	0.6	3.65	12.01	137.83	0.84831
10	849	N	A-14	721726	1107739	10.0149	11.0228	69	4.8	1.6	2.2	13.4	0.79	3.07	18.85	139.52	0.84849
10	897	O	A-15	721760	1107775	10.0152	11.0231	76	3.6	3.6	2.4	18.4	0.42	7.62	15.02	149.29	0.84878
10	939	P	A-16	721796	1107809	10.0155	11.0235	105	6.6	3.2	1.8	26.6	1.21	5.6	14.28	183.61	0.84899
Profile	**RECE_fid**	**MarkSpot**	**StationPt**	**Xco_m**	**Yco_m**	**Lat_deg**	**Lon_deg**	**TC_cps**	**K_cps**	**U_cps**	**Th_cps**	**Cs_cps**	**cK_PCT**	**cU_PPM**	**cTh_PPM**	**Dose_nGypH**	**ThPeak1**
10	**1011**	**Q**	**A-17**	**721835**	**1107844**	**10.0158**	**11.0238**	**83**	**2.4**	**2.2**	**2.4**	**22.6**	**0.48**	**2.62**	**19.16**	**144.9**	**0.84891**
10	**1074**	**R**	**A-18**	**721868**	**1107881**	**10.0162**	**11.0241**	**72**	**5**	**1.2**	**2.4**	**17.4**	**0.78**	**2.92**	**21.52**	**136.35**	**0.84833**
10	**1117**	**S**	**A-19**	**721900**	**1107917**	**10.0165**	**11.0244**	**60**	**3.6**	**1.2**	**1.8**	**15.8**	**0.6**	**1.4**	**13.93**	**109.82**	**0.84829**
10	**1179**	**T**	**A-20**	**721936**	**1107951**	**10.0168**	**11.0248**	**55**	**2**	**1**	**1**	**15**	**0.33**	**2.36**	**7.79**	**102.43**	**0.8478**
10	**1228**	**U**	**A-21**	**721972**	**1107988**	**10.0171**	**11.0251**	**66**	**2.8**	**1.2**	**2**	**17**	**0.45**	**4.12**	**12.73**	**123.85**	**0.84769**
10	**1274**	**V**	**A-22**	**722007**	**1108023**	**10.0174**	**11.0254**	**67**	**4**	**2.2**	**2**	**16.4**	**0.51**	**5.21**	**13.08**	**124.32**	**0.8481**
10	**1322**	**W**	**A-23**	**722043**	**1108058**	**10.0177**	**11.0257**	**61**	**4**	**1.8**	**0.6**	**13.8**	**0.65**	**4.77**	**8.15**	**111.69**	**0.84805**
10	**1371**	**X**	**A-24**	**722078**	**1108094**	**10.0181**	**11.0261**	**55**	**3.2**	**0.8**	**0.8**	**12.4**	**0.54**	**2.12**	**10.65**	**102.23**	**0.84781**
10	**1416**	**Y**	**A-25**	**722114**	**1108129**	**10.0184**	**11.0264**	**68**	**2.6**	**1.6**	**2.2**	**12.6**	**0.43**	**4.08**	**12.34**	**119.71**	**0.84818**
10	**1462**	**Z**	**A-26**	**722149**	**1108164**	**10.0187**	**11.0267**	**70**	**5.4**	**1.4**	**1.2**	**17**	**0.97**	**4.2**	**11.63**	**130.34**	**0.84794**

10	1509	a	A-27	722184	1108198	10.019	11.027	72	4.2	2.2	1.6	15.2	0.71	6.15	12.2	135.23	0.84775
10	1812	b	A-28	722222	1108231	10.0193	11.0274	72	4	1.8	1.8	17	0.62	3.43	12.81	126.06	0.84723
10	1856	c	A-29	722253	1108269	10.0196	11.0277	88	4.8	3.4	2.4	19.6	0.79	5.27	18.76	158.43	0.84767
10	1959	d	A-30	722287	1108306	10.02	11.028	89	5	3.8	2	21	0.53	8.34	13.04	168.09	0.84745

Appendix IV: Results of conversion of activity concentration of radionuclides of rock samples from Bq/kg to ppm and results of calculations of dose rate

Sample ID	U^{238} (Bq/kg)	U^{238} (ppm)	Th^{-232} (Bq/kg)	Th^{-232} (ppm)	K^{-40} (Bq/kg)	K^{-40} (%)	Dose ($nGyph^{-1}$)
Composite 1	29.1774	2.6286	43.1471	10.6274	127.6827	0.4079	44.8651
Composite 2	25.7822	2.3227	45.2338	11.1413	291.5272	0.9314	51.3892
Composite 3	13.9050	1.2527	69.0992	17.0195	52.4106	0.1675	50.3455
Composite 4	11.0545	0.9959	89.1676	21.9625	64.8523	0.2072	61.6687
Composite 5	23.9861	2.1609	82.3261	20.2774	70.2955	0.2246	63.7379
Composite 6	39.5481	3.5629	48.6887	11.9923	88.4915	0.2827	51.3693
Composite 7	44.2642	3.9878	67.1608	16.5421	38.1026	0.1217	62.6040
Composite 8	11.2399	1.0126	72.2919	17.8059	27.7450	0.0886	50.0141
Composite 9	44.0324	3.9669	40.1026	9.8775	64.2302	0.2052	47.2434

Conversion factors used for the above table.

1 ppm of ^{226}Ra = 11.1 (Bq/kg)
1 ppm of ^{232}Th = 4.06 (Bq/kg)
1 % of ^{40}K = 313 (Bq/kg) (Abdul-Razek *et al.*, 2013)

$D = (0.462C_U + 0.604C_{Th} + 0.0417C_K)$ $nGyph^{-1}$ (Ramasamy et al., 2010)

Where: C_U, C_{Th} and C_K are the activity concentrations (Bq/kg) of ^{238}U, ^{232}Th and ^{40}K respectively.

$nGyph^{-1}$ = nanogray per hour

Appendix V: Results of laboratory gamma ray spectrometer Analysis

Centre for Energy Research and Training

Ahmadu Bello University Zaria

Results of Analysis

S/No.	Sample ID	K-40 (CPS)	Error ± (CPS)	K-40 (Bq/Kg)	Error ± (Bq/Kg)	Ra-226 (CPS)	Error ± (CPS)	Ra-226 (Bq/Kg)	Error ± (Bq/Kg)	Th-232 (CPS)	Error ± (CPS)	Th-232 (Bq/Kg)	Error ± (Bq/Kg)
1.	Composite 1	0.0821	0.001843	127.6827	2.866252	0.02518	0.00149	29.17729	1.726535	0.03784	0.00867	43.14709	9.885975
2.	Composite 2	0.187452	0.01843	291.5272	28.66252	0.02225	0.0013	25.78216	1.506373	0.03967	0.00846	45.23375	9.646522
3.	Composite 3	0.0337	0.0042	52.41058	6.531882	0.012	0.00054	13.90498	0.625724	0.0606	0.0016	69.09920	1.824401
4.	Composite4	0.0417	0.004562	64.85226	7.094868	0.00954	0.0034	11.05446	3.939745	0.0782	0.00098	89.1676	1.117446
5.	Composite5	0.0452	0.00584	70.29549	9.082426	0.0207	0.002	23.9861	2.317497	0.0722	0.0008	82.32611	0.912201
6.	Composite6	0.0569	0.003	88.49145	4.66563	0.03413	0.0017	39.54809	1.969873	0.0427	0.00243	48.68871	2.77081
7.	Composite 7	0.0245	0.0024	38.10264	3.732504	0.0382	0.0027	44.26419	3.128621	0.0589	0.0013	67.16077	1.482326
8.	Composite 8	0.01784	0.00501	27.74495	7.791602	0.0097	0.00292	11.23986	3.383546	0.0634	0.0011	72.29190	1.254276
9.	Composite 9	0.0413	0.0037	64.23017	5.754277	0.038	0.00333	44.03244	3.858633	0.03517	0.00095	40.1026	1.08324

CPS= Count per second **Bq/Kg** = Becquerel per kilogram

Calibration factors: K-40 = 0.000643, Ra-226= 0.000863, Th-232 = 0.000877 **Conversion factor:** $x10^{-4}$ cps/Bq-kg^{-1}

Analyzed and Compiled by: *I.A.Bappah* ***Signature:*** ***Date:*** 23/02/2015

Checked and Approved by: Dr. D.J. Adeyemo ***Signature:*** ***Date:*** 26/02/2015

Appendix VI: Frequency distribution of total count rates of gamma ray energy of the study area

Total Count (cps)	Frequency
5.0	0
10.0	7
15.0	76
20.0	171
25.0	93
30.0	16
35.0	4
40.0	12
45.0	6
50.0	7
55.0	1
60.0	1
65.0	0
TOTAL	394

PLATES



Plate I: The Researcher taking readings with the scintillometer in the study Area



Plate II: A Field Assistant recording the readings taken by the researcher



Plate III: The PGIS-SP strapped at the back of the researcher during the spectrometric survey